

Molecular Photodynamics in Rare Gas Solids

V. A. Apkarian*

Department of Chemistry, University of California, Irvine, California 92697-2025

N. Schwentner†

*Institut für Experimentalphysik, Freie Universität Berlin, Arnimallee 14, D-14195 Berlin**Received October 19, 1998 (Revised Manuscript Received March 18, 1999)*

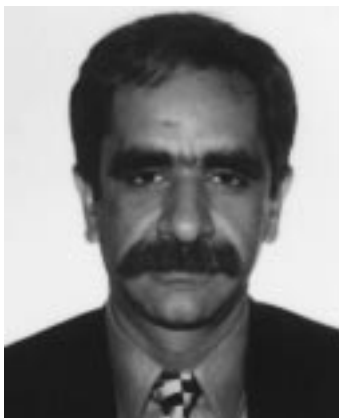
Contents

I. Introduction	1481	C. H ₂ S, D ₂ S	1502
A. The Staging of Barrier Crossings: Atomic Mobility	1482	D. Cl ₂ in Xe—Dissociation without Cage Exit	1502
B. The Fundamental Issue: Potential Energy Matrixes	1483	IX. Forced and Delayed Cage Exit	1503
1. $L = 0$ Atoms	1484	A. Cl ₂ in Ar	1503
2. $L > 0$ Atoms	1485	B. Cl ₂ in Kr and Xe	1504
3. Molecules	1487	X. Channeled Migration	1504
C. The Challenge to Theory: Quantum Many-Body Dynamics	1488	A. F Atoms	1504
II. Matrix Isolation Spectroscopy and Relaxation Processes	1490	B. O Atoms	1505
III. Sample Preparation and Morphology	1492	C. H Atoms	1506
IV. Photon-Induced Dissociation	1493	XI. Photon-Induced Harpooning	1508
V. Perfect Caging	1494	XII. Acknowledgments	1510
A. Direct Observation of the Caging Process	1494	XIII. References	1510
B. Stabilization of Fragments and Isomerization	1495		
1. OCIO	1495		
2. ICN	1496		
VI. Predissociation	1497		
A. Electronic Caging by Solvent Symmetry	1497		
B. Differential Solvation	1497		
VII. Dissociation through Sudden Cage Exit	1499		
A. F(² P)	1500		
B. O(¹ D)	1500		
C. S(¹ D)	1500		
VIII. Delayed versus Sudden Exit	1500		
A. HI, HCl	1500		
B. H ₂ O, D ₂ O	1502		

I. Introduction

A molecular level understanding of dynamics in condensed media is one of the current challenges to chemical physics. The challenge stems from the many-body nature of interactions, which lead to inseparable dynamics on a wide range of time and length scales. Progress in this field has been slow, since the experimental tools for probing the microscopic world, namely, spectroscopies, in the case of condensed media are blunted by structural and dynamical averaging. Interpretations of experiments must rely heavily on theory, and the required theoretical methods for handling extended systems are themselves in a formative state. Ideally, what is required is the exact determination of the time-dependent quantum Hamiltonian for assemblies of hundreds of particles. While this feat is not feasible

* To whom correspondence should be addressed. E-mail: apkaria@uci.edu.
† E-mail: Nikolaus.Schwentner@physik.fu-berlin.de.



V. Ara Apkarian was born in 1955 in Damascus, Syria. A graduate of the Hovagimian-Manouguian School in Beirut, Lebanon, 1973, he obtained a B.S. in Chemistry from the University of Southern California in 1976. He obtained his Ph.D. in Chemistry from Northwestern University in 1980 under the supervision of Prof. E. Weitz for a dissertation on vibrational energy transfer processes in polyatomics. He developed his interest in energy transfer processes of matrix-isolated molecules while at Northwestern, where he stayed for a postdoctoral period, 1980–1981. He then joined Professors P. L. Houston and R. P. Merrill at Cornell University, 1981–1983, to carry out postdoctoral studies on gas–surface interactions. He was appointed Assistant Professor of Chemistry at the University of California, Irvine, in 1983, where he is currently. His research focuses mainly on fundamental aspects of chemical dynamics and photophysics in condensed media.

at present, classical and semiclassical computational tools for handling mesoscopic dynamics on an atom-by-atom basis are becoming possible. Model systems, which are amenable to both experimental and theoretical scrutiny at a commensurate level of detail, are therefore highly desirable for developing both experimental and theoretical tools and for converging on accurate descriptions of many-body interactions and dynamics. That the photodynamics of small molecules in rare gas solids (RGS) represent ideal model systems for this purpose has been the motive for a significant body of work, which is the subject of this review. From this limited perspective, the field is young but poised for accelerated progress in the coming years due to the widening accessibility of the two most incisive tools: ultrafast lasers, which enable experiments on time scales of relevance to elementary processes in condensed matter and computational tools, which enable large-scale simulations. Neither of these tools can credibly develop alone, while the synergy between the two can transform a well-devised study into a fundamental learning experience. Recent examples from the literature, which will be reviewed here, were chosen to validate this contention. We must apologize at the onset for not compiling an all inclusive list of related works, our aim is to provide through examples a critical assessment of the field and a chart for future progress. To establish a unified theme for the selected subjects, we offer several considerations.

A. The Staging of Barrier Crossings: Atomic Mobility

The most rudimentary abstraction of chemical change is the crossing of a barrier separating reagents from products. The generalization of this



Nikolaus Schwentner was born in Rosenheim, Germany, in 1945. He received his Diploma in 1971 and his Ph.D. in 1975 from the University of Munich under the supervision of Professor Wulf Steinmann. His Ph.D. work was centered on the photoelectron emission from pure and doped rare gas films with experiments at DESY in Hamburg and Tel Aviv. Then he carried out postdoctoral research at the University of Kiel with Professor Ruprecht Haensel, starting with structural investigations using X-ray absorption fine structure. He became interested in nonradiative processes and studied light-induced fluorescence at the synchrotron radiation laboratories in Hamburg and Paris and finished his habilitation in 1980 with the topic of energy dissipation in solid and liquid rare gases. He has been a Professor at the Physics Department of the Free University in Berlin since 1982. His research interests, broadly, are in nonradiative transitions and light-induced photochemical reactions with ultrashort laser pulses. He also works on materials for short wavelength lasers and on the microstructuring of metals and semiconductors by light-induced dry etching.

picture to complex reactions entails mapping of multidimensional phase space on a single coordinate, with the result that the complexity of the reaction is transformed to the nature of the barrier. It is in this context that the seminal work by Kramers on passage over dissipative barriers has served as the cornerstone of modern theories of condensed-phase reactivity.^{1,2} In principle, well-defined barriers of varying complexity can be staged in ordered, inert, crystalline hosts to serve as models for both laboratory and computer experimentation. To be concrete, consider the mobility of an impurity atom trapped as a point defect in a host with long-range order (see Figure 1). The defect is presumably stationary by virtue of being surrounded by thermally inaccessible potential energy barriers. Mobility, which must involve barrier crossing, can then be induced either thermally or via a variety of photoinduced processes.

The thermal diffusion of point defects in solids is a well-developed field;^{3,4} although thermal mobility of guests in rare gas matrixes is well-known and widely used for chemistry,⁵ few quantitative studies of the process have been reported. Where quantified experimentally, such as in the case of atomic oxygen in both free-standing crystals^{6,7} and in matrixes,^{7–10} the theoretical rationalization of the observed process, and experimentally extracted quantities such as activation energies of interstitial and substitutional O atoms, has failed.^{11,12} The results of these simple experiments await interpretation. The key, as we will argue below, lies in the proper description of potential energy surfaces.

A variety of photoinduced methods can be employed to promote atomic mobility, as illustrated schematically in Figure 1.

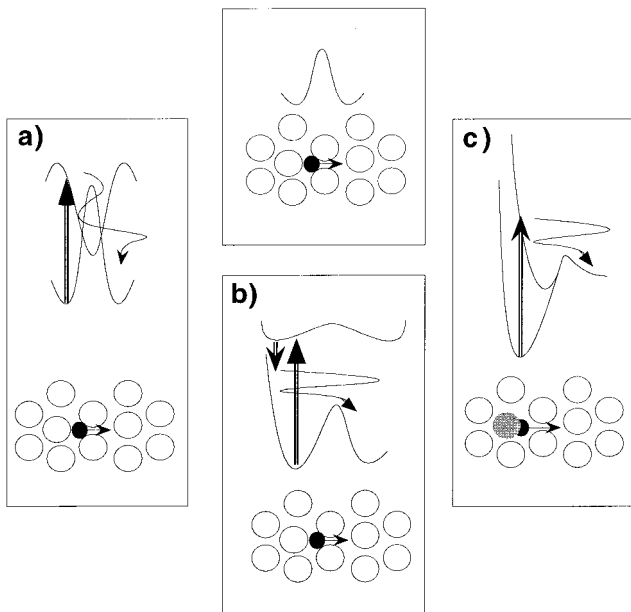


Figure 1. Staging of barrier crossings. An interstitial atomic impurity (●) must overcome a barrier to reach the new trapping site. This can be induced thermally or optically. Three photoinduced mechanism are shown: (a) accessing an excited surface which shows a minimum where the ground-state barrier occurs (need not necessarily cross); (b) accessing an exciplexic state, where the excited state is more tightly bound than the ground state, and subsequent radiative dissociation; (c) photodissociation of a diatomic impurity.

(a) *Electronic excitation of the atom, such that the barrier on the ground surface is replaced by a well on the excited surface.* The photomobility of atomic oxygen in free-standing crystals of Kr and Xe^{6,13,14} and in matrixes^{8,9,15} and photomobility of metal atoms such as Ag^{16,17} and Cu¹⁸ which show extensive photo-induced aggregation are examples. Note, this process entails electronic curve crossings.

(b) *Photoinduced relay between electronic surfaces to reach a repulsive configuration on the ground surface.* Electronic transitions forming guest–host exciplexes and their subsequent radiative relaxation (dissociation) fall in this category. Photomobility of halogen atoms such as F¹⁹ and Cl²⁰ can be induced by this photocycle and has been the subject of some of the more refined theoretical analysis,²¹ with less than satisfactory agreement with experiment in the final analysis.

(d) *Photodissociation,* which in contrast with the gas phase is now controlled mainly by the crossing of the cage barrier by photofragments, can lead to a large range of mechanisms for barrier hopping, from forced to sudden to delayed cage exit scenarios. A number of examples will be given in this context.

(e) *Tunneling mobility* is mainly reserved to quantum hosts, such as solid H₂ and He, in which it has been shown that this is the main mechanism for the migration of vacancies.²² Vacancies in turn serve as the means for both self-diffusion²³ and interdiffusion of impurities such as H atoms in solid H₂.^{24,25} Tunneling via both physical exchange^{26,27} and chemical exchange²⁸ has been considered for H-atom diffusion theoretically and has been used to rationalize the

extensive measurements by the Miyazaki group in pure and isotopically mixed solids of hydrogen.^{29–32} Tunneling contributions to H-atom diffusion in heavier rare gases, although not significant, have been suggested as a possibility.^{33,34}

The nature of the barrier crossed in these cases varies dramatically. In the thermal process, the barrier is one of free energy in character. In the case of photoinduced crossings, a wide range of behaviors may be expected, from strictly sudden transitions to fully accommodated adiabatic processes involving a number of active degrees of freedom which in turn are coupled to the bath. Statistical treatments of such a barrier crossing process may be possible at either extreme, thermal⁴ or sudden;³⁵ however, the more general situation occurs between these two limits, where the only viable means for elucidation of the controlling many-body dynamics are explicit simulations.

To stage one of these scenarios with a clearly identifiable reaction coordinate or to interpret observations, the crucial ingredient is the understanding of excited- and ground-state potential energy landscapes together with their nonadiabatic couplings. This may indeed be regarded as the ultimate goal of the field and deserves commentary before proceeding with detailed case studies.

B. The Fundamental Issue: Potential Energy Matrices

Since model systems, not chosen for immediate applications of practical utility, are the subject of this review, identification of the most fundamental issues to be addressed by such studies is valuable. To this end, consider the conceptual framework behind numerical treatments of classical molecular dynamics (MD). Newton's equations of motion are deterministic and defined given the instantaneous force acting on each particle. The common numerical method for propagation of trajectories, the Verlet algorithm³⁶

$$\mathbf{r}_i(t + \delta t) = 2\mathbf{r}_i(t) - \mathbf{r}_i(t - \delta t) + \frac{\mathbf{F}_i}{m_i} \delta t^2 \quad i = 1, \dots, n \quad (1)$$

makes it clear that given initial positions of particles *i* at times *t* and *t*−*δt*, the future positions can be predicted as long as the instantaneous force acting on the particle, \mathbf{F}_i , is prescribed. If the forces were prescribable, then just the fact that *n* is a large number produces collective dynamics, which with proper time and ensemble averages leads to statistical mechanics. Given the nontrivial connection between statistical mechanics and single-particle trajectories, classical simulations under assumed forces and sound statistical analysis are in themselves valuable for producing an atomistic view of macroscopic observables. Yet, the prescription of forces and torques is the more fundamental issue and the challenge in multibody systems. For nondissipative systems, we may generally expect that the forces can be derived from a scalar potential, i.e., a function of only nuclear positions

$$\mathbf{F}_i = \nabla_i V(\{\mathbf{r}^n\}) \quad (2)$$

It is not conceivable that a function of the full set of positions, which must contain hundreds of elements to render a realistic treatment of condensed-phase dynamics, will be of any use. It is then surmised that to a good approximation, this function may be expressible in terms of pair interactions, the most primitive assumption being that of pairwise additivity

$$V(\{\mathbf{r}^n\}) = \frac{1}{2} \sum_{i,j=1}^n V(|\mathbf{r}_i - \mathbf{r}_j|) \quad (3)$$

which, due to its convenience, is also the most widely used. Were this approximation valid, then pair potentials would be the required input for the prediction of many-body dynamics. Given that at present pair potentials can be obtained at high levels of precision, both from electronic structure calculations and from experiments, the challenge in describing inter- and intramolecular forces in condensed phase may be summarized under the rubric of the *nonadditivity of pair interactions*.

Implicit in the assumption of a single potential energy surface (PES) in eq 2 is the Born–Oppenheimer approximation, which is invariably inadequate where chemistry is at play: the making and breaking of bonds necessarily involves coupling between electronic and nuclear degrees of freedom. Implicit in eq 3 is the assumption that atom–atom interactions are angularly isotropic, which is not the case where open-shell structures are involved.^{37,38} Also, the assumption of a scalar potential presumes the absence of electrostatic forces, such as induction forces, which are vectorial in nature.³⁹ In the case of interactions among closed-shell atoms, such as rare gases for which the pair potentials are well-characterized,⁴⁰ deviations from additivity arise from the fact that dispersion forces originate from fluctuating charge distributions, which must also be correlated vectorially. The well-known three-body dispersion term, the Axilrod–Teller–Muto potential, is such an example.^{41,42} This third-order perturbation correction in transition dipoles accounts for the three-body van der Waals interaction which is operative at long range. At short range, in small clusters, the quadrupole exchange interaction has been recognized as a dominant source of nonadditivity.⁴³ Although such contributions may be rather small, on the order of 5%, compared to pair terms, their effect on structure and dynamics can be profound in dense media, where many are involved simultaneously. For example, the equilibrium fcc structure of rare gas crystals cannot be obtained without the inclusion of three-body forces.⁴⁴

1. $L = 0$ Atoms

Since the photodissociation of hydrides is one that plays a prominent role in this subject, let us use it as a case for warnings. The H–Rg pair potentials have been studied experimentally through scattering experiments that measure orbiting resonances, which give detailed information about the bound region of

the potential.^{45,46} The repulsive walls of interaction at short range are more reliably obtained from ab initio calculations.⁴⁷ The parametrization of Tang and Toennies is informative.⁴⁸ The potential is given as a sum of the Born–Mayer exponential repulsion and a dispersion expansion in even powers of inverse R

$$V(R) = A \exp(-bR) - \sum_{n=3} \frac{f_{2n}(R) C_{2n}}{R^{2n}} \quad (4)$$

in which $f_{2n}(R)$ is a damping function given in terms of the Born–Mayer range parameter b and is devised to smoothly join the long-range attraction due to dispersion with the exponential repulsion arising from overlap of charge densities. The form is the same as that used earlier for the description of closed-shell atoms,⁴⁹ except in the combining rules for the Born–Mayer parameters. The critical evaluation of combining rules and their theoretical justification gives physical motivations for the various terms. In the case of H–Rg, it is found that, in effect, only one-half of the outer-shell electrons of Rg need to be considered in the overlap-induced repulsion (the Pauli force is only due to the electron density with spin parallel to that of the H electron).⁴⁸ This force generates a polarization of both Rg and H charge densities and, therefore, produces collision-induced multipoles along the Rg–H coordinate. The dispersion coefficients in eq 4 reflect the multipole expansion of the perturbation operator,^{50,51} with the identification of C_6 as dipole–dipole, C_8 as dipole–quadrupole, and C_{10} as the sum of dipole–octupole and quadrupole–quadrupole terms. Viewed as such, it would seem that none of the terms in this expansion are pairwise additive. Yet, to date, in all treatments of H in RGS, this assumption has been made.

Now consider the photodissociation of a diatomic hydride, which is only completed upon cage exit of the H atom. The potential barrier along the minimum energy path passes through the center of three-mutual nearest neighbors,⁵² corresponding to a tight structure high up the repulsive curve of individual pair interactions. Within the range of known accuracies of potentials, using either high-level ab initio potentials^{53,54} or the semiempirical Tang–Toennies potential,⁴⁸ at the equilibrium geometry of the lattice, the barrier height determination is subject to $\sim 25\%$ (~ 0.25 eV) uncertainty.⁵⁵ This large variation is in part the result of the amplification of the uncertainty in the pair potential, due to the fact that three Rg atoms are simultaneously repelled. Note, the inclusion of thermal and zero-point amplitudes of lattice vibrations produces a barrier height distribution which is significantly broader than this uncertainty.³⁵ We can, therefore, expect that measurements of near-threshold photodissociation of a diatomic hydride, which may be quite aptly regarded as an experiment in *scattering from within* the crystal, can experimentally refine our knowledge of the H–Rg interaction in the barrier region. The caveat remains that we must be prepared to address the nonadditivity issue, since that too will be amplified at nonstationary points such as at tight potential barriers. Moreover, host-induced perturbations of electronic surfaces

complicate this simple proposition of a scattering experiment, necessitating the consideration of electronic manifolds and nonadiabatic dynamics, as we amplify next.

2. $L > 0$ Atoms

In the case of open-shell atoms with orbital angular momentum $L > 0$, we must account for the angular anisotropy of electron densities and the multiplicity of electronic surfaces that arise from orbital degeneracy. Variations of the environment from perfect symmetry, be it static or due to nuclear dynamics, will lift the degeneracy of electronic surfaces, and now the coupling between nuclear and electronic degrees of freedom needs to be taken into account to describe the instantaneous forces. This breakdown of the Born–Oppenheimer approximation implies that no longer can the forces be obtained from a potential function of coordinates alone, and if we insist on a classical model, we must be prepared to consider velocity-dependent forces. The anisotropic potentials that arise from an open-shell atom interacting with the closed-shell rare gas atoms can quite generally be described through the electrostatic expansion

$$V_{X-Rg}(r, R_1, R_2, \dots, R_n) = \sum_{k=1}^n \sum_{L=0}^{\infty} V_L(r, R_k) P_L(\vec{R}_k \cdot \vec{r}) \quad (5)$$

in which r denotes the electronic coordinate on open-shell atom X, R_k are the coordinates of the closed-shell Rg atoms, and P_L is the Legendre polynomial. The potential is now evaluated as an expectation value over r , in the relevant basis set of electronic wave functions of atom X. The simplest case we may imagine is that of a p-hole ($L = 1$), as in the case of X = halogen atom. Neglecting spin, the minimal basis set required for describing the potential matrix is Y_{1m} ($m = 1, 0, -1$). This limits the summation over L to only two terms, $L = 0$ and 2, and leads to a 3×3 matrix with elements

$$V_{mm'} = \sum_k \sum_{L=0,2} \frac{4\pi}{2L+1} \times \langle Y_{lm'} | \sum_{M=-L}^L Y_{LM} | Y_{l,m'} \rangle V_L(R_k) Y_{LM}^*(\vartheta_k, \varphi_k) \quad (6)$$

in which the radial functions, V_0 and V_2 , describe the isotropic and anisotropic parts of the X–Rg pair interaction, respectively, and may be related to the diatomic Σ and Π potentials through⁵⁶

$$V_0 = \frac{1}{3}(V_\Sigma + 2V_\Pi) \quad (7a)$$

$$V_2 = \frac{5}{3}(V_\Sigma + 2V_\Pi) \quad (7b)$$

The adiabatic surfaces are now obtained by diagonalizing the potential matrix, and nonadiabatic dynamics are controlled by off-diagonal surfaces. The barrier for cage exit now depends on orbital orientation, as illustrated in Figure 2.

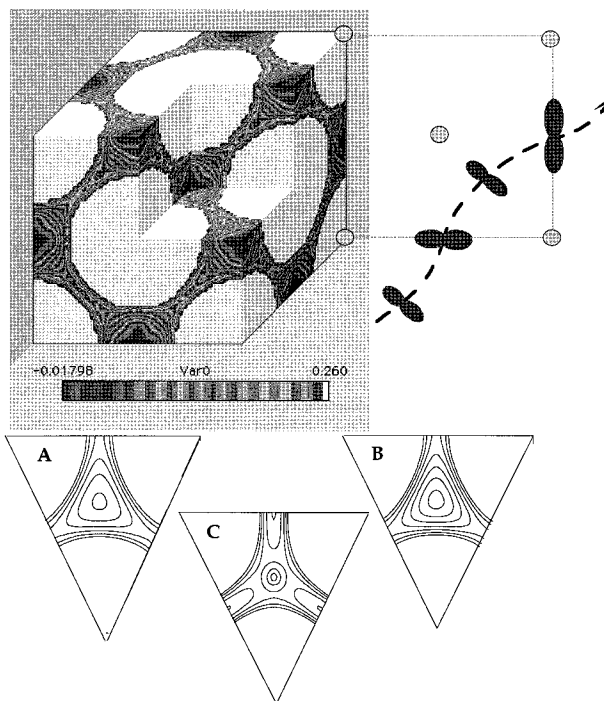


Figure 2. Three-dimensional contour map for the lowest energy surface of an F atom on a unit cell of Kr is shown. The minima occur at the octahedral interstitial sites, which are directly connected via minimum energy paths, the midpoint of which corresponds to insertion of the F atom between two nearest neighbors of the lattice. This is clarified with the trajectory showing the p orbital of the F atom, where it is clear that at the midpoint it forms two Σ -type interactions. Whether migrating in a perfect lattice or after photodissociation from an impurity site, access of the interstitial O_h site is mandated with the triangular faces of the octahedron acting as dividing planes. The energy contour maps on the triangular face of the octahedron are shown. There are three such surfaces, as a result of the splitting of the 2P state degeneracy: (A) highest energy surface with the P-hole perpendicular to it (minimum energy contour at center, at $E = 0.75$ eV, contour spacing of 0.25 eV), (B) middle energy surface with topology similar to A (minimum energy contour at $E = 0.5$ eV), (C) the minimum energy surface, where the lowest energy occurs at the bisectors of the sides, with the P-hole in the plane (minimum energy contour at $E = 0.15$ eV, central hill at $E = 0.26$ eV).⁸⁷

The above construct is valid beyond the electrostatic limit, being in effect a limited-basis diatomics-in-molecules (DIM) treatment. The DIM formalism, originally developed by Ellison,⁵⁷ partitions the electronic Hamiltonian of a polyatomic in terms of atomic and diatomic constituent fragments

$$H = \sum_a \sum_{b>a} H_{ab} - \sum_a H_a \quad (8)$$

The partitioning is exact when complete basis sets are used. In practice, the bases are invariably truncated and the formalism is implemented semiempirically. The approach is well-developed for describing intramolecular potentials of small molecules and has found wide use in gas-phase reactive dynamics in which global excited and ground electronic surfaces that can be efficiently evaluated through the solution of algebraic equations are quite useful.^{58,59} These considerations are even more pressing in the case of

condensed-phase chemical dynamics dictated by many-body interactions. Indeed, the principle sophistication in treatments of chemical dynamics in RGS has occurred through adaptations of the DIM framework for describing potential energy matrixes, even if the authors have not specifically acknowledged this relation. The unity in theme of these methods is the construction of potential energy manifolds based on pair parameters, without making the assumption of simple pairwise additivity. A review of such implementations in RGS illustrates the sophistication that has evolved over the past decade.

The first realistic treatment of open-shell atoms isolated in rare gas matrixes was a direct extension of the three-body treatment by Bayliss,^{37,38} extended now to the analysis of trapping sites and site-specific electronic absorption spectra of alkali atoms trapped in rare gas matrixes.⁶⁰ The same formalism, limited to the p-basis set, was later implemented using accurate pair potentials as input.⁶¹ With the same motivations, interpretation of electronic spectra and local structure, Maillard et al. addressed the energetics of O(³P, ¹D, ¹S) atoms isolated in high-symmetry sites of a rare gas lattice.⁶² The work of Balling and Wright has been influential since it was formulated for numerical implementations not limited to a specific local symmetry.⁶¹ These treatments limited the DIM bases to term states of the ground electronic surface. An important extension of the DIM procedure was made by Last and George in describing the delocalized charge-transfer states of Cl atoms isolated in solid xenon and coined the term diatomics-in-ionic-systems (DIIS).^{63,64} Deviating from strict adherence to the DIM procedure, DIIS does not limit energetics to purely pair interactions, rather in the case of ionic configurations, it takes proper account of the vectorial nature of induction terms. To describe the mixed covalent and ionic states of a Cl atom isolated in a substitutional site of the Xe lattice, the DIM basis must now include the Xe⁺(²P) states on the cage atoms, minimally requiring a 39 × 39 matrix to treat the 13-atom system submerged in the dielectric of the host. Moreover, they explicitly included the admixture between ionic and neutral manifolds in their analysis. While in this specific case the excited state is believed to be delocalized beyond the immediate cage and a Wannier-type Rydberg progression of hole states is the more accepted picture,^{65,66} inclusion of the ionic admixture yields an improved description of the ground-state interactions. The significance of this development transcends the specifics of the system under consideration, and its broader implications are only recently being appreciated. For example, in recent test cases in such species as HF–Ar_n, He–Cl₂, Ar–Cl₂, and HF–HF, for which detailed many-body surfaces exist, it has been demonstrated that the proper inclusion of the lowest ionic states in the DIM matrix provides a convenient means for the incorporation of nonadditivities in induction and dispersion terms to give a quantitative description of both inter- and intramolecular potential surfaces of aggregates in the ground state.^{67–70} An important extension of DIM is due to Gabriel and co-workers, who showed that the basis could be used

to describe truly extended electronic states, first describing the band structure of pure solids⁷¹ and more recently for doped solids, readdressing the nature of halogenic hole states in solid xenon.⁷²

Tests of the utility of the DIM approach for quantitative descriptions of interactions come mainly from the analyses of electronic spectra of atomic impurities. Lawrence included the spin-orbit interaction in the DIM matrixes to describe the Jahn-Teller split potential surfaces and spectra of atomic iodine in crystalline Kr and Xe.⁷³ They showed that, although small, adjustment of input pair parameters were necessary to reproduce the spectra in the limited six-dimensional basis arising from interactions of Rg(¹S)–(²P_{1/2}, ²P_{3/2}) states. Fajardo et al. used the method to interpret the site-specific spectra of matrix-isolated alkali atoms,^{74–77} where the site induced splitting of the degeneracy of $L = 1$ excited states serves as the important diagnostic.^{78–80} More extended basis treatments of the same systems were given by Langhoff et al., now in the formalism of the spectral theory which shares attributes of the DIM formalism, although in constructing the matrixes it relies on dipolar expansions in unsymmetrized polyatomic basis sets.⁸¹ Site-specific spectra, interstitial versus substitutional, of the two-hole oxygen atom isolated in free-standing crystals were reproduced through simulations.⁶ This study also showed the inadequacy of the limited basis representation in the analysis of O-atom mobilities. The same treatment was extended to O-doped in solid *para*-hydrogen where, by using accurate ab initio points, surfaces coupled within the manifolds of term states were generated.⁸² This limited basis set treatment failed to reproduce the surprising stability of O(¹D) in solid deuterium, which was discovered experimentally.^{82,83} Using the same ab initio input, but now with a much larger expansion of the basis set, including the O[–]H⁺ and H⁺O[–]H⁺ charge-transfer configurations, it was shown that a barrier to insertion of O(¹D) in H₂ arises naturally as strictly a many-body effect.⁸⁴

In the description of interactions of an open-shell atom, the off-diagonal elements of the Hamiltonian matrix are as important as the diagonal ones. While in the case of thermal interactions at cryogenic temperatures we may expect the adiabatic following limit to be operative, nonadiabatic effects can play an important role. Using DIM Hamiltonians, dynamics including nonadiabatic transitions among spin-orbit split states of F(²P_{1/2}, ²P_{3/2}) atoms in solid Kr have been analyzed to show that nonadiabatic transitions can lead to orbital reorientation on time scales of <20 fs.⁸⁵ This mixed quantum-classical treatment of coupled electronic-nuclear degrees of freedom was extended to include explicit consideration of electronic phases, Berry phase that arise from Kramers degeneracy, for an isolated Cl atom.⁸⁶ The finding of very rapid orbital reorientation justifies the assumption of and adiabatic orbital following even in the case of atomic motions at several electronvolts of kinetic energy—a conclusion also reached by a careful statistical analysis of the experimental data on cage exit of F atoms.⁸⁷ Analysis of the spectroscopy and inter-

system crossing dynamics of Hg⁸⁸ and Zn^{89,90} are valuable studies in this regard.

In summary, the consideration of interactions of a single open-shell atomic impurity in the lattice of closed-shell rare gas atoms demonstrates the nuances in quantitative treatments of many-body interactions. The DIM framework is a useful means for injecting the necessary physics in such analyses and with astutely chosen bases and pair parameters may lead to quantitative results. To date, the indication is that minimal basis constructs are successful in the analysis of atoms trapped at stationary points, such as potential minima; however, it would seem that such a treatment is insufficient to quantify potential barriers. It is perhaps not surprising that nonadditivities are significantly more severe in the latter case, and contributions from excited-state configurations, and in particular from charge-transfer states, must be included, as in DIIS, to be quantitative. Since, invariably, truncated bases are used in these treatments; tests of the adequacy of the representation vis-à-vis experiment are crucial to establish the accuracy of the approach and the reliability of predictions. Such rigorous comparisons are becoming possible with the increase of detail in experimental observables.

3. Molecules

While the conceptual framework does not change in proceeding beyond a single open-shell atom, the bases required for describing interactions increases exponentially with the number of open-shell fragments. To describe the electronic surfaces relevant to photodissociation of a diatomic impurity, inter- and intramolecular global surfaces are required. And although single-surface classical molecular dynamics was initially employed gainfully, e.g., the photodissociation of HI in solid Xe,⁹¹ rigorous treatments could not be considered, since on a single dissociative electronic surface recombination cannot be described. The first explicit treatment of recombination is that of Gersonde and Gabriel who simulated the photodissociation of matrix-isolated Cl₂⁹² and subsequently of HCl.⁹³ They used a minimal basis DIM Hamiltonian neglecting spin-orbit coupling (9×9 matrix in the case of Cl₂). Recombination, and more generally nonadiabatic dynamics, could now be explicitly considered through semiclassical surface-hopping algorithms while propagating the nuclear motions classically. Krylov and Gerber used DIM matrixes to carry out simulations of nonadiabatic dynamics now including spin-orbit coupling in their treatment of the photodissociation of HCl in solid Ar.⁹⁴ Batista and Coker have carried out simulations of nonadiabatic dynamics using the DIIS Hamiltonian of the full stack of covalent and ion-pair states of molecular iodine both in matrixes⁹⁵ and in liquid Xe.⁹⁶ The construct of the DIIS matrix of 23 covalent states and 18 ion-pair states (with the neglect of coupling between ionic and covalent manifolds) is semiempirical *de-jure*. Despite the care for detail, there is significant uncertainty in such constructs, as can be gleaned by a comparison of the DIM matrixes of Coker and Batista with those of Buchachenko and

Stepanov, who gave an explicit analysis of the I₂-Ar case.^{97,98} Initial comparisons with experiments in the solid and liquid phase show qualitative success; however, the simulations overestimate the predissociation probability of the B state by an order of magnitude.^{99,100} The origin of this discrepancy, whether algorithmic or due to overestimates of off-diagonal elements in the DIIS matrix, is not yet clear. However, given the fact that detailed time-resolved measurements of this system are possible, significant refinements of method and model can be expected. More recently, Alberti et al. have reported simulations of the photodynamics of ICN isolated in solid Ar, using DIM matrixes to include the four electronic surfaces that correlate with I(²P_{1/2}) + CN and I(²P_{3/2}) + CN limit.¹⁰¹ Although the fragments do not exit the cage, recombination can be defined by electronic populations: 44% of the trajectories reach the ground electronic surface within 3 ps, with curve crossings controlled by the bending angle which occur on the picosecond time scale. The data are not directly compared to experiments, since the stiff CN bond remains highly vibrationally excited, and classical MD simulations are inadequate for the direct description of vibrational thermalization for modes that are much higher than the Debye limit of the solid.¹⁰¹ Note, in all cases to date the nonadiabatic dynamics is simulated using classical trajectories and surface hopping, a method pioneered by Tully.^{102,103}

Last and George extended their DIIS analysis of charge-transfer states to molecular impurities, in particular to HCl isolated in solid Xe.¹⁰⁴ This study was motivated in part by the recognition that the incipient bonding between halogens, X, and the heavier rare gas atoms, as in Rg,X, could be naturally described via DIIS as mixing between ionic and neutral configurations. Their calculations correctly predicted the existence of (HXe)⁺Cl⁻ as a ground-state ionic molecule,¹⁰⁴ a finding that was directly verified experimentally in the family of HRgX, where Rg = Kr or Xe and X = Cl, Br, or I,^{105,106} and is expected to be valid for the entire family of halogens and heavier rare gases. Using DIIS, Last and George had also made predictions of structure and stability of positively charged rare gas clusters containing atomic and molecular hydrogen;¹⁰⁷ these too were subsequently verified experimentally as charge-separated centers generated via optically accessed delocalized charge-transfer states.^{108,109} Infrared spectroscopy of UV-irradiated solids containing halogen and hydrogen atoms along with high-level ab initio theoretical analysis have led to the identification of a large number of new ionic centers, such as (RgH-Rg)⁺ and (RgH)⁺,^{108,110-114} RgHX⁺,¹¹³ HX₂⁻,¹⁰⁹ and ion-pair states, such as HRgH or HRgD.¹¹⁵

Two important conclusions can be reiterated from these works: first, in considering the energetics of a system such as a hydrogen halide, *even in the "ground" electronic surface*, ionic configurations cannot be ignored; second, DIIS can be useful in such treatments by including the mixing between ionic and covalent manifolds of states, the alternative of all-electron calculations being rather impractical where dynamics is of interest. These conclusions are

further supported by the works of Nemukhin et al., who more recently used the approach to simulate the emission spectrum of the matrix-isolated ion-pair state of Cl_2 .⁷⁰

Global surfaces have also been constructed effectively through ab initio methods to treat reactive dynamics in RGS. The bimolecular reaction of F_2 with ethylene is an example.^{116,117} The utility of the semiempirical DIIS methods in constructing global surfaces in matrixes stems from the fact that the host is composed of closed-shell atoms, and if represented by $^1\text{S}_0$ wave functions, then one isotropic function is required per host atom. If the excited-state p-hole is to be taken into account on the Rg atoms, which is required for inclusion of charge-transfer contributions, then to represent N Rg atoms, 3^N basis functions are required. Thus, DIIS matrixes can rapidly become unmanageable. An alternative is the use of pseudo-potentials to describe ground- and excited-state interactions of the valence electron of the impurity with its polarizable ion core as well as e–Rg interactions, as recently implemented in the description of Na atom and dimer spectra in Ar clusters and matrixes.¹¹⁸ All of the discussed methods are rather prohibitive in the treatment of reactive dynamics in molecular solids. In such systems, empirical, effective bond order methods, such as that of Tersoff,¹¹⁹ become more useful.

Iteration between detailed experiments and simulations can be expected to provide descriptions of the many-body forces and torques that are at the heart of all descriptions of chemical physics in condensed media and may be regarded as the most fundamental issue addressed through studies of matrix-isolated dynamics.

C. The Challenge to Theory: Quantum Many-Body Dynamics

For a realistic representation of condensed-phase dynamics, the simulation of a system containing $>10^2$ nuclear degrees of freedom is necessary. Exact quantum propagation of dynamics in all degrees of freedom is not possible and is seldom warranted. Yet, besides the inherently quantum nature of dynamics involving electronic degrees of freedom, quantum aspects of nuclear dynamics play an important role in cryogenic solids and are necessary to rigorously define macroscopic observables.

Although to date the majority of simulations of matrix-isolated dynamics has been classical, the cryogenic temperatures involved imply that zero-point effects cannot be ignored. This difficulty has been recognized in the first classical simulations aimed at describing vibrational relaxation of Cl_2 isolated in solid Ar.^{120,121} Quite clearly, the results in this case are sensitive to the description of the spectral density, the proper representation of the full density of phonon states and phonon–phonon scattering processes, descriptions which are suspect in a strictly classical simulation in a finite cell. There have been several partial remedies used to address this deficiency, the combined semiclassical/classical molecular dynamics algorithm being one.¹²² Classical simulations at temperatures scaled to reproduce the

vibrational amplitude of the Debye mode has been another expedient solution, which has been used with some success in the interpretation of time-resolved measurements of vibronic coherences of I_2 .¹²³ The success of the approach may be related to the fact that the short time dynamics of relevance in this case is not sensitive to the exact description of long-wave phonons. Pseudo-potentials that freeze the zero-point energy by convoluting it into the potential have been used to describe impurity rotations in the quantum crystals of solid hydrogen.¹²⁴ While it has been demonstrated that the proper density of states and structure of the lattice can be reproduced by this approach, the reliability of dynamical descriptions remains to be tested.^{82,125} For systems at or near thermal equilibrium, quantum path integral methods, such as centroid dynamics, can be used to treat quantum statistical dynamics¹²⁶ and have been implemented for the calculation of diffusion-controlled recombination of Li atoms in solid *para*- H_2 .¹²⁷ Nevertheless, there is not a fully satisfactory solution for explicit dynamical simulations far from equilibrium.

Spectroscopic observables in condensed media are most naturally formulated in terms of quantum correlation functions^{128–133} and as such serve as a useful test of methods. The information content or the dynamical memory in spectra is limited by the decay time of the supersystem (all coordinates) correlation function. Where correlations decay on a time shorter than any dynamical recurrences to the Franck–Condon region, the classical Franck principle applies, in which case the spectrum can be regarded as a reflection of the initial state distribution function over the final state potentials. In this limit, spectra can be simulated using Monte Carlo methods⁷³ and can be used for testing the accuracy of representations of the initial state quantum distributions and the assumed system potentials but provide little to test the quantum propagation. With these considerations in mind, methods have been advanced and tested.

Mixed quantum–classical descriptions of nuclear dynamics in matrixes were first implemented by Alimi and Gerber to describe the photodissociation of HI by propagating the lattice coordinates classically while propagating the H atom as a Gaussian packet.¹³⁴ Zero-point effects of the guest degrees of freedom, in particular the proper description of its librational and rotational degrees of freedom, can be expected to be rather important in describing the photodissociation of a diatomic hydride. The first quantum treatment of the rotational wave function, and its consequence on dissociation dynamics, has recently appeared.¹³⁵ Although limited to a rigid lattice, these simulations make it clear that dissociation yields will be controlled by the initial rotational state of the parent molecule, which in turn controls the distribution of the relative guest–lattice orientations as illustrated in Figure 3. The effect of a dissipative lattice was introduced in the quantum calculation of HCl photodissociation in solid Ar by using the reduced density matrix approach.^{136,137} In this approach, the H–Cl coordinate is treated as a three-dimensional quantum degree of freedom which

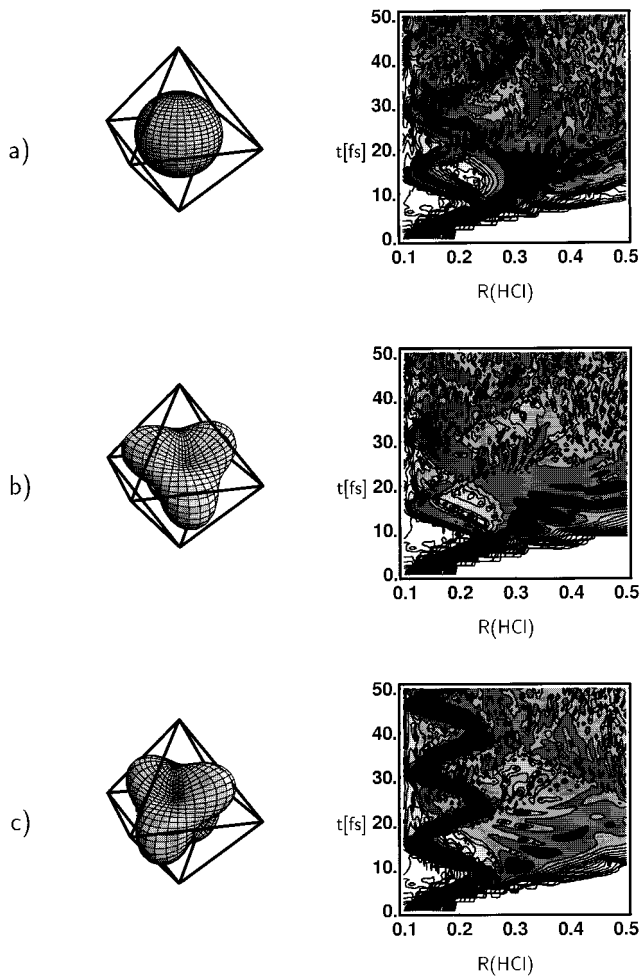


Figure 3. Quantum wave packet dynamics for photodissociation of HCl ($v = 0$) in fcc Ar with initial rotational wave functions: (a) $J = 0$ (A_{1g}), (b) $J = 3$ (A_{2u}), (c) $J = 3$ (T_{2u}).¹³⁵ In each case the modulus of the radial function of the H–Cl distance, R , versus time, t , is shown for initial excitation to the repulsive $^1\Pi$ potential. The A_{2u} distribution along the $\langle 111 \rangle$ axis leads to efficient exit around 8 fs, when the wave packet reaches the cage for the first time, while oscillating patterns are observed for T_{2u} orientation along $\langle 110 \rangle$, due to strong reflections. The isotropic orientational distribution in $J=0$ leads to behavior intermediate between the other two cases.

is linearly coupled to fluctuations of the spatially localized lattice points and the fluctuations dissipate on a phonon–phonon correlation time scale. The coupling is taken as an adjustable parameter. All of these simulations show a highly coherent packet for the H motion with persistent recurrences. This alone is not sufficient to generate structure in the absorption spectrum, which is known to be absent in the experiments.¹³⁸ The overall correlation function will decay due to the decay of overlap in momentum of the host atoms, which can be illustrated in one-dimensional analysis of systems such as IHXe.¹³⁹ In the reduced density approach, the structure can be completely eliminated by increasing the strength of the phenomenological coupling constant,¹³⁷ but now, the physical basis for the decay of correlations is less clear. We should note that these model treatments ignore the electronic density of states that were included in the quantum–classical electronic–nuclear dynamics^{93,94} and the latter ignore the ionic configura-

rations which for excited states of HCl should become important even in solid Ar.¹³⁸

The time-dependent Hartree method was used to construct the $A \rightarrow X$ emission spectrum of matrix-isolated iodine by carrying out wave packet propagation for a Morse oscillator coupled to a linear chain of harmonic oscillators.¹⁴⁰ Good agreement with experiment was obtained by extending the chain to 25 oscillators. Mixed quantum–classical calculations of time-resolved observables on the same state with a reduced representation of the matrix were given by Liu and Guo.^{141,142} The resonant Raman spectra of matrix-isolated iodine, which show long progressions,^{143,144} have served as a focus for developing methods. The first theoretical analysis used one-dimensional wave packet propagation and introduced a damping factor in the constructed correlation functions to represent the effect of the lattice.¹⁴⁵ However, the required excitation-dependent damping function could not be directly interpreted. The same method was further extended to scrutinize the non-monotonic decay of RR progressions in the liquid phase to suggest that ultrafast predissociation plays a role in shaping the intensity profile.¹⁴⁶ Time-dependent self-consistent field (TDSCF) treatments advanced by Gerber et al., where one degree of freedom is propagated quantum mechanically on the dynamically averaged mean potential of the rest of the system, has been implemented to calculate the same spectrum.^{147,148} This variant of TDSCF uses classically based separation of potentials, where classical trajectories are first propagated and stored, then one degree of freedom is propagated quantum mechanically over the dynamically averaged potential of all other degrees of freedom. Separability and averaging of dynamics are assumptions in the approach which can be improved upon by methods of configuration interaction, similar to CI in electronic structure calculations.¹³⁹ The general trend of RR progressions of matrix-isolated I_2 is reproduced by the method but not the details of nonmonotonicity. The mixed-order semiclassical molecular dynamics method was introduced by Ovchinnikov, first in a coordinate representation^{149,150} and subsequently in a coherent state representation,¹⁵¹ to construct quantum correlation functions in full dimensionality of the supersystem. In its final form, the method consists of propagating few coordinates (selected as such, either because of their low occupation number, $\hbar\omega/KT \gg 1$, or because of their high anharmonicity) by the Herman and Kluk propagator^{152,153} while the rest of the degrees of freedom are propagated as Heller's frozen Gaussians.¹⁵⁴ This semiclassical initial value method for carrying out path integrals in full dimensionality is valid for relatively short times, however, long enough to be useful in explicit simulations of spectroscopy in condensed media. The method was implemented in the coordinate representation to analyze absorption, emission, and RR spectra of matrix-isolated iodine.¹⁴⁹ It was shown, by nearly an exact reproduction, that the structure in the intensity profile of RR progressions in matrixes arises from interference between packets propagating on two surfaces, B and B'', simultaneously.¹⁵⁰ The analysis

makes it clear that the RR intensities are defined by the many-body correlation function. In contrast, the B → X absorption spectrum of matrix-isolated Cl₂ shows a strong vibration-dependent "electron–phonon" coupling, which is quite sensitive to the quantum correlation functions that arise from the details of collective dynamics.¹⁵¹ The successful simulation of the features of this spectrum is quite encouraging. Moreover, it has already been demonstrated that this initial value semiclassical method of propagation can be successful in reproducing quantum dynamics in the deep tunneling regime.¹⁵⁵ Extensions of these methods to include nonadiabaticity and quantum electronic degrees of freedom are to be expected soon.

The above examples were limited to simulations of relatively short time dynamics. In treating processes of low probability, such as the vibrational relaxation of a high-frequency mode or thermally activated barrier crossings, appropriate sampling methods and statistical treatments are required. Such examples can be found in the treatment of diffusion-controlled bimolecular reactions including effects of lattice morphology^{156,157} and the nonstatistical dynamics of isomerization of HONO.¹⁵⁸

The conceptual and methodological refinements in simulations are now sufficiently advanced to test their accuracy versus experimental reality and to develop predictive theories at least in the case of model systems such as the ones which form the body of this review. To this end, detailed experimental observables are crucial and time-resolved measurements in condensed media provide such data.

II. Matrix Isolation Spectroscopy and Relaxation Processes

The phenomenology of many of the processes discussed below is well-established in the mature literature of matrix isolation spectroscopy (MIS), which besides the spectroscopic background, provides a compendium for accessible reactivities.^{159–162} Traditionally, the main emphasis in MIS has been the spectroscopic characterization of transient species in which strong guest–host interactions are unwanted complications. A review of more recent developments in MIS has been provided by Bondybey.¹⁶³ And although qualitative descriptions of dynamics leading to the *in situ* generation of neutral and ionic fragments and the photochemistry of small molecules has been given in a pair of insightful reviews by Perutz,^{5,164} quantitative descriptions of such phenomena are relatively recent. The change in emphasis to dynamical studies in matrixes is noted by a recent volume of *Chemical Physics* dedicated to photophysics of matrix-isolated species.¹⁶⁵ Reviews of photodissociation dynamics in rare gas matrixes and clusters, in the very spirit of the present work, already exist.^{166–168} Contemporaneous with the writing of the present work is the review article by Haas and Samuni on reactions in rare gas matrixes, with an emphasis on site effects.¹⁶⁹ An earlier volume on electronic excitations in condensed rare gases,¹⁷⁰ a series on the properties of the rare gas host crystals,^{171–173} and the more recent book on chemical dynamics at low temperatures¹⁷⁴ provide useful back-

ground material for the general field. Also relevant are the reviews on simulations of dynamical processes in solids,^{175,176} of molecular dynamics of chemical reactions in solutions,¹⁷⁷ and of photochemical reactions in weakly bound clusters.¹⁷⁸

Relevant to reactive dynamics is the understanding of energy flow from internal degrees of freedom of a guest to lattice modes of the host and host-induced energy cascade within the guest. Vibrational energy relaxation and energy transfer among isolated molecules has been characterized for some time, and the general principles are relatively well-established.^{179,180} In this context, a new chapter has been added in the work of Dubost et al. on O₂/CO-doped matrixes in which vibrational relaxation, energy pooling via long-range energy transfer (now via induced quadrupoles), and vibrational up-pumping have been characterized.¹⁸¹ The recent theoretical analysis of vibrational energy relaxation, which has been specifically applied to O₂,^{182–185} is an important contribution toward exact treatments that explicitly consider the lattice acceptor modes in multiphonon relaxation. The impressive efficiency in up-pumping, via long-range vibrational pooling through induced dipoles, has been illustrated in NO where electronically excited states are reached and even molecular dissociation is affected by IR excitation using an F-center laser.^{186,187} It is also important to note that stimulated emission can be a very efficient channel for vibrational relaxation in cryogenic matrixes,¹⁸⁸ as recently demonstrated for matrix-isolated ozone¹⁸⁹ and earlier for CO isolated in crystalline N₂.¹⁹⁰

Detailed analysis of vibronic dynamics in electronically excited states of diatomics, such as N₂,^{191,192} CO,¹⁹³ and NO,^{194–196} have been given with a dissection of the contributions of internal nonadiabatic matrix elements of the molecule and the coupling between guest and host nuclear degrees of freedom. The theme that emerges from these studies is that where intersystem crossing is governed by spin–orbit coupling with significant matrix elements, the lattice modification of the matrix elements are small, and if internal Franck–Condon factors are large, these routes of energy flow are preferred. However, energy flow is dictated by energy gaps, which are determined by differential solvation of electronic states, and which are bridged by lattice phonons and, therefore, external Franck–Condon factors. The large variation in relevant Franck–Condon factors leads to a large spread in relaxation time constants, covering the range from seconds to picoseconds.

In contrast with the above-mentioned molecules, with characteristic vibrational spacings significantly larger than the Debye limit of the host, time-resolved measurements on picosecond and femtosecond time scales have been carried out in systems with smaller energy gaps. Detailed measurements using optical Kerr gating have been reported on the vibronic relaxation channels of the Xe⁺F[−](B_{1/2}, C_{3/2}) charge-transfer states in solid Ar.¹⁹⁷ Although the overall picture is complicated by site-dependent dynamics controlling population flow between these nested potentials, the sequential vibrational cascade shows relaxation times increasing from 1 ps to 1 ns with

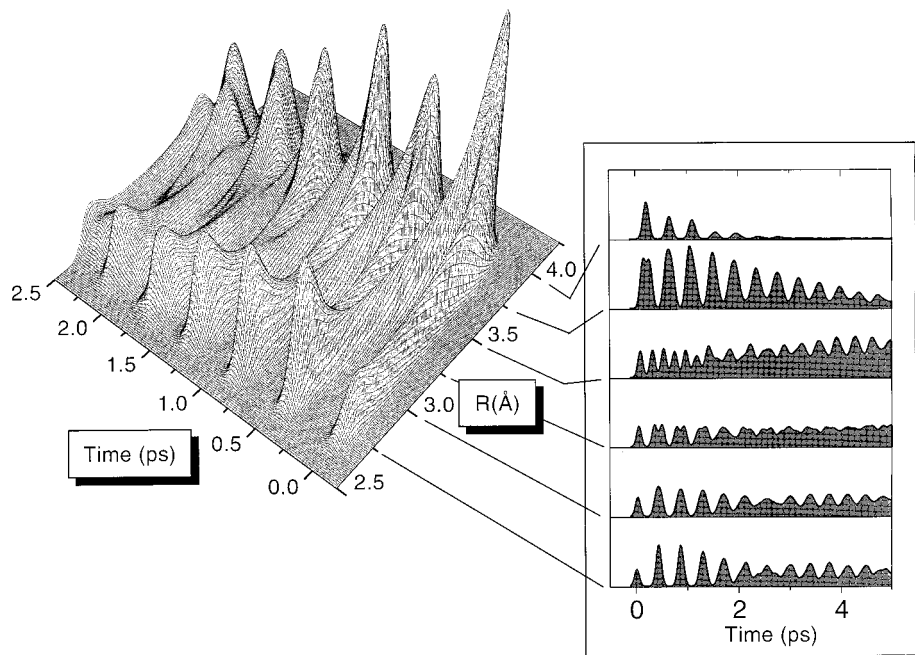


Figure 4. Time evolution of the density on the $I_2(B)$ state in solid Xe, constructed from a swarm of classical trajectories obtained from molecular dynamics simulations of a 500-atom cell. The initial conditions correspond to preparation with a 80 fs pump pulse, at 545 nm, and the observable signal for various probe windows is shown in the inset. Predissociation is not included in the reconstruction.

an increase in vibrational spacing of only 20%. Vibrational relaxation in matrix-isolated I_2 in both A^{123,198,199} and B^{99,200} states has been measured in femtosecond pump–probe studies and implicitly analyzed by reconstructing the signal from swarms of classical trajectories, as in Figure 4. The nearly exact reproduction of the observed signal through molecular dynamics simulations shows the adequacy of classical treatments of energy flow in such systems. In both the A and B states of I_2 , vibrational relaxation is completed on a time scale of ~ 10 ps, with a bimodal energy decay rate characteristic of Morse oscillators in condensed media.²⁰¹ When prepared in the anharmonic region near or above the dissociation limit of the Morse potential, impulsive energy loss in the first period of vibration (~ 1000 cm⁻¹ in one period) drops the molecule to the harmonic region, where exponential energy loss characteristic of creating a phonon per period takes over.⁹⁹ Note, an exponential energy decay from molecule to bath implies that the rate of energy transfer is proportional to the energy content in the molecule, a result that is generally valid for harmonic vibrations that are linearly coupled to the bath. Descriptions of molecule–cage motions during vibrational relaxation, in particular energy back-flow from the cage into the molecule, have been documented for different initial preparations, clearly depicting the molecular nature of the “bath”.^{199,200} Beyond determining relaxation times, femtosecond pump–probe experiments with chirped pulses have been used to characterize phase-space evolution (classical coherence) during vibrational relaxation within $I_2(B)$ in solid Kr²⁰² and in the elementary step of a wave packet bouncing off of the cage wall in $I_2(A)$.²⁰³ It has been shown that the system retains memory of the pump pulse coherence for as many as ~ 15 vibrational periods of the guest—a dramatic demonstration of the feasibility for coherent control

of molecular dynamics in condensed media. Also, it has been demonstrated that vibrational coherences survive in indirectly prepared states, such as after cage-induced recombination,^{123,198,199} and after electronic curve crossing.²⁰⁰ To date, fast relaxation processes were experimentally only probed in electronically excited states. Recently, free-electron lasers have provided a convenient route to probe vibrational relaxation in the ground electronic state on the picosecond time scales²⁰⁴ and has been applied to studies of molecular isomerization processes in RGS.^{205,206}

Rotational degrees of freedom of guest molecules can be generally expected to be arrested in matrixes and converted to small amplitude librational motion; however, in the case of small molecules such as hydrides and methyl groups, free rotation is observed. These general rules are evident in infrared absorption spectra.¹⁵⁹ A careful analysis of the effect of hindered rotations on IR line shapes has been given by Winn et al.,²⁰⁷ with implementations for matrix-isolated HF and OCS.^{208,209} More recently, rotationally unrelaxed emission in electronically excited states of CN have been observed in all matrixes.^{210,211} These studies are particularly notable in that they illustrate the role of the isotropy of potentials in classical solids where the cage symmetry is preserved. Despite the very strong directional binding of CN to Xe, the high symmetry of the cavity produces isotropic interaction potentials for CN isolated in neat Xe hosts and allows nearly free rotation. In contrast, when only one of the nearest neighbors to CN is Xe in an otherwise Ar lattice, rotation is completely arrested.²¹² A similar analysis of rovibrational lines and site symmetry was given earlier for the case on NH.^{213,214} It is also worth noting that in soft lattices, such as that of hydrogen, local distortion of the cage around the molecule may lead to blocking of rota-

tions, and now the molecule can reorient only by dragging or following the cage deformation.¹²⁵ These considerations are valid for thermally occupied rotational levels. In the case of photodissociation–recombination processes, highly excited rotational states can arise and rotational relaxation can serve as an important dissipation channel, as illustrated in the case study of HCl in matrix Ar.²¹⁵

III. Sample Preparation and Morphology

Sample preparation and characterization is one of the most tedious aspects of experiments. Usually, empirical recipes are followed, since the rigorous characterization tools such as X-ray or neutron scattering, which have been implemented, are seldom available to the photochemists. The classic methods applied by the matrix isolation community for deposition of a premixed gas sample on a cold window are well-established, and the merits of various approaches of pulsed deposition versus slow spray-on have been reviewed.²¹⁶ These have been devised with the main goals of optimizing isolation of a guest, and spectroscopic measures such as minimization of inhomogeneous contributions to observed line widths are used as measures of local order at the isolation site. Disorder on the scale of visible wavelengths, in the form of voids created between grains, is evidenced by the scattering appearance of films. In contrast, films deposited by a single pulse are usually transparent, indicative of dense packing on micrometer scales, similar to solids formed from the melt. In the case of spray-on deposition, higher temperatures favor dense packing²¹⁷ while lower temperatures are required to prevent clustering of the dopant.²¹⁸ Despite the years of experience in this field, there is room for improvement to meet the requirements for different applications. A few such developments are mentioned here.

Microchannel plate dosers have recently been employed for the preparation of high-quality films that show damage thresholds in excess of 300 W cm^{-2} in frequency tripling applications.^{219,220} Laser ablation coupled with microchannel plate deposition has been shown to produce high-quality samples with metal-atom dopants in studies of Ag-doped matrixes, including the notoriously difficult Xe host.¹⁷ The films prepared by this method are of sufficiently high quality to enable time-resolved studies, which are sensitive to light scattering. A systematic discussion of various sources for metal-atom deposition, from Knudson ovens to laser ablation, has been given^{78,79} along with theoretical analysis of structures and site-specific spectra.^{75,77} Among the important findings of this study was the remarkable difference in isolation sites of alkali atoms when deposited via laser ablation versus oven evaporation. The initial assignment of this difference to hot atoms has now been revised and demonstrated to originate from the ion content in the ablated pulses.²²¹ In the course of this work, a velocity selector for depositing alkali atoms with a much narrower kinetic energy distribution than that obtained by direct ablation has been developed.²²² Deposition from pulsed discharged supersonic nozzles

has been used to prepare high-quality films doped with radicals.²²³

Different solid morphologies are suited for different applications. In time-independent laser-induced fluorescence spectroscopy, scattering solids are preferred since multiple scattering in the film from grain boundaries effectively increases the radiation interaction length and yields a higher signal. The same effect also increases the residence time of photons in the solid, completely degrading the time response of ultrafast time-resolved studies. Thus, thermal cycling, which produces local annealing and is widely practiced in infrared studies, is deleterious to ultrafast measurements. For such applications, especially where the guest molecules may undergo efficient separation on walls during slow deposition and where thin transparent films are desirable, condensation of a single gas pulse is commonly used. Pulsed deposition has in the past been evaluated as a means for producing nonscattering solids with good isolation properties, and the quality of such solids is primarily attributed to self-annealing in the process of accommodating the latent heat of fusion of the gas pulse.

Local order may be sufficient for the study of many spectroscopic and dynamical processes. However, for processes such as migration of atoms and excitons which may entail length scales of micrometers,²²⁴ it is necessary to experiment in samples with long-range crystallinity. Near epitaxial growth in ultrahigh-vacuum chambers has been feasible to this end and implemented in sophisticated experiments involving carefully prepared multilayer sandwiches in which the transport of atoms from one layer to another is measured.²²⁵ Free-standing crystals (FSC), quickly grown by using latent heat annealing, can be prepared to have grain sizes in excess of 0.1 mm.^{226,227} The high optical quality of such crystals has been demonstrated by the construction of rare gas halide lasers in such solids.^{166,228} The method, however, suffers from a serious deficiency in that only commensurate guests can be isolated in a given host. Aggregation of guest molecules, due to their high mobility during condensation, is quite severe. While there may be much unpublished data on this issue, a few examples have been given in the literature. For example, it is trivial to isolate Cl₂ in any of the rare gases by vapor deposition techniques, yet it has been nearly impossible to do so in FSC Ar or Kr.²²⁹ At dilutions as high as 1:50000, although monomers can be clearly identified, dimers and clusters are the dominant species. Although it is less direct to interpret the Xe case, since the emission spectrum of the isolated molecule is already quite broad, it would seem that Cl₂ can be isolated there. The case is clearer for N₂O, which has been studied by infrared spectroscopy.²³⁰ In Ar, attempts to prepare free-standing crystals lead to segregation; in Kr, extensive dimerization is observed; in Xe monomers prevail. The dimer content of H₂S-doped Kr free-standing crystals can be reduced to ~1% by using dilutions of 1:20000, which is quite sufficient to carry out IR spectroscopic studies.²³¹ However, in photodissociation studies, the S₂ fluorescence from the dimer dissociation product causes a serious background

emission, such that the particular set of experiments were moved to thin films. F₂ and O₂ can be doped in free-standing crystals without difficulty and can be verified to be well isolated,^{19,232} but I₂ and ClF segregate even in Xe. The case of I₂ may be complicated by the fact that chromatography on the walls of the deposition lines causes partial separation between the guest and the host prior to condensation; however, even when heated lines are used, mainly I₂ dimers are observed, as verified by resonance Raman spectroscopy.²³³

Establishing the effect of the range of crystalline order on a particular dynamical observable is important. The comparative study on long-range migration of F atoms, which shows that the migration range of F atoms is an order of magnitude longer in FSC than in vapor-deposited films,²³⁴ and the demonstration of a large distribution in activation energies for thermal diffusion of O atoms trapped in Xe as compared to a single-rate process in FSC Xe⁶ are examples.

We should mention that there have been theoretical simulations dedicated to the study of condensation and matrix deposition.^{235–237} These are well-reviewed in the article by Haas.¹⁶⁹ The simulations should be interpreted with caution, since they suffer from the difficulty of mimicking heat transport at realistic cooling rates. Moreover, the simulations do not address structure on long scales. On the microscopic level of identifying trapping sites and structures, Monte Carlo simulations such as those of Fajardo may be as representative.⁷⁴ In this regard, Schurath's group has successfully modeled site-specific vibronic spectra and line shapes of NBr^{238,239} and NH/ND,^{213,214} the latter showing rotational structure and splittings that are quite sensitive to the local structure.

In addition to the standard matrix materials, which form classical inert solids upon condensation, doped quantum solids of H₂^{83,240–243} and He^{244,245} have recently become the subject of increased research. Isolation of atomic fragments in solid He is achieved by direct ablation in a pressurized cell. While in classical hosts such a process would destroy the solid, leaving behind a highly scattering trail, in solid He the lattice heals within minutes without leaving any damage marks. These quantum hosts provide fascinating media to explore the effects of collective dynamics, issues that will present a serious challenge to theory. A rather thorough review of the spectroscopy of atoms and molecules in liquid He, in particular in large He clusters, has recently appeared.²⁴⁶

IV. Photon-Induced Dissociation

Photon-induced dissociation of molecular impurities may be classified on the basis of the nature of the initial excitation into three distinct categories: (a) Direct excitation of molecular dissociative or predissociative states, which may be regarded as the import of a gas-phase single-molecule problem into the solid state. For this view to hold, the transition dipole involved in the dissociative absorption should be localized on the guest and at least near the Franck–Condon region the electronic surfaces should be subject to minor perturbation by the host. Reliance

on the lighter rare gases, with their larger band gaps, and on dissociative transitions in the visible or the near-UV spectral regions best approximate these requirements.

(b) Electronic excitation of the host, followed by excitonic transport and localization at guest sites, is a characteristically solid-state process. Whether the localization of the exciton will proceed via dissociative trapping or not will depend on the details of the guest–host excited electronic manifold, and examples of either outcome can be found. We hasten to note that direct access of the excitonic bands is not necessary for this process to be active. Due to dilution factors and large mobility of excitons, where pulsed lasers are used, multiphoton-accessed exciton-mediated dynamics may compete with single-photon direct excitation of the impurity. Two-photon and three-photon versions of this mechanism have been characterized in solid¹⁴ and liquid²⁴⁷ Kr.

(c) Excitation of guest–host intermolecular transitions, which in the gas phase would correspond to excitation of collision complexes, is a natural consideration in condensed media. Perhaps the best characterized in this family are harpoon reactions initiated by excitation to guest–host charge-transfer potentials.^{65,248,249} Optical access of intermolecular potentials can also occur among geminate guests, a dissected example being that of CO and O.²⁵⁰

Quite often the above distinctions are blurred, since electronically excited states of the guest molecule may be significantly modified by the matrix.²⁵¹ The quantitative understanding of these modifications, which we expand under the discussion of predissociation, remains a serious challenge.

An alternate classification of photon-induced dissociation is possible based on mechanistic considerations of the nuclear motions involved during cage exit. The cage, as viewed by an isolated molecule, consists of the shell of atoms immediately surrounding it. In classical solids, the shell structure is defined by the rest of the lattice and its integrity is maintained by the mutual contact among the constituent atoms or equivalently by the repulsive interatomic potential walls which prevent the collapse of the shell even if the cavity is empty. To a photofragment, the centers of the shell atoms represent infinite potential barriers while the contact seams between the shell atoms enclose areas where the cage exit barrier is of finite height. Areas where this potential barrier is smaller than the kinetic energy of the photofragment can be regarded as *cage windows*, while the rest of the shell represents the *cage wall*. In rare gas solids, cage windows exist only for the “smallest” of photofragments, where size is determined by the fragment–host internuclear potentials and even then the windows constitute a very small fraction of the shell area. With this picture in mind, see Figure 5, we may classify the exit dynamics mechanistically: (a) *Sudden exit* describes the exit of photofragments through cage windows, without significant deformation of the cage structure. The ingredients that make this a process of significant probability are a small effective radius of the fragment as compared to that of host atoms, little momentum transfer between the photof-

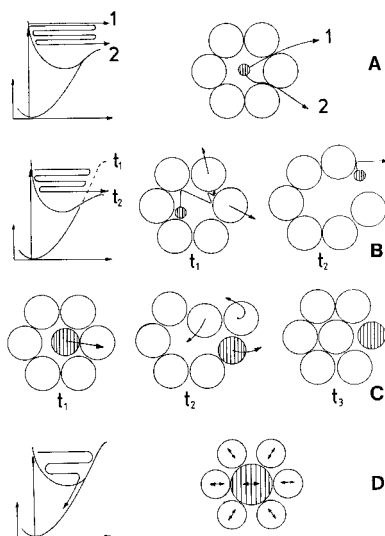


Figure 5. Schematic of barriers and trajectories of the escaping fragment (counter-fragment not shown) representing the classification of various cage exit mechanisms: (a) sudden exit for two initial orientations, (b) delayed exit due to the lowering of the barrier between t_1 and t_2 , through momentum transfer to the cage atoms and opening of a window, (c) forced exit by displacement of a lattice atom at t_2 , and subsequent rearrangement at t_3 with the net result of exchange in atomic positions, (d) perfect caging, recombination after vibrational excitation of the cage atoms.

ragment and host during cage exit (therefore $m_g/m_h \ll 1$), photofragments generated with high kinetic energy, and proper initial orientation of the photofragment momentum toward the cage window. Note, in cases where the mass asymmetry is large, e.g., H atoms in rare gas hosts, even if the projectile is not properly oriented initially, sudden exit in our sense can occur after multiple trials until the projectile is funneled toward the window and prior to losing enough energy to fall below the barrier.

(b) *Forced exit* describes a process in which the fragment possesses sufficient momentum to displace cage atoms. The net scrambling of positions of the photofragment and cage atom, which becomes permanent upon cooling of the site, leads effectively to cage exit. Note, such a rearrangement does not imply melting, since it is limited to only atoms involved in the direct impact of collision. This is a general process which should occur for all fragments provided the required kinetic energy of ~ 4 eV or more can be delivered.

(c) *Delayed exit* describes the process in which the photofragment opens its own windows through momentum transfer to the shell atoms and distortion of the cage structure. The fragment must transfer sufficient momentum to the shell atoms to widen the window or equivalently to lower the cage exit barrier while maintaining the requisite kinetic energy to pass through. This requires a delicate timing between collisions and correlation among atomic motions.

(d) *Perfect caging* is the rule rather than the exception in photodissociation studies in matrixes when standard light sources of $\hbar\omega = 6.5$ eV (ArF laser) is used. This occurs because for most photofragments the barrier heights for sudden cage exit are

larger than 2 eV and since molecular binding energies are typically on the order of 2–4 eV. Moreover, if the required excess energy for sudden exit could not be provided, for photofragments of mass comparable to that of the host, rapid momentum transfer and energy dissipation away from the isolation site will usually prevent delayed exit.

Let us note that where cage exit occurs, the mechanism will most likely not fall exclusively in any of the above classifications. Sudden, delayed, and forced exit mechanisms with different probabilities may coexist under any given set of conditions of a system and may need to be invoked to explain the observables. In time-independent studies, which constitute the majority of the work to date, the characterization of reagent and product trapping sites, the extent of separation of photofragments, and determination of probabilities of various dissociation channels as a function of excitation energy and thermodynamic variables (P, T) are the sought after quantities. Such thorough determinations have only been possible in very few systems. Generally, it is necessary to rely on complementary data from different sources to construct a complete picture. This practice should be exercised with caution since, especially in vapor-deposited matrixes, a great variation in sample morphologies is attained under presumably similar preparation conditions and many dynamical observables are sensitive to such variations.

V. Perfect Caging

A. Direct Observation of the Caging Process

It has been possible to follow the caging process directly, in real-time studies of I_2 isolated in thin films of Ar and Kr.^{123,198–200} In these pump–probe studies with a time resolution of ~ 100 fs, the molecule was excited on the repulsive wall of the $A(^3\Pi_{1u})$ state at excess energies of 1000–3000 cm⁻¹ and the subsequent dynamics of recombination was followed by laser-induced fluorescence via the ion-pair states which had previously been characterized in matrixes.^{252,253} The experiments were interpreted rather successfully by classical molecular dynamics simulations. These experiments rely on the creation of a wave packet by the pump pulse, and the short probe pulse along with fast dephasing of the states accessed in the ion-pair states allow a purely classical interpretation of the observables (see Figure 4). Due to the fact that the population coherence persists for many picoseconds, surviving extensive energy transfer to the lattice, the essential steps of the process—the initial wave packet, its collision with the cage, recoil, recombination and subsequent coherence during vibrational relaxation in the bound $I_2(A)$ state—could be followed. Given the detail in observables, extensive analysis is possible, and besides the original classical calculations on a single electronic surface, there are now semiclassical dynamics simulations using the full manifold of covalent electronic states correlating with $I(^2P) + I(^2P)^{95}$ and mixed quantum classical calculations.^{141,142} Among the notable findings are (a) The extent of coherence in the

population is dictated by the initial impact parameters of the collision of I₂ with the cage, which in turn is mainly dictated by the zero-point amplitude of atomic motions; (b) despite the fact that there are 10 electronic states that correlate with the atomic fragments, the process remains highly adiabatic, limited to the A/A' surfaces and without any detectable population leakage to the ground, X, state in Ar and Kr. Theory predicts that the process will be nonadiabatic in the case of Xe, marked by efficient transfer from A to X, due to the larger cage which allows the access of the crossing between these states.⁹⁵ (c) Frequency analysis of the transients allows direct observation of the excited cage motions that project back on the I–I coordinate. In addition to the Debye frequency of the lattice, which is always present, a low-frequency collective lattice mode is observed which corresponds to the initial driving period of the E_g cage mode. At higher excitation energies, the entire phonon spectrum of the lattice is reflected in the I–I oscillations.²⁰⁰ (d) Energy dissipation into the lattice is a highly nonlinear process, and the main impact of the collision with the cage is absorbed and dispersed very rapidly through the generation of shock waves.^{254–256} Nevertheless, significant energy remains localized on the cage, and the energy transferred back to the I–I coordinate is sufficient to drive the molecule above dissociation after its initial recombination.¹⁹⁹ (e) Finally, in addition to the atomistic descriptions, dynamics on a longer scale is probed by these experiments. For example, the recoil of the I atoms after pushing several layers into the solid is a result of the bulk elastic response of the solid. To maintain coherence in the recombination process, the recoil must be sudden, on a time scale shorter than the vibrational period in the bound potential. Sudden recoil, in turn, implies elasticity in the response of the driven cage. The comparisons between Ar and Kr show that the tighter the fit between molecule and trap site and the larger the mass asymmetry between guest and host atoms, the more elastic is the bulk response and therefore the more coherent is the vibrational motion in the reformed molecule.¹⁹⁹

These initial studies illustrate the level of detail that can be expected from ultrafast time-resolved studies, details that may force rigor in both development and applications of theory.

B. Stabilization of Fragments and Isomerization

The stabilization of fragments in the perfect cage has been exploited in a large variety of photochemical studies in matrixes. The prevention of separation between photofragments by the lattice can force contact between otherwise purely repulsive pairs, e.g., CH₃–I*²⁵⁷ and I*–I*,²⁵⁸ which relax radiatively. Perfect caging also makes dissociative pumping an effective method for preparing the full stack of electronically excited states that correlate with term states of open-shell photofragments and can be used to access states that are not optically allowed. As an example, near-UV excitation of O₂ in Ar and Kr matrixes populates all of the bound states that correlate with O(³P) + O(³P), including the meta-

stable a(¹Δ) and b(¹Σ) states which can be seen in emission and which could not be easily accessed by direct excitation due to the highly nonallowed nature of absorptions to these states from the molecular ground state.²⁵⁹ In fact, it is this recombinant emission that is most conveniently used to assess the efficiency of caging. The persistence of recombinant emission as a function of excitation fluence establishes upper bounds for photodissociation quantum yields. At excess energies (energy above dissociation limit of the free molecule) of <2 eV, the photodissociation quantum yields of ICl,^{260,261} Cl₂,²⁶² Br₂,^{263–265} and I₂²⁶⁶ are less than 10⁻⁷.²⁶⁷ This is typical of what is referred to as perfect caging. One should be forewarned though that matrixes are not perfect crystals and there will always be a population of the guest molecules in defect sites, in particular at grain boundaries, which may undergo facile photodissociation. With a sensitive probe, such as ESR or LIF, such products can be observed without a significant loss of the parent population. Experimentally, the obvious means of determining whether the observed photofragmentation is representative of the guest population is to drive the process to completion.

1. OCIO

When polyatomics are excited above dissociation, steric hindrance leads to the formation of cage-bound, unusual chemical isomers, which in the absence of the cage would be strictly transient. This principle is of course the basis of the utility of MIS for trapping and spectroscopic analysis of transient species. From the myriad of such examples, the photogeneration of Cl–O–O from O–Cl–O is an informative case, which due to its potential role in stratospheric ozone depletion has been the subject of extensive experimentation in the gas phase, in clusters, in the liquid phase, and in rare gas solids. Extensive references to work in other media are contained in the most recent studies in RGS by Lee et al.^{268,269} Closely related is the study on reversible photoisomerization between BrOBr and BrBrO.²⁷⁰ Besides the practical motivations, the OCIO system is informative because it illustrates site selectivity and mode specificity and serves as a model system for studying the modification of dynamics by the presence of the host. Both OCIO and its in-cage photodissociation product ClOO exist in numerous matrix sites.^{271–273} This had created some difficulty in accounting for all of the IR bands observed after UV irradiation of the parent molecule,²⁷⁴ although the assignment of the product to ClOO was definitive in the early works which involved photodissociation of isotopically labeled OCIO^{275,276} and contributions from dimers to form (ClO)₂ were known.²⁷⁷ The vibronic spectrum of OCIO Å(²A₂), which shows activity along all three molecular vibrations, remains well-resolved in matrixes and shows site splittings. This enables the study of site- and mode-specific photodynamics.²⁶⁸ In dilute samples, where the only observed dissociation product is ClOO, near-threshold excitation shows site-specificity with partial scrambling as the excess energy is increased. The observed scrambling hints at structural changes that are not strictly local, as evidenced by the observation that irradiation of a molecule causes site

conversion of a neighbor. The rate of photoinduced isomerization is observed to be 2–3 times faster in Ne than in Ar and Kr and is observed to be strongly enhanced when the asymmetric ν_3 mode is excited and less so when the bending ν_2 mode is excited. These results are well-rationalized using the detailed ab initio potential energy surfaces of the molecule, which clearly demonstrate that curve crossings via spin-orbit coupling between 2A_2 and 2A_1 and vibronic coupling to 2B_2 via the asymmetric stretch occur in near-threshold photodissociation.^{278,279} This, in the gas phase, can lead to mode-selective enhancement of branching between the ClO + O and Cl + O₂ channels. And although the observed mode selectivity in matrixes would indicate that the same predissociation channels are operative in the condensed phase, the final products are indistinguishable: the perfect caging decrees that the only observed final product is ClOO. At what stage does the matrix effect the dynamics? A direct clue is provided in OCIO, since vibrationally unrelaxed emission from the $\tilde{\Lambda}$ state is observed.²⁶⁹ The fluorescence yield is now determined by predissociation, which is much faster for ν_2 than for ν_1 , and no fluorescence is reported for excitation into the asymmetric ν_3 mode. These are consistent with the theoretical surfaces for the gas-phase molecule, although in Ar and Kr the $\tilde{\Lambda}$ state is significantly solvated and stabilized with respect to predissociation. In effect, and in particular in Ne, we may conclude that the initial dynamics of curve crossings and arrival to the transition state for dissociation seem to be controlled by the molecular electronic surfaces and the matrix effect, which controls the final products, sets in later. Note, this is in contradiction with recent resonant Raman studies of OCIO in cyclohexane, where it is concluded that solvation dramatically alters the initial dynamics.²⁸⁰ On the basis of comparison of absolute RR intensities with simulations using the gas-phase potentials, it is concluded that while the 2A_2 surface along the ν_1 and ν_2 coordinate is not effected, solvation (by 2000 cm⁻¹) dramatically changes structure, forcing C_{2v} geometry on the excited surface, and therefore enhancing the symmetric dissociation product of Cl + O₂.

2. ICN

To our knowledge, for well-isolated molecules, there has not been any documentation of photodissociation which proceeds via cage exit of molecular fragments. This point is well made by the experimental and theoretical analysis of matrix-isolated ICN. The photodissociation of ICN through its first absorption band has been well-characterized in the gas phase.²⁸¹ For our purposes, we note that in the free molecule dissociation is a direct process, though branching to yield both I and I* product channels occurs. Detailed ab initio potential energy surfaces now exist for both free ICN^{282,283} and for ICN in Ar.²⁸⁴ The photodissociation of the molecule has been simulated theoretically, with various levels of sophistication in the treatment of electronic degrees of freedom, in solid Ar^{101,285} as well as in liquid Ar^{284,286} and chloroform.²⁸⁷ The experimental studies of Haas et al. were designed to characterize the photodissociation process

in RGS.^{288–291} They use UV lasers to initiate dissociation and IR spectroscopy to analyze the final products. Though not all features in the IR spectra are interpreted, the conclusion that while ICN isomerizes to INC it does not undergo permanent dissociation, is robust. The earlier ESR reports of photodissociation of ICN should be ascribed to be limited to molecules at defect sites.²⁹² Note, in the liquid phase, the molecule dissociates and recombines on different time scales.²⁹³

Since the simulations are consistent with the experimental findings, let us consider the analysis of the trajectory data. Given the disparity of masses, CN receives the main component of momentum in the excitation, and the absence of dissociation may be entirely attributed to the failure of the CN radical to exit the cage. This result holds even when the simulation is carried out at an excess energy of 4 eV. This cannot be entirely attributed to CN–Rg potentials, since for the very comparable system of Cl–Rg, at similar excess energies, cage exit is observed.⁸⁶ Steric considerations do play a role. Within the classically allowed librational amplitudes, the suddenly generated CN projectile is aimed at “unfavorable” initial impact with the cage. Note, however, in the comparable case of Cl-atom exit in solid Ar, the mechanism involves displacement of a cage atom, which is not very sensitive to initial alignment. The more important considerations may be dynamical in nature. Upon collision with the cage, rotations and vibrations of the CN radical are excited, channels absent in the case of an atomic projectile. A rotating CN molecule is effectively larger than the nonrotor, but more importantly can be regarded as an effective shock absorber. In the simulations in solid Ar, at the end of the trajectory run of 3 ps, the CN fragment is observed to contain ~2.5 eV of internal vibrational energy.¹⁰¹ This is sufficient for the fragment to undergo ICN \leftrightarrow INC isomerization during vibrational relaxation, which can be expected to occur on millisecond time scales. With this consideration in mind and the recognition that MD simulations are inadequate for describing the relaxation of the high-frequency mode, it is difficult to compare the “hot” INC isomer yield of 70% in the simulation with that of the cold isomer yield of 2.6% measured experimentally.²⁹⁰

ICN constitutes a candidate for the investigation of cage-induced isomerization. The UV absorption is dominated by optical access to two electronic surfaces, the $^3\Pi_0^+$ and $^1\Pi_1$ surfaces which correlate with CN–I* and CN–I, in which the angular anisotropies of the CN radical are quite different. The branching ratio between ICN and INC depends on the partition between these surfaces and has very different dynamics. In the anisotropic potential, the fate of the orientation is sealed early on, since after one or two collisions the energy loss is sufficient for the radical to fall into one of its orientational minima. In contrast, in the isotropic potential, this fate will not be determined until complete relaxation. Such details are in principle accessible by real-time experimentation. Finally, as would be expected, theory predicts very different probabilities of photodissociation in the

liquid phase, and a comparison between liquid and solid state would be quite informative.

VI. Predissociation

Predissociation describes access of repulsive electronic surfaces via nonadiabatic transitions. After the curve-crossing occurs, the matrix effects operative in direct photodissociation are also applicable in this case. At issue here is how the matrix modifies the distinguishing step, namely, the nonadiabatic transition from bound to the repulsive states. This, for example, is the main matrix effect observed on the predissociation of OCLO in proceeding from Ne, which is gaslike, to Ar and Kr.^{268,269} The theoretical considerations of matrix effects on nonadiabatic transitions are of general relevance to the subject. We categorize the role of the host under two different mechanisms: (a) modification of off-diagonal coupling elements among electronic surfaces, (b) differential solvation of electronic states, leading to dramatically different dynamics between free and matrix-isolated molecule.

A. Electronic Caging by Solvent Symmetry

The predissociation of the $B(^3\Pi_{0u}^+)$ state of I_2 , which is crossed by six dissociative electronic states that correlate with the ground-state atoms,²⁹⁴ is a particularly useful test case for the investigation of the effect of the solvent on nonadiabaticity. The utility of this model system stems from the fact that in the free molecule predissociation is negligible, predissociation rates being smaller than radiative relaxation; yet upon collisions,^{295,296} complexation,²⁹⁷ or solvation,^{298–300} predissociation in the subpicosecond time scale is observed. With the advent of femtosecond sources, this solvent-induced predissociation has been extensively investigated in real-time, in small³⁰¹ and large van der Waals complexes,³⁰² in high-pressure gas,³⁰³ in the liquid phase,^{100,304} and in rare gas matrixes.^{99,200} An even shorter time scale glimpse of dynamics is provided by resonant Raman spectra, which were obtained in liquid Xe and CCl_4 ^{146,305,306} and compared with the earlier matrix spectra^{143,144} to discern the possible role of predissociation on the observed nonmonotonic decay of intensities in the RR progressions. Explicit simulations of the matrix spectra indicate that the structure is mainly due to quantum interference between scattering from the B and B'' surfaces which are simultaneously prepared.¹⁵⁰ The comparison between predissociation of $I_2(B)$ in simple liquids and in rare gas matrixes is quite illuminating, more so because the state-of-the-art in theoretical analysis of this condensed-phase nonadiabatic process has been implemented for rare gas liquids^{96,307,308} and solids.⁹⁵

Using time-resolved circular dichroism measurements, $I_2(B)$ is observed to predissociate coherently, with a half-life of 230 fs in *n*-hexane.³⁰⁴ Moreover, based on the appearance time of the transient at different probe wavelengths, among the various electronic surfaces, the process is assigned to the crossing with the $a(1_g)$ state. The same conclusions are reached in pump–probe studies in CCl_4 ,¹⁰⁰ establishing that ~60% of the population predissociates

per period independent of the initial vibrational state prepared and that the main crossing occurs near the bottom of the potential at $3.05 \text{ \AA} < R < 3.8 \text{ \AA}$, consistent with the $a(1_g)$ crossing. That polarizable collision partners should predominantly induce the $B(0_u) - a(1_g)$ nonadiabatic coupling is expected since to first order the perturbation in such interactions is electrostatic with a dipolar leading term.³⁰⁹ Indeed, focusing on this transition dipole–induced dipole coupling, the liquid-phase data were reproduced and the strong dependence of the process on local solvent density due to the R^{-6} dependence of the coupling efficiency were noted.³⁰⁸ While the local density of perturbers in the solid state is increased nearly 2-fold, the predissociation of $I_2(B)$ in rare gas solids proceeds on a time scale of 5 ps, namely, a factor of 20 slower than in the liquid phase.⁹⁹ This is consistently explained by noting that since the V_{B-a} coupling matrix element must have odd inversion symmetry, summation over perturbers arranged in cubic symmetry, as in a rare gas lattice, will lead to cancellation of the coupling.¹⁰⁰ Accordingly, predissociation occurs only through dynamic asymmetric distortions of the local solvent cage, a consideration that also explains the fact that the larger the vibrational amplitude of the molecule, a stronger effective coupling between potential energy surfaces is observed. The liquid- and solid-state data can be quantitatively rationalized within this model using Landau–Zener probabilities and the off-diagonal coupling surface obtained from the DIM Hamiltonian of Batista and Coker.⁹⁵ Somewhat surprisingly, the more rigorous simulations by the latter group does not reproduce this effect, overestimating solid-state predissociation probabilities by an order of magnitude.⁹⁵ Moreover, they observe efficient predissociation via a variety of crossings, some of which are predicted to be strictly many-body in nature. In principle, even if weaker, the different channels can be verified experimentally by preparing wave packets near the crossing points. However, Franck–Condon factors limit the accessibility of such configurations, and to-date the solid-state measurements are limited to B state energies far from the crossings.

The observed symmetry-induced caging of the electronic predissociation should be a phenomenon of some generality. In cases where the off-diagonal coupling between electronic states is due to a dipolar perturbation, cancellation is to be expected in sites of high symmetry. Electronic couplings induced or modulated by collective cage coordinates are predicted in treatments of nonadiabatic processes that explicitly consider vibronic interactions, such as is afforded through the DIM Hamiltonian.⁹⁴ Quite generally, where the coupling between surfaces is via spin–orbit coupling, then the matrix perturbations are rather small. Yet differential solvation can occur in such manifolds, leading to significant differences between gas and condensed phases.

B. Differential Solvation

Qualitative predictions regarding differential solvation can be made by recognizing generalizations based on the generic character of electronic states as valence, Rydberg, or ionic (charge transfer).²⁵¹

In valence to valence transitions the spatial extension of the outer wing of the electronic wave function, which governs the guest-host interaction, changes only weakly. The observation that zero-phonon lines with well-resolved phonon sidebands accompany such transitions is a direct indication of the similarity in molecule–lattice interactions in initial and final states and that little rearrangement of the lattice is induced by the excitation. The direct connection between spectroscopy and dynamics in such transitions has been made through explicit simulations of quantum correlations.¹⁵¹ Energy shifts associated with such transitions are small, of the order of a few tenths of an electronvolt, and usually to the red.

Valence to Rydberg transitions shift considerably to the blue due to the repulsion of the more extended Rydberg orbital by the cage-atom electrons. The shift increases with the increase in tightness of the cage, from Xe to Ne, and may exceed 1 eV, and the lattice rearrangements cause a broad convolution of phonon sidebands. A detailed case study of differential shifts involved in valence to valence and valence to Rydberg transitions is provided in the spectroscopic studies of NO,¹⁹⁵ along with a scrutiny of the perturbations and deperturbations.^{196,310–312} The connection between spectroscopy and dynamics in this system is most directly made through direct time-resolved measurements in both rare gas solids^{313,314} and in solid hydrogen.³¹⁵ These measurements should allow a detailed description of the nuclear motions, information which is buried in the structureless spectral profiles, which may be retrieved through the interplay of time-resolved experiments with simulations.³¹⁶ In a very recent work, the hitherto unknown 193 nm induced photodissociation of NO in Ar, Kr, and Xe was reported.³¹⁷ This observation adds incentive for scrutiny of the electronic–nuclear coupled dynamics in this model system.

Valence to ionic state transitions shift to the red by several tenths to an electronvolt, due to the solvation of the ionic state through induction forces which scale with the polarizability of the matrix. Numerous studies have documented this effect.^{72,248,318–320} Semiquantitative treatments, such as the Onsager cavity model, while useful, remain limited by ambiguities, such as the definition of cavity radius. More rigorous treatments rely on self-consistent expansions of electrostatic interactions, including induced multipoles, and are relatively successful where implemented.^{65,72,200}

The largest differential shifts are to be expected between ionic and Rydberg states. In dense electronic manifolds, the potential surfaces become rather complex due to multiple crossings of Rydberg and intramolecular ionic states, leading to double minima and changing state character with internuclear separation. The dramatic changes on the order of electronvolts for energies of curve crossings, their spatial locations, the resulting deperturbations, and the changing sequence of the character of states were exemplified for the Rydberg progression and several ionic states in the case of F₂ in Ne.³²¹ For Cl₂ and its lowest ionic states, a similar study was carried out earlier with buffer gas pressure rising up to solid Ar

and Ne matrixes.^{322–324} For both molecules a high propensity for predissociation results from these matrix effects,³²¹ a result that has been exploited in the forced cage exit study of Cl₂ in Ar.³²⁴ In addition to the intramolecular ionic states, intermolecular charge-transfer states of the type X₂[−]Rg⁺ arise in matrixes for which transition energies scale with the rare gas ionization energy and the halogen electron affinity. For Cl₂, for example, the transition energy varies from 6.88 to 8 to 10.3 eV in going from Xe to Kr to Ar matrix.³²⁵ Thus, especially in Xe, a completely new route for photodissociation via intermolecular charge-transfer surfaces becomes available, a mechanism which has been extensively discussed under the heading of harpooning.²⁴⁸ Solvation effects also contribute to repulsive surfaces and therefore can have a profound effect on dissociation dynamics. This has been illustrated experimentally for HCl in Xe, Kr, and Ar³²⁶ and verified through calculation.⁹⁴ Differential solvation can occur along one surface, as in the case of H₂O where the Rydberg character increases with the H–OH elongation.^{311,327}

While the above represent examples in which predissociation channels are enhanced by differential solvation, the opposite, namely, suppression of predissociation, can also occur as exemplified in the case of SH.³²⁸ In SH(A), which correlates with S(^1D) + H, the vibrationally relaxed state is known to predissociate in the free radical on a time scale of 10^{−9}s.³²⁹ The A state is crossed by several repulsive potentials which correlate with S(^3P) + H, among which a(^4Σ[−]) is the main predissociation channel.³³⁰ A rather thorough analysis of the predissociation in the gas-phase radical was recently developed.³³¹ In RGS, the vibrationally relaxed SH(A) decays radiatively with a lifetime of ~700 ns.³²⁸ On the basis of the consideration of the diatomic fragment interactions, S(^1D)–Rg and S(^3P)–Rg, it is possible to rationalize that the A state will have an attractive interaction with the lattice while states that correlate with the ground state will have a repulsive interaction. Using qualitative curves, it has been possible to explain the absence of predissociation in matrix-isolated SH(A) and to fit the excitation and emission profiles, with the prediction that the same should happen in SH:Rg 1:1 complexes.³²⁸ In essence, relaxation along the SH–Rg coordinate in the excited state lowers the electronic A surface below the crossing, permanently shutting down the predissociation channel. A similar stabilization is active for OH.³³² This dramatic caging effect was verified for the SH–Ar complex,³³³ and through the analysis of high-resolution spectra,³³⁴ empirical potentials that embody the relevant physics³³⁵ have been extracted.³³⁶ In the more recent studies of H₂S dissociation in matrixes, the spectroscopy of SH in Ne through Xe has been reanalyzed, drawing parallels between OH and SH.³³⁷ This combined UV–IR study illustrates the interplay between charge-transfer and covalent interactions between guest and host. Quite notable are the observations of the spin–orbit split states of SH(X) in Ne and the observation of the insertion product HXeSH in Xe. The latter observation would clearly suggest that in Xe the photodissociation of H₂S will

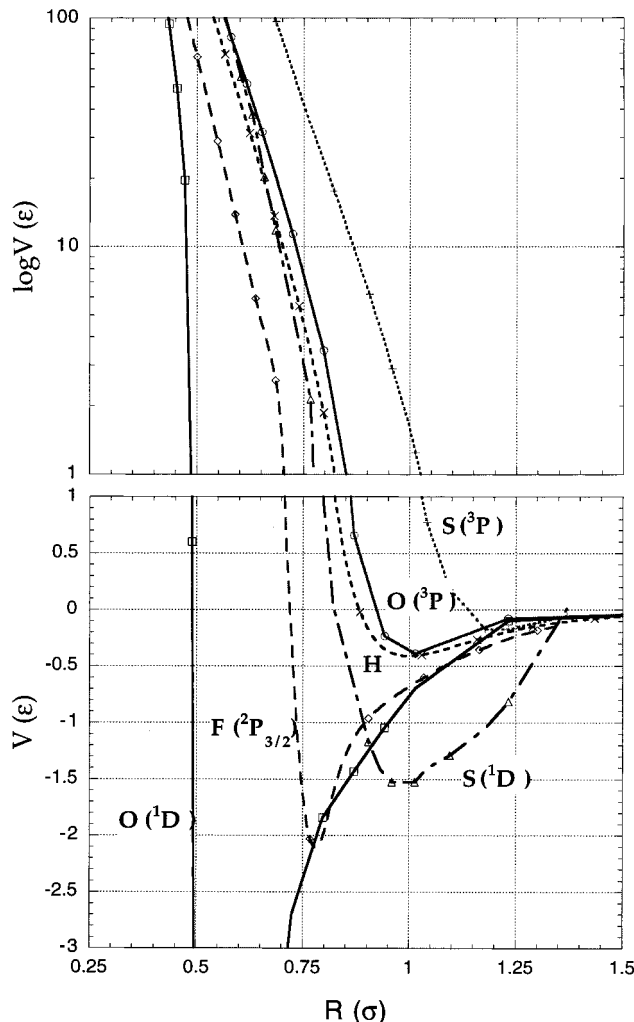


Figure 6. The sizes of atoms, as discerned from pair potentials with Kr, scaled to the Kr–Kr Lennard–Jones parameters. The lowest energy surface from each of the spin–orbit terms is shown, and the curves are shifted to have a common dissociation limit at zero. The diatomic states corresponding to the various atomic terms are $RgX(^3\Pi)$ for $X = O(^3P)$ and $S(^3P)$, $RgX(^1\Sigma^+)$ for $X = O(^1D)$, $S(^1D)$, and $H(^1S_0)$, $RgX(I_{1/2})$ for $X = F(^2P)$.

have a significant contribution from photoinduced harpooning. Further, the analysis suggests a reassignment of the emission band origin in Kr, although, the suggestion is not wholly satisfactory.³³⁷

VII. Dissociation through Sudden Cage Exit

Sudden cage exit was defined as the ejection of a photofragment through open windows without significant cage distortion in the process. The process is reserved to the smallest atomic photofragments, most notably to $O(^1D)$, $F(^2P)$, $S(^1D)$, and $H(^2S)$, atoms for which long-range migration is also relevant. As a measure of the sizes of these atoms, their pair potentials with Kr, $KrO(^1\Sigma^+)$,^{338,339} $KrF(I_{1/2})$,^{340–342} $KrS(^1\Sigma^+)$,³⁴³ and KrH^{48} are shown in Figure 6. The incipient bonding character of $O(^1D)$, $F(^2P)$, and $S(^1D)$ with rare gases is evidenced by the deep potential minima that arise at internuclear distances that are significantly shorter than what would be predicted based on van der Waals radii. In all three cases this arises from partial charge transfer or equivalently

due to the admixture of the Rg^+X^- character in these surfaces. Accordingly, these potentials are further solvated in the solid state, as demonstrated spectroscopically for $XeO(^1\Sigma^+)$ ^{13,344} and XeF .^{320,345} After cautioning that these potentials are not pairwise additive, we remark that where thermal processes are involved, the potential minima are of relevance and that where kinetically hot atoms are involved, the repulsive walls determine size. In either case, $O(^1D)$, $F(^2P_{3/2})$, and $S(^1D)$ are significantly smaller than H atoms, which when cold is comparable in size to Kr. For further insight in the description of binding in xenon and krypton halides, we refer to the most recent high-level ab initio calculations.^{346,347}

The cage window, i.e., the potential barrier along the minimum energy path, is the dividing surface between the initial isolation site and the final trapping site that must be reached for successful permanent dissociation (see Figure 2). In perfect solids, the closest new such site corresponds to the interstitial octahedral cavity. What constitutes a *window* or a *wall* to enter the octahedron depends on the guest and host. In the case of H atoms, where the guest–host interaction is isotropic and repulsive, the window corresponds to the center of the face of the octahedron or the center of any three mutual nearest neighbors where electron–electron repulsion between H and Rg is minimized.⁵² For halogen atoms, the window corresponds to insertion between a pair of nearest neighbors (see Figure 2).⁸⁷ This orientation maximizes attractive Σ interactions and minimizes electron–electron repulsion by limiting the Π interaction to the more distant host atom at the apex of the triangle. This path will be taken if the F atom moves slowly enough to adiabatically follow the lattice motions. If, on the other hand, a sudden collision were to bring the p-hole pointing at the octahedron face, then the minimum pass would be the window for repulsive interactions, the path that minimizes contact pairs and therefore the center of the three atom face (see contours in Figure 2). The minimum energy path is the insertion between a pair of host atoms in the case of $O(^1D)$ atoms as well.¹¹ Direct cage exit through undistorted cage windows is already prohibitive in the case of Cl atoms.⁸⁷ The more massive Cl atoms exit after distorting the cage, nevertheless the discussion regarding relative orbital orientations remains valid.⁹² In all cases of attractive windows of insertion, it can be expected that charge-transfer contributions will play a role to further minimize the cage exit barrier. While this consideration has been noted, it has not been implemented in simulations. Nevertheless, it is possible to generalize that the direct cage exit will be limited to “small” atoms, where small implies host–guest potentials that are attractive at short range. H atoms are unique in this regard, since at the internuclear distances of relevance their interactions with the lattice are strictly repulsive. Indeed, as we will expand on in the next section, the sudden channel for cage exit of H atoms opens at excess energies above 1.7 eV and the delayed exit mechanism dominates at lower energies.

A. F(²P)

The most convincing demonstration of direct exit is based on orientation dependence. This has been experimentally demonstrated for F and O(¹D). In the first case, an anomalous temperature dependence of dissociation probabilities of F₂ was demonstrated, whereby the probability increases at 4.5 K to above what is observed at 12 K.³⁴⁸ This dependence was predicted in simulations.^{349,350} At 12 K, the molecule is a free rotor; therefore, photodissociation is initiated isotropically, with initial F-atom momenta pointing with unbiased probability toward windows and walls of the cage. At 4.5 K, the molecule orients with its axis pointing toward windows, thus enhancing its sudden exit probability. Good agreement is found between experiment and simulations of photodissociation of F₂ as a function of excess energy.³⁵⁰

B. O(¹D)

The case of O(¹D) is established from studies of ozone in solid Ar, where a thermally activated photodissociation quantum yield is observed.³⁵¹ In the measured temperature range of 10–35 K, the quantum yield increases by a factor of ~20 to reach a probability of ~15%. Since the thermal energy is insignificant in comparison to the excess energy at 266 nm, the thermal activation must entirely be ascribed to population of the molecular librational coordinate, i.e., to thermally induced molecule–lattice reorientations. The data can be rationalized under the assumption that at low temperature the molecule points at the cage wall while at high temperatures it has sufficient librational amplitude to access cage windows. As dramatic a demonstration of the effect of relative molecule–lattice alignment on photodissociation is provided in studies of O₃ in matrix and FSC Xe, where it is observed that of the two main sites of isolation, one leads to complete caging while the other can be driven to complete dissociation.⁷ The two main sites of isolation of O₃ have been analyzed experimentally³⁵² and theoretically³⁵³ to be the singly substituted and doubly substituted sites, as in the case of CO₂.³⁵⁴ Evidently, for O₃ in the first site, the direct exit path is blocked, leading to efficient recombination. However, proper molecule–cage alignment can lead to dissociation, which has to be sudden to compete with recombination.

In the reactive hosts of O₂^{355–357} and N₂,³⁵⁸ the photodissociation of ozone and its subsequent thermal and photoinduced nonadiabatic dynamics presents a fascinating subject. Very efficient photodissociation of O₃, with a temperature-independent quantum yield of ~0.7, is observed in solid N₂ and interpreted as direct cage exit of O(¹D). It is estimated that the atom undergoes some 10 collisions before switching to the triplet surface.³⁵⁸ The observed decay of the O₃ concentration is bimodal, and only the slow decay was analyzed in this study. With very similar data and a careful analysis of the IR absorption profiles of N₂O formed during dissociation of O₃ and upon thermal cycling of the solids, a different interpretation is reached, namely, the primary channel

of photodissociation is the reaction of O(¹D) with the cage wall to form in-cage N₂O–O₂ pairs, which can subsequently be optically excited to yield either cage exit of O atoms or recombination.³⁵⁹ In solid oxygen, the identification of the final products of dissociation, O atoms and O–O₃ complexes,³⁵⁵ is the subject of fascination and controversy.³⁵⁷

C. S(¹D)

The experimental evidence for direct cage exit of S(¹D) atoms is circumstantial. In photodissociation studies of H₂S with an initial excitation leading to the SH + H coordinate, in addition to cage exit of H, a small channel leading to cage exit of S atoms is observed.^{35,328} Characteristically, the photogenerated S atoms are found in thermally unstable interstitial sites. An indirect mechanism between H atoms that fail to undergo sudden cage exit and parent fragment, SH + H → S + H₂, is responsible for this channel. The energetics of the system force the conclusion that the exiting atom must be S(¹D) and must exit prior to momentum transfer to the cage. Similarly, in photodissociation studies of OCS, facile dissociation to generate isolated S atoms is observed.³⁶⁰ These observations are used to infer that the cage exit of S atoms is quite facile, and according to Figure 6, that would only be consistent with S(¹D). We should note that in the more recent study of H₂S photodissociation, the S + H₂ channel was not detected, neither were they able to observe interstitial S atoms.³³⁷ The latter observation would suggest that the differences are due to lattice morphology, resulting from different sample preparation methods: pulsed versus slow spray. This system should then afford the opportunity for more detailed investigations of structural control of local dynamics.

VIII. Delayed versus Sudden Exit

Judging from pair potentials alone, it can be easily concluded that H atoms are effectively larger than either F or O(¹D). Accordingly, cage exit of H atoms is expected to be less facile. In simulations of photodissociation of hydrogen halides, both direct and delayed exit of H atoms after significant rattling in the original cage of isolation is observed. The same systems have been difficult to study experimentally. However, systematic experimental studies on the triatomics, H₂O and H₂S, have been carried out. A picture consistent with the simulations has been inferred from rather detailed statistical analyses of the experimental data. A somewhat different picture emerges in the case of Cl₂ in Xe, as discussed below.

A. HI, HCl

The description of permanent bond breaking in HI and HCl is mainly controlled by the cage exit dynamics of the H atom. Given the existence of reliable H–Rg potentials and its isotropic nature, the system is amenable to simulations on Born–Oppenheimer surfaces and constitutes perhaps the best case for the assumption of pairwise additivity of interactions. In fact, theoretical modeling is now most advanced in the treatment of H-atom cage exit. It has evolved

from the first classical MD simulations⁹¹ to the wave packet treatment of the H atoms¹³⁷ to semiclassical simulations that include nonadiabatic transitions^{93,94} and a quantum mechanical description of rotations of the parent molecule.¹³⁵

The photodissociation of HI in solid Xe was the first system singled out for scrutiny for several reasons.^{91,134,361} The fact that its first dissociative absorption continuum lies in the near-UV makes it amenable for experimentation with conventional lasers. Given the similarity of Xe–I and Xe–Xe pair potentials and the negligible anisotropy of HI–Xe potentials, it was recognized that high-quality inclusion crystals could be grown from the melt.³⁶² Finally, the similarity of I and Xe masses and the very large mass asymmetry between them and H would ensure the dynamics to be dictated by the H-atom motion. Simulations meet these expectations. They revealed that due to the poor momentum transfer between H and lattice, the fragment undergoes nearly elastic collisions and loses its kinetic energy after hundreds of collisions. The H–Xe potential used was sufficiently repulsive to not allow direct cage exit but rather a delayed exit which occurs over a reduced barrier caused by the opening of a passage after the cage atoms are set in a sluggish motion by the cumulative energy loss of photofragments.⁹¹ These simulations were followed by a mixed quantum-classical treatment of the H atom as a wave packet, while all other coordinates are propagated classically.¹³⁴ The simulations revealed that the delayed exit results in persistent recursions in the H wave packet motion. The first experiments were conducted in inclusion crystals grown from liquid HI/Xe solutions.³⁶² The utility of these single-crystal solids was limited to a narrow range of temperatures, due to cracking upon cooling below 100 K. The experiments were subsequently carried out in FSC Xe.⁷³ Despite extensive efforts, little systematic information in the dissociation process itself could be extracted, mainly because of interferences from ionic channels that could not be fully understood. UV excitation of these solids leads to access of delocalized charge-transfer states, such as $\text{Xe}_n^+ \text{I}^-$ and $\text{Xe}_n^+ \text{H}^-$, which in turn lead to charge separation and trapping, creating ionic centers such as Xe_2H^+ .^{65,249} While these were anticipated, it has now become clear that the localized charge-transfer state, $(\text{HXe})^+\text{I}^-$, is the lowest energy configuration of the system and can be directly formed from the neutral ground-state atoms in the absence of UV radiation.¹⁰⁶ Notwithstanding the experimental evidence for the important role played by ionic surfaces, theoretical modeling of this and related systems remains limited to neutral interactions.

The HCl/Xe system has been the focus of semiclassical treatments, including nonadiabatic dynamics. The first such study focused on nonadiabatic transitions among the three repulsive surfaces of HCl in Xe (neglecting spin–orbit interaction) and their role on recombination in the ground state.⁹² The study established the time scales for nonadiabatic transitions to be in the subpicosecond and picosecond range. For kinetic energies ~ 1 eV below the static

barrier, they predicted a contribution due to delayed exit with a quantum efficiency on the order of 0.01. Sudden exit was predicted to occur at excess energies above the exit barrier, with efficiencies increasing to 60% at excess energies of 4 eV. The simulations also show a high probability for cage re-entry at these high energies. The treatment was further advanced in the case of HCl in solid Ar to now include spin–orbit splittings and nonadiabatic dynamics among the full stack of states and for photodissociation at an excess energy of 2.5 eV.⁹⁴ Once more, redistribution in the manifold of electronic states on a sub-picosecond time scale is predicted. Fast recombination events within 200 fs and delayed recombination events on a picosecond time scale with extensive rattling and heating of the lattice are observed. The fate of exit versus recombination is determined after 2 ps, and a cage exit probability of about 50% is predicted.

Experiments on this system delivered quantum efficiencies for HCl dissociation in Xe, Kr, and Ar matrixes by using synchrotron radiation in the spectral range from 6 to 10 eV.³²⁶ The absolute value for Ar matrixes varies between 20% and 40% for kinetic energies between 2 and 4 eV. The observed quantum yield of 40% at 2.5 eV is in reasonable agreement with the calculation. In Xe matrixes, a systematic comparison of the energy dependence in the range from 1 to 4 eV was attempted. Between 1.4 and 2.4 eV, convincing agreement with simulations is obtained. Below 1.4 eV, due to the small absorption coefficient, the experiment is inconclusive with regard to the predicted contribution of delayed exit. Above 2.4 eV, saturation of the process at a quantum yield of 40% is observed. This is in contradiction with the simulations which predict a further increase in dissociation efficiency. Deviations from a classical behavior of the nuclear motions are to be expected to be most severe for H atoms, as already pointed out in the mixed quantum–classical simulations of HI, since both zero-point energy and tunneling may play a role.³⁶¹ These considerations have inspired the quantum mechanical treatment of the initial rotational degrees of freedom of HCl/DCl in Ar and the wave packet motion of the H atom on the dissociative surface, albeit in a rigid lattice (see Figure 3).¹³⁵ While the orientational distribution in $J=0$ is isotropic, preferential orientation in the $\langle 100 \rangle$, $\langle 110 \rangle$, and $\langle 111 \rangle$ directions is predicted for $J=1$ and the sublevels of $J=2$ and 3 are split by the crystal field. The H-atom wave packet splits up in the course of dissociation when it approaches the shell of nearest Ar neighbors into escaping and returning oscillatory parts. The probability for cage exit within 15 fs strongly depends on the correlation between the initial angular distribution of the packet and the cage geometry and thus on the initial J sublevel. The angular correlations are smeared out after several periods, on the time scale of ~ 150 fs. These new developments in modeling present a challenge for future real-time experimental investigations of cage exit.

B. H₂O, D₂O

Experimental rigor on the photodissociation of hydrides was first provided by a series of systematic studies on H₂O/D₂O in Ar, Kr, and Xe matrixes as a function of excess energy from 1.4 to 3 eV and as a function of temperature.^{52,55,363,364} The energy dependence of quantum yields, in particular the observation of a sharp threshold as a function of excess energy, was taken to indicate sudden cage exit of H, in apparent contradiction with the delayed exit scenario suggested by the HI/Xe simulations. This thesis was supported by presenting a qualitative statistical prediction for sudden exit dynamics near the threshold of a sharp barrier to dissociation, in the form of a quadratic power law for quantum yields. The model was in acceptable agreement with experiments,³⁶³ and the threshold behavior was confirmed in later studies in Ne.³⁶⁵ However, with a careful analysis of the first absorption continuum, it is now established that in Ne, Ar, and Kr, the observed photodissociation threshold of 1.7 eV is not dynamical in origin but rather determined by the threshold of absorption to the repulsive Å state. There remains a difference of 0.2 eV between photodissociation and absorption threshold in Xe, where the absorption threshold is red-shifted by 0.5 eV relative to the gas phase. The latter observation is explained by attributing charge-transfer character to the repulsive H₂O(Å) state in Xe,³²⁷ energetics which has been quantified in some detail in the analogous system of the linear HCl–Xe complex.³⁶⁶ This consideration changes the premises of the kinematics assumed in the experimental design and in the analyses through simulations. A likely outcome of accessing the charge-transfer potential is the formation of HOXeH, the analogue of the recently identified HSXeH.³³⁷ The framework of mixed quantum–classical calculations has been applied to H₂O in Ar.³⁶⁷ The threshold behavior was well-reproduced, indicating a rising contribution of sudden exit with energy. The delayed exit contribution, which appears mainly below the exit barrier, has a low quantum efficiency and escaped experimental scrutiny due to weak absorption and therefore limited detection efficiency. This treatment failed to reproduce the pronounced isotope and temperature effects. In an early statistical model³⁶³ the isotope effect was explained by a cooling rate increasing with the mass ratio of H (or D) to matrix atoms, and local heating was invoked to explain the temperature dependence.³⁶⁸ The latter picture was later questioned, in view of the efficient cooling that can be expected through the generation of shock waves.²⁵⁴

C. H₂S, D₂S

While H₂O has the advantage that dissociation proceeds presumably on one repulsive electronic surface, the investigations on H₂S in Ar and Kr, where two distinct channels of permanent dissociation—SH + H and S + H₂—coexist, allowed a more detailed analysis. The experiments were analyzed through a more refined statistical theory³⁵ to clearly extract the contributions of sudden and delayed exit in the photodissociation process. For

both matrixes quantum efficiencies were determined from the flux required to drive the reaction to completion. The branching ratio of the channels was measured directly in Kr by further dissociating the SH photoproduct through two-photon access of charge-transfer states, which have recently been analyzed through ab initio calculations and show that S⁻H⁺ and S⁺H⁻ states are closely nested.³⁴³ The essentially constant S + H₂ contribution, which is not observed in the more recent study,³³⁷ could be subtracted from the overall yield in Ar. The study provided absolute values for H-atom cage exit probabilities, for excess energies of 1–3 eV. The lower limit of photodissociation is limited by the absorption threshold, and a significant quantum yield of 2% to 4% is observed for excess energies between 1 and 1.7 eV, indicating that cage exit occurs below the potential barrier in the undistorted cage. This clear evidence for delayed exit is in good accord with the early MD simulations of HI in Xe⁹¹ and with the mixed quantum–classical calculations for HCl in Xe and H₂O in Ar.^{92,93} Above an excess energy of 1.7 eV, a significant rise in dissociation probabilities (15% around 2.5 eV) is observed and attributed to the opening of the sudden exit channel on the basis of the statistical model.³⁵

The statistical model considers a substitutionally trapped parent molecule with cage exit windows located in the center of the triangular faces formed by mutual nearest-neighbor cage atoms. The probability for cage exit is related to the area within the triangle for which the excess energy lies above the local barrier height. The fractional energy loss in an unsuccessful exit attempt is given by the mass ratio, and the probabilities for a sequence of attempts is obtained as a sum over scattering events that drop the energy of the H atom below the barrier. As a major improvement in this model, instead of a static barrier fixed by the equilibrium structure of the lattice, barrier height distributions arising from both zero-point and thermal fluctuations are considered and the initial molecule–cage orientations are explicitly included. The model is useful in the quantitative analysis of sudden dissociation, in terms of the dependence of probabilities on excess energy, temperature, and isotopic substitution. It has been convincingly applied to the data on H₂S/D₂S to extract contributions from sudden exit and to identify the contributions from delayed exit. The derived picture is equally valid for the prior studies on H₂O and HCl. Deviations from the treatment, such as the saturation effect observed in the case of HCl/Xe near 2.4 eV, are believed to indicate the need for a more thorough understanding of the nature of the optically accessed electronic surfaces.

D. Cl₂ in Xe—Dissociation without Cage Exit

Depending on the excitation energy, the photodissociation of Cl₂ in Xe proceeds via very different mechanisms.¹⁶⁷ A rather unique mechanism of delayed dissociation occurs at excess energies below 3 eV, whereby the fragment Cl atoms get metastably buried in the cage wall. The parent molecule, Cl₂, is stabilized in the singly substitutional site of Xe, with orientation along the ⟨110⟩ direction and carries out

only small amplitude librations at 5 K.^{92,369,370} The Cl atoms create potential pockets, with the most stable configuration corresponding to the D₂ insertion site between two Xe atoms with its empty p orbital aligned along Xe–Xe. The experimental verification of this picture comes from the observation of efficient dissociation at excess energies below 1 eV and the observation that up to excess energies of 3 eV the product Cl atoms are trapped in thermally unstable sites, such that annealing at 40 K leads to complete recovery of the parent molecule.³²⁴ The mixed classical–quantum MD calculation (without spin–orbit coupling) predicted four different sites for the Cl atoms, with preference for the D₂ site for in-cage dissociation at low excess energies.⁹² Moreover, the calculations showed that a temperature increase to 40 K leads to recombination of in-cage pairs. Thus, the modeling successfully reproduced the experiments. This gives credence to mechanistic details that can be extracted from the trajectory data but which are not direct observables. For example, the trapping in the D₂ site occurs after a time delay of 1–2 ps, after creating the pocket through momentum transfer and subsequent cooling of the cage; the initial orientation of the molecule does not play a role in controlling this outcome. At excess energies above 3 eV, in the simulations, sites of D₂ symmetry farther removed from the parent site appear. Consistent with this, experimentally, it is noted that now the photofragments are thermally stable. The simulations indicate a forced exit mechanism in which cage atoms are significantly displaced to create windows. The experiments, however, indicate that at excess energies above 3 eV, the harpoon mechanism is in effect, a mechanism which is not addressed in the simulations.

IX. Forced and Delayed Cage Exit

A. Cl₂ in Ar

At high enough excess energies, *forced exit*, during which cage atoms are scrambled, becomes accessible. This process is common to high-energy excitations, such as X- and γ -rays, electrons, ions, and α -particles and may contribute to radiation damage, i.e., chemistry, sputtering, and desorption. Despite its potential ubiquity, the process has received little quantitative attention in matrix studies, the photodissociation of Cl₂ in solid Ar being a rather clear example.^{324,371} In well-annealed Ar matrixes, Cl₂ isolates in doubly substitutional sites. This has been established experimentally, based on analysis of the molecular A' → X emission and on post photolysis analysis of the Cl atom spectra in the VUV. The same conclusion is also derived in theoretical analysis of trap site energetics and recent simulations of the B → X excitation spectrum. Given the similarity in size of Cl and Ar atoms, the cage does not provide energetically accessible windows for sudden exit. Given the similarity in masses of Cl and Ar, after a failed attempt at cage exit, ~50% of the kinetic energy of the atom will be lost, dramatically reducing its chances of exit in subsequent attempts. Indeed, cage exit probabilities remain less than 10⁻⁶ for excitation

energies up to 6.1 eV (excess energies of 3.6 eV). At excess energies between 3.6 and 7 eV, a finite dissociation probability of ~2% is observed.³²⁴ At excess energies above 7 eV, a sudden increase in dissociation efficiency to about 30% is observed. Moreover, in all cases, post photolysis analysis of the atomic spectra shows that Cl atoms now occupy separate, singly substitutional sites.

These experimental observations, the photodissociation efficiencies throughout the excitation energy range and the fact that an initial doubly substituted molecule leads to final singly substituted pair of atoms, are remarkably well reproduced through classical MD simulations.³⁷¹ The simulations indicate a changeover in the mechanism of dissociation near 7 eV. Below this excess energy, the two hot Cl atoms deposit a large amount of energy in a first hard collision with the cage and heat it up locally. While executing large amplitude motions, occasionally, and after a rather long delay of ~3 ps, one of the Cl atoms replaces an Ar atom, with the net result of the permanent separation of substitutionally trapped Cl atoms as second nearest neighbors. The very low efficiency results from the low probability that the Cl atoms will retain sufficient kinetic energy for a long enough period to execute the exchange. Above 7 eV, the calculations show that the Cl atoms now possess sufficient energy to execute two hard collisions, the first destabilizes the cage and the second dislodges an Ar atom from the second shell. The dislodged Ar atom stays transiently in an interstitial site until it relaxes to the vacancy created by the Cl atom. As before, the net result is the permanent separation of a pair of substitutionally trapped Cl atoms, but now the process is characterized as direct, the result of impulsive dynamics.

Despite the excellent reproduction of the experimental observables, the microscopic interpretations should be made with some caution. The simulations are strictly classical, carried out on a single repulsive surface, and pairwise additive Cl–Ar potentials parametrized as ArCl($\Sigma_{1/2}$) are used. The experiments involve excitation at energies between 6 and 10 eV, which accesses a dense manifold of electronic states, which besides the repulsive surfaces include the bound 1¹ Σ_u^+ and Ar⁺Cl charge-transfer states.^{372,373} Excitation into the bound states followed by rapid predissociation is involved in the cage exit and scrambling. Since charge-transfer states are involved, the possibility of a strict harpooning was considered in the analysis of the experiments and rejected on the basis that emission from Ar⁺Cl⁻ could not be observed. Moreover, it was concluded that predissociation occurs with a probability of 50%, prior to electronic and vibrational relaxation. The latter aspect may explain the insensitivity of the process to the details of electronic dynamics—the initial excitation is efficiently converted to center of mass motion, which evidently can be well-represented by direct access of a single repulsive potential.

The Ar/Cl₂ system also serves as an example of a successful predissociation, one which involves cage modification in the process. Remarkably, despite the extensive transient scrambling, when the initial site

of the molecule is well defined as a double vacancy site, only well-defined product sites of singly substituted Cl atoms occur. When the sample is prepared with a distribution of different Cl_2 sites, a distribution of different product sites for Cl atoms results.³²⁴

B. Cl_2 in Kr and Xe

The influence of cage size and modification of electronic surfaces by the cage is illustrated by contrasting the behavior of Cl_2/Ar with that observed in the heavier rare gases. In Xe, molecular Cl_2 resides in singly substitutional sites. At low energies, in-cage dissociation dominates, while harpooning prevails at higher energies.³²⁵ In Kr, molecular Cl_2 isolates in both single- and double-substitutional sites. This leads to an interesting and complex superposition of features¹⁶⁷ from the Ar matrix, i.e., high energies for the onset of dissociation, with those from Xe, i.e., thermally unstable sites. Dissociation to thermally stable Cl sites starts at excess energies above 3 eV and thus at slightly lower energies than in Ar, while the production of Cl in thermally unstable sites occurs at excess energies of about 5 eV. Annealing to 25 K leads to a conversion mainly of stable sites produced at smaller excess energies to a new site and the thermally unstable sites are completely quenched. Surprisingly, dissociation at 25 K supports all three sites and the thermally unstable site gains probability at excess energies between 3 and 5 eV while absent at 5 K. This rather involved competition of different dissociation channels awaits modeling.

X. Channeled Migration

Up to this point the cage exit probabilities of atoms were considered without comment about their subsequent fate. In general, photodissociation leads to the stabilization of fragments as second nearest neighbors. However, in the case of "small" or light atomic photofragments, the initial impulse can induce long-range migration, displacing the hot atom by several lattice sites away from its origin. The best characterized case is that of F atoms, the long-range migration of which has been key to the construction of solid-state exciplex lasers and for inducing hot atom chemistry in cryogenic solids. Long-range migration has also been documented for both photo-mobilized and thermally activated atomic oxygen. In the case of atomic H, which by virtue of its light mass loses kinetic energy over many collisions, the details of the process remain unclear. We expand on these three systems below.

A. F Atoms

The high probability of XeF formation upon photodissociation of F_2 in free-standing Ar crystals doped with Xe and F_2 was the first recognition that F atoms must undergo long-range migration.²²⁸ This was exploited for the *in situ* synthesis of XeF in crystalline solids at densities on the order of 10^{18} cm^{-3} and led to the development of solid-state exciplex lasers with interesting gain properties.^{228,374–378}

Direct confirmation of the large migration length of impulsively generated F atoms was first provided

through shuttling experiments in FSC Ar triply doped with Xe, Kr, and F_2 .³⁷⁹ Photodissociation of F_2 leads to trapping of F atoms at Kr and Xe sites. The atoms are then reversibly shuttled between these two sites by taking advantage of the bound-to-repulsive nature of exciplex emissions, whereby F atoms are mobilized on the ground electronic surface through radiative dissociation (see Figure 1b). Upon excitation of the XeF exciplex at 308 nm, the Xe trap sites are completely depleted and the Kr sites are populated. Subsequent excitation of the KrF exciplex at 248 nm depletes the Kr sites and populates the Xe sites. The process can be repeated. On the basis of the assumption of a statistical spatial distribution of dopants, it could be inferred that with an initial excess energy of ~ 0.5 eV, the F atoms migrate an average length of 10–15 lattice constants (50–80 Å). The same principles were used in FSC F/Ar, where now the bimolecular recombination of F atoms was monitored through the bleaching of the Ar_2F emission to establish an average migration length of ~ 70 Å, with an estimated initial F-atom kinetic energy of 0.7 eV.¹⁹ Note, in contrast with the photodissociation of a diatomic, in the case of radiative dissociation of exciplexes, the partitioning of the repulsive energy along coordinates of the chromophore is less well-defined and only inferred from spectral analysis. The initial energy dependence for long-range migration was demonstrated in FSC Kr codoped with F_2 and Xe by monitoring the XeF yield upon photodissociation of F_2 .³⁸⁰ It was established that at excess energies below 1.9 eV, while F_2 can be completely dissociated the photofragments remain localized, while at excess energies above 2.4 eV, the F atoms migrate an average length of 80 ± 40 Å. This series of studies also conclude that the migration is not diffusive but rather a channeled motion guided by the lattice.

The long-range mobility of F atoms provides an opportunity for investigating low-temperature chemistry with translationally hot atoms. This was exploited in a series of studies by a combined ESR and IR analysis of addition and abstraction reactions of F atoms with C_2H_4 , CH_4 , H_2 , NH_3 , CO , and O_2 isolated in matrixes.^{381–383} The hot atom chemistry initiated by F_2 photodissociation could be contrasted with cold atom chemistry initiated by thermally activated diffusion of F atoms trapped in the lattice. The hot atoms promote abstraction and invariably produce isolated free radicals, e.g., $\text{F} + \text{CH}_4 \rightarrow \text{CH}_3 + \text{HF}$; $\text{F} + \text{H}_2 \rightarrow \text{H} + \text{HF}$; while the cold atoms lead to insertion, producing radicals complexed to the parent molecular fragment, e.g., $\text{F} + \text{CH}_4 \rightarrow \text{CH}_3-\text{HF}$; $\text{F} + \text{H}_2 \rightarrow \text{H}-\text{HF}$; $\text{F} + \text{NH}_3 \rightarrow \text{NH}_2-\text{HF}$. The structures formed in the latter case can be well-correlated to configurations of local minima on the reaction coordinate of the particular reactions. Evidently, in these gentle reactions, the cooling rate of the lattice is sufficient to trap transition-state intermediates. Although the contrast is quite dramatic, it is not yet clear as to which aspect of the hot atom chemistry, structure or dynamics, imposes its reaction specificity. However, the nature of the hot atoms was rather definitively established by the same group by contrasting the addition reactions of F to CO and O_2 in

vapor-deposited matrixes of Ar with those of FSC Ar.²³⁴ In these studies, the atom migration lengths are obtained through the kinetics of photoinduced complex formation, subject to the assumption of a statistical distribution of guests. The latter assumption is checked and justified, since the IR detection scheme allows the observation of dimers and clusters. The comparison between matrix and FSC shows a dramatic difference in the migration length of hot F atoms: 7–14 Å in the vapor-deposited matrixes versus 140± 60 Å in FSC. Within the reported experimental error bars, the latter value is in agreement with the earlier measurements in FSC. This order of magnitude difference caused by lattice morphology is rather convincing evidence that the long-range migration of F atoms is a nondiffusive, channeled motion through the ordered lattice and that the thermalization length is controlled by structural defects.

Contemporaneous with the first experimental measurements, classical MD studies predicted the long-range migration of F atoms in crystalline Ar.³⁴⁹ Photodissociation above an excess energy of 2 eV produced several trajectories that showed long-range channeling motion of F atoms in the thermal lattice (wiggly trajectories along the channels of the lattice, with few large angle scattering events). The length of travel of these trajectories was limited by the size of the simulation cell to 30 Å. These simulations provided the plausibility and mechanistic interpretation of channeled migration but not a quantitative agreement. Only 10% of dissociation events above 2 eV lead to long-range migration in the simulations, while the experiments indicate 100% probability. The simulations were based on the assumption of a pairwise additive isotropic F–Ar potential, fitted to V_{Σ} of the pair potential given by Becker.³⁸⁴ More refined treatments of this potential were subsequently implemented, including orbital anisotropy and spin-orbit interactions, as already discussed.²¹ These refined treatments, however, failed to show the channeling mobility. It would seem that the original potential, although formally not justifiable, is a more realistic representation of the effective interaction of the F atom with the lattice. Quite clearly, there is room for more rigorous theoretical analysis and more quantitative experiments to warrant such analyses. We should point out that of the two KrF potentials obtained by molecular beam scattering,^{341,384} the earlier work of Becker et al. is the more reliable. This had been recognized through MD simulations of spectral line shapes of F-doped Kr³⁷⁹ and more directly demonstrated in the gas-phase spectroscopic measurements by Lo and Setser.³⁴²

All of the experiments described above rely on the assumption of statistical spatial distribution of dopants and extract quantities as averages over distributions. This gives cause for concern since the assumption is difficult to verify. Furthermore, a mismatch in sizes of guest and host can lead to strain fields that may attract or repel migrating atoms, distorting the premise of a homogeneous site distribution. With these concerns in mind, experiments in the sandwich geometry were introduced.²²⁵ The layout consists of

a top layer of F₂-doped Ar, a spacer layer of pure Ar with thickness controlled in the monolayer regime, followed by a substrate of pure Kr in which the arrival of atoms is monitored. F atoms in the Ar layer, in the Kr layer, and at the Ar/Kr interface can be distinguished spectroscopically through their characteristic emissions.³⁸⁰ By varying the thickness of the spacer layer, the distribution of penetration depths and its average value can be extracted. Moreover, by separating the dissociation and transport volumes spatially and by following transport in the pure substrate, suspected sources of “hidden process” are eliminated. When F₂ is dissociated with 10.15 eV in the top layer, imparting a mean kinetic energy of 4.3 eV to each F atom, an exponential distribution of penetration probabilities with a 1/e value of 10 monolayers of Ar (28 Å) is obtained. The compactness of the films and the absence of multiple excitation of F atoms in the spacer layer was carefully checked. The sensitivity of detection of F atoms was increased to 1/1000 of a monolayer of F atoms using energy transfer from Kr excitons. The F atoms are injected isotropically in the spacer layer, and the values for the average length of travel derived from the average penetration depth depends on the type of motion. Assuming the less likely purely rectilinear motion leads to an average length of travel of 30 Å, a more likely Brownian type of motion is consistent with a mean free path between large angle scattering events of around 4 monolayers and an average length of travel up to 27 monolayers (70 Å).²²⁵ Thus, the travel length observed in these carefully prepared sandwiches exceed those obtained in the vapor-deposited matrixes (7 Å)²³⁴ by an order of magnitude and represent the lower bound of those observed in doped FSC. The sandwich experiments primarily determine the penetration depth of hot atoms, while the measurement in the doped solids yield the volume sampled by migrating atoms.¹⁹ Both techniques yield large migration lengths, on the order of 100 Å, for samples with long-range order, confirming the model of channeled migration.

B. O Atoms

As in the case of F atoms, the radiative dissociation of Rg⁺O[−] charge-transfer states leads to photomobility of O atoms. This has been demonstrated in matrix Xe^{9,10} and in FSC Kr and Xe.^{6,14} In the matrixes, atomic oxygen is prepared by 193 nm photolysis of N₂O, which at this wavelength occurs with near-unit quantum efficiency, implying direct cage exit of O(¹D).^{9,10} After establishing that the O atoms in their ground ³P state are permanently trapped in the Xe matrix,⁸ it is demonstrated that 248 nm access of the charge-transfer state leads to bleaching of the exciplex emission, due to depletion of the atomic O concentration by formation of O₂. The observed fluorescence depletion curves could be treated by homogeneous kinetics and fit the form expected for bimolecular kinetics. The analysis yields a migration length of ~400 Å.⁹ Note, the migration length will depend on the assumed contact cross section for recombination, σ , which can be argued to be underestimated in these analyses.²³⁴ In essence, a migra-

tion length of the photomobilized O atoms is comparable to that of F atoms. Since this result is difficult to rationalize if the mobile species were O(³P), it has been suggested that the observed mobility must occur at defects and voids.¹² It is difficult to accept this hypothesis since all O atoms can be made to recombine, and it would be surprising if all atoms were created at defects. Further, the grain boundary argument cannot be used for the FSC studies, in which photomobility is observed.^{13,14} To explain the observed photomobility of O atoms in FSC Kr, it has been suggested that the motion must occur on the ¹D surface. Direct evidence for this suggestion is provided by the observation of a photostationary state between N₂O and O at 248 nm, a process that cannot occur on the triplet surface where the barrier to recombination is more than 1 eV.¹⁴

Perhaps the more surprising observation pertains to the deduced *channeled mobility of thermally activated O atoms* in FSC Kr and Xe.⁶ In these experiments, after photodissociation of N₂O at 193 nm, the thermally induced reaction of O atoms to form O₂ is monitored—the O atoms are monitored through site-specific LIF, while O₂ is monitored via its thermoluminescence. Analysis of the kinetic data obtained by both programmed temperature ramp measurement (glow curves) and temperature jump measurements yield first-order kinetics and lead to the extraction of migration lengths of ~300 Å. Further, it is shown that the mobility is activated, and well-defined activation energies for interstitial and substitutional sites are extracted. A good indication that long-range order is necessary for the observed mobility is provided through the comparison between FSC and vapor-deposited matrixes and the observation that in the latter a continuous distribution of activation energies and recombination rates arise. These results are in general accord with the matrix measurements of the same process, where thermally induced long-range mobility of O atoms, second-order recombination kinetics to form O₂, and at least two main low-temperature ensembles of O atoms are observed in Xe.^{9,10,15} Again, these observations cannot be explained based on O(³P)—Rg potentials.¹² Instead, it is suggested that in these heavy rare gas solids the singlet and triplet surfaces crisscross and that at least in Xe,¹³ in the D₂ insertion sites the singlet surface is lower in energy than the triplet.¹¹ However, with a DIM basis set limited to neutrals, the model is unable to explain the observed activation energies quantitatively. Noting that the binding nature of the RgO(¹Σ) state is wholly derived from its mixing with the Rg⁺O⁻ charge-transfer state, it is suggested that a realistic treatment of the nonadiabatic dynamics in this case would necessarily require the inclusion of ionic states in the electronic basis.¹³ This conclusion was also derived from the discrepancy between experiment and theory in the case of F atoms. The only theoretical implementation of this concept is the recent treatment of O(¹D) in solid H₂, in which a dramatic modification of the potential energy surfaces (a many-body barrier along the H—O—H coordinate) is obtained when including the coupling between ionic and covalent surfaces.⁸⁴

In the seemingly similar set of studies of photodissociation and recombination of ozone in both FSC and matrix Xe, very different photophysics is realized.⁷ Photodissociation of O₃ in the doubly substituted isolation site is affected at 266 nm. Upon warm-up, it is observed that ~90% of the O₂/O pairs undergo geminate recombination to reform ozone. This would immediately imply a short-range separation between the photofragments and a short range for the thermally activated mobility of the O atoms. Indeed, the analysis of the data produces a migration range comparable to the initial separation range of ~20 Å and, as importantly, produces a large recombination cross section with a capture radius comparable to the migration range of 20 Å. In essence, the photodissociation of ozone generates an O atom which remains coupled to its parent site, presumably through the structural defect that connects the two through a strain field (a Frenkel pair). In terms of kinetic diffusion constants, the extracted value for matrixes shows a large dispersion around an average value of $6 \times 10^{-19} \text{ cm}^2 \text{ s}^{-1}$ at 15 K extracted from the O₃/Xe matrix experiments, to be compared with 3×10^{-19} and $1 \times 10^{-21} \text{ cm}^2 \text{ s}^{-1}$ for the fast and slow subensembles observed in the N₂O/Xe matrix experiments.^{9,10} The dispersion in these values is a good reflection of the structural disorder in matrixes. Although consistently larger, a variation in diffusion constants measured in FSC Xe is also observed, with diffusion constants as high as $1.5 \times 10^{-17} \text{ cm}^2 \text{ s}^{-1}$. Note, these experiments are designed to probe the tail of the activated mobility of O atoms by restricting the measurement temperatures to $T = 15\text{--}17$ K. The thermally activated channeled mobility in FSC Xe is observed at significantly higher temperatures, with glow curve maxima at 40.5 and 47.5 K for interstitial and substitutional O and a third unidentified site that peaks near 61 K.⁶ These complementary data produce a very complete experimental picture for O-atom dynamics in solids, making the system ripe for more refined theoretical scrutiny.

C. H Atoms

Much of the information regarding the possibility of impulsive migration of H atoms comes from studies of photodissociation, followed by thermally activated recombination aimed at retracing the original spatial distribution of photofragments. Since the conclusions are less firm, we examine the details of experiment and theory.

Early indications of long-range mobility of H atoms are derived from UV photolysis of HI in solid Xe codoped with C₂H₆ with ESR analysis of reaction products.^{385,386} The experiments demonstrated a competition between abstraction reactions of the hot H atoms with HI and ethane to form H₂, instead of addition to the radicals. These observations are quite similar to those of F atoms³⁸² and would imply long-range migration of H atoms. The unusual abstraction reaction with ethane, along with a very large isotope effect, is ascribed to reaction via tunneling.^{385,386}

In thermal mobility studies, H and D atoms were produced by X-ray and VUV excitation from a large variety of hydrocarbons and triatomic and diatomic

parent molecules in Xe, Kr, and Ar matrixes.^{387–389} The atoms are stable for weeks at low temperatures but bleach at elevated temperatures through thermally activated diffusion. Bleaching time constants, which were determined over 6 orders of magnitude, do not show a sufficiently strong deuteration effect, hence, tunneling contribution to the thermally activated mobility is deemed insignificant. The temperature dependence of rate constants follows a stretched exponential that can be treated in terms of continuous-time random walk models, implying a dispersion in activation energies. In the earlier studies, the bleaching of H atoms was attributed to reversible recombination with the parent fragment.³⁸⁷ In more recent experiments it was recognized that this is a minor channel, especially in Xe but also in Kr.³⁸⁸ While the main bleaching channels, presumably formation of H₂, is not well-characterized, the observation of negligible recombination would imply a large initial separation between the H atom and its parent and therefore a propensity for migration of the atoms during photogeneration. Analysis of competing channels in the thermal bleaching of H atoms could determine their initial distribution, as in the implementation in HCl/Xe and HCl/Ar.³²⁶ Such measurements were recently reported using EPR for detection of the H atoms.³⁹⁰ In Ar, geminate recombination between photofragments dominates, while in Kr, bimolecular rates and permanent bleaching of the precursor clearly show the contribution from H₂ formation. The observed kinetics has been analyzed to extract activation energies for thermal diffusion of 6–7 kJ/mol in Ar and 9–14 kJ/mol in Kr.

Direct evidence for long-range migration of photo-allytically generated H atoms was reported in photodissociation studies of HBr/Xe matrixes, with dissociation carried out at 248 and 193 nm (excess energies of 1.25 and 2.59 eV, respectively).³⁹¹ Modification of the accessed electronic states is implicated by the fact that at both wavelengths the dissociation efficiency exceeds gas-phase absorption cross sections. In these experiments, the H and Br atoms are followed via the Xe₂H and Xe₂Br emissions and the loss of HBr is monitored through IR absorption. The combined IR/UV studies also allow characterization of the role of clusters. At dilutions of 1:800, the Br production is second order in the 193 nm laser intensity, indicating that the photogenerated H atom produces a secondary Br atom through the abstraction reaction H + HBr → H₂ + Br. At larger dilutions, at 1:10⁵, the Br growth reverts to first order. From the turnover concentration for the kinetic order of 1:10⁴, the mean travel distance of H atoms can be derived as ~100 Å. Consistent with the reduced excess energy, at 248 nm the turnover concentration is observed to occur at a dilution of 4 × 10³. An intriguing observation in these studies is the observation of an induction time in the kinetic curves. This delayed onset was taken to suggest that the radiation initially creates defects, and only subsequently do H atoms migrate through defect-rich areas. This is shown to be the case for thermal diffusion of H atoms through measurements conducted in matrixes deposited at different temperatures, where a 5-fold

decrease in the thermal diffusion constant of H atoms at 40 K is observed for matrixes deposited at 28 K versus those deposited at 10 K.³⁸⁹ This is consistent with the notion that quench condensation of matrixes leads to increased defect concentration through the formation of smaller crystalline domains and therefore a larger contribution from grain boundaries.²¹⁸ A consistency check for this picture was provided by investigating the thermal diffusion of the HBr molecules via dimer formation: The defect-enhanced mobility in the 28 K deposit leads to a higher dimer content after annealing to 50 K than samples deposited and kept at 60 K, despite the higher original dimer content from the deposition at 60 K.³⁹² The conclusions reached in these studies were more recently reproduced in photodissociation studies of HBr, now combining LiF and EPR tools for analysis.³⁹³ The studies show that when the dissociation is carried out at an excess energy of 2.6 eV, while in Ar the H atoms remain near the parent trapping site, in both Kr and Xe they undergo long-range migration. This study also included simulations which support these conclusions.

In a related study, now using synchrotron radiation, H atoms produced by photodissociation of HCl in slowly deposited Xe films at excess energies of 1.8, 2.2, 2.6, and 3.1 eV and at dilutions between 10⁻³ and 10⁻⁴ were studied.³²⁶ Initially, 97% of the original HCl is dissociated. The photofragments are then mobilized by warming the sample up to $T = 44$ K, and the concentrations of H and Cl are followed by monitoring the Xe₂H and Xe₂Cl emissions, respectively. The atom concentrations evolve due to three main channels: (1) H + Cl recombination, (2) formation of H₂ from H + H, (3) Cl production via the abstraction H + HCl → H₂ + Cl. At dilutions of 10⁻³, for all excess energies, the Cl content remained essentially constant or slightly increased whereas the H content completely disappeared. This would indicate that under the experimental conditions, process 2 dominates and a possible weak contribution of process 1 is compensated or even overcompensated by process 3. The preference of processes 2 and 3 demonstrates that the initial photodissociation creates H and Cl atoms that are separated by at least one-half the mean HCl–HCl distance, suggesting an H-atom migration length of at least 19 Å. At dilutions of 10⁻⁴, when the atoms are prepared with an excess energy of 1.8 eV, complete loss of both H and Cl is observed. This would imply that in this case, process 1 dominates and establishes a migration length of ~19 Å at this excess energy. At larger excess energies, partial loss of Cl is observed and migration lengths between 20 and 40 Å are deduced. On the basis of similar arguments, H-migration lengths in Ar matrixes of 27 Å are deduced for dissociation with an excess energy of 2.5 eV.³²⁶

The rather large H-migration lengths are in contradiction with simulations carried out in crystalline cells.^{91,93,394} However, the experimental evidence for migration of H atoms is based on studies in matrixes, and in contrast with the case of F atoms, defects are implicated in the migration process. Simulations have been carried out in cells that model the deposi-

tion process.^{157,169} In the case of Ar deposited at 12 K, a lattice density 82% of the perfect fcc structure is obtained, with ~3 vacancies around the H₂ impurity and a radial distribution function indicating disorder which does not anneal at 50 K.¹⁵⁷ In more recent simulations of H-atom diffusion in imperfect xenon matrixes using the classical variational transition-state approach, it was again concluded that the experimentally measured thermal rates are only compatible with diffusion at grain boundaries.³⁴

Seemingly, theory remains in contradiction with measurements performed in thin films carefully prepared by slow condensation at elevated substrate temperatures. At least the notion that large defect concentrations are required for H-atom mobility can be eliminated by experiments performed in well-prepared samples, the integrity of which is verified through measurements of spectral inhomogeneity and measurements of packing density.^{17,225} The optical scattering properties of such films are also indicative of a microcrystalline composition, which is further supported by the observation of fcc–hcp phase transitions.^{320,395,396} While defects cannot be suppressed completely and it is difficult to specify their density quantitatively, it is legitimate to attribute the main features of photochemical results to a well-ordered local geometry as long as indicators, such as low optical scattering and sharp spectral lines, are verified. Indeed, photochemical processes are less susceptible to defects than thermal processes. In thermal diffusion, barrier distributions are sampled with rates on the order of 10¹² s⁻¹ and the Boltzmann tail in the kinetic energies exponentially enhances contributions from lower barriers associated with defects. In short, since several features in the HBr/Xe experiments are corroborated by the HCl studies in very differently prepared films, we may conclude that experiment and theory remain at odds with respect to long-range migration of H atoms.

In principle, investigations of H-atom mobility in free-standing crystals could be quite informative. The only such reported studies, namely, photodissociation of HI in FSC Kr and Xe, have been silent on this subject due to complications arising from the “hidden processes” associated with ionic centers.^{73,362} In effect, where H atoms are generated with a counterfragment of significant electron affinity, as is the case in the photodissociation of hydrogen halides, then photoinduced charge-transfer processes create a variety of photoactive ionic centers, which have broad and intense absorptions throughout the spectrum, and interference with the targeted dynamics in the H-atom mobility measurements. We expand on the photophysics of such ionic centers in the next section.

XI. Photon-Induced Harpooning

An underlying theme of the entire presentation above is the importance of direct and indirect contributions of ionic surfaces on dynamics. Although this consideration is well-established experimentally, it has, for the most part, been bypassed in theoretical analyses due to the challenges involved in rigorous treatments. Photoinduced harpoon reactions, in which guest–host intermolecular charge-transfer states are

accessed optically, are designed to probe reactive dynamics over ionic surfaces and serve as model systems to advance theoretical rigor. The classic case of Cl₂/Xe, which has been extensively studied in the gas phase,^{397–399} in small^{400–402} and large^{403,404} van der Waals clusters, in the supercritical fluid,⁴⁰⁵ in the liquid phase,^{406–409} in matrixes,^{65,248,249,267,325} and in solids under pressure,^{20,410} serves as a useful example to highlight the distinctive features of dynamics on ionic surfaces.

The intermolecular charge-transfer transition of the Xe···Cl₂ contact pair can be directly accessed optically.^{397,411} In condensed media, dielectric solvation of the ionic terminal state shifts this transition to the near-UV, and a relatively simple model can reproduce the absorption bands, as shown for all the molecular halogens in liquid Xe⁶⁵ as well as in solids of Xe and Kr.³²⁵ Upon excitation, the vertically created Xe⁺Cl₂⁻ ion-pair state, which was recently isolated in liquid Ar,⁴⁰⁹ evolves along the attractive Xe⁺···Cl⁻ coordinate and the repulsive Cl⁻···Cl coordinate, toward the Xe⁺Cl⁻ + Cl product of the harpoon reaction. This evolution is probed in real time in liquid Xe, where it has been shown that the reaction can be arrested by stimulating the transition from the ionic to the neutral surface.⁴⁰⁸ While this would complete the process in gas-phase collision complexes, in condensed media, collective host coordinates are set into motion due to the sudden creation of the ionic moiety. As long as the host is more polarizable than Cl, the driving force for solvation would dictate that the neutral Cl be expelled from the first shell while the solvent crowds about the dipolar center by polarization forces. This tendency is the basis of the “negative” cage effect which has been invoked to explain the near-unit yield of cage exit of Cl atoms via this mechanism.²⁴⁸ Further, if the host is Xe, then the vertically created hole is delocalized over nearest neighbors and will only successfully self-trap by localization as Xe₂⁺, which has a bond length more than 1 Å shorter than the nearest-neighbor distance in the lattice.⁶⁵ This delocalization and self-trapping result in photophysics peculiar to the solid state.²⁴⁹ The process terminates with radiation of the Xe₂⁺Cl⁻ exciplex, the net reaction being the breaking of the Cl₂ bond with permanent separation of Cl atoms. This occurs with near-unit efficiency in the solid-state despite the fact that the sudden barrier for Cl(²P) exit in Xe is ~20 eV.⁸⁷ Mechanistically, the most profound difference between dissociation via the ionic surfaces versus dissociation via a neutral repulsive surface is the driving force. In the latter case, it is the *repulsive release of energy* that leads to products, hence, the crucial role of excess energies in the processes discussed in the prior sections. In the case of the ionic surfaces, the driving force is the *attractive release of energy* as the system evolves toward the formation of a tightly solvated ion-pair state. Indeed, it is now possible to break a bond by supplying optical excitation that is less than the dissociation limit of the free molecule. These principles along with significant detail regarding ionic intermediates and evolution on various surfaces have been established through the

studies of the two-photon-induced harpoon reaction of molecular halogens and hydrogen halides in condensed rare gases. Besides the dynamical motivation, these studies were initiated to probe the photophysics of cooperative transitions⁴¹² and condensed-phase exciplex lasers and as minimalist models for optical energy storage and retrieval.²⁴⁹ We only give highlights relevant to our subject.

Perhaps the clearest and the most dramatic contrast between dissociation via ionic versus neutral surfaces is given in the studies of solids under pressure. Using a diamond anvil cell (DAC), Cl₂-doped solid Xe was investigated under pressure, $P = 2\text{--}10 \text{ GPa}$, and as a function of temperature, $T = 30\text{--}300 \text{ K}$.²⁰ It could be shown that photodissociation via the repulsive $^1\Pi_u$ surface of the molecule, at an excess energy of 1.5 eV (308 nm), is completely blocked (upper limit of quantum yield of 10^{-4}) under these conditions. Earlier simulations had shown that at zero pressure, the dissociation of Cl₂ could only be affected at temperatures above 100 K.³⁶⁹ Subsequent simulations showed that at $T = 100 \text{ K}$, upon application of pressure, the dissociation quantum yield dropped from $\phi = 0.3$ at $P = 0 \text{ GPa}$ to $\phi = 0$ at $P = 2.5 \text{ GPa}$, the dissociation being blocked by the increased barrier for cage exit and complete arrest of molecular librations.³⁷⁰ The latter prediction was verified through polarization measurements, although the zero-pressure dissociation could not be tested.⁴¹⁰ In short, based on both experiment and simulation it could be established that dissociation via neutral surfaces does not occur. Nevertheless, throughout the studied range of up to 8 GPa, the two-photon-induced harpoon reaction is effective in producing Cl atoms with a quantum yield at least 5 orders of magnitude larger than the neutral channel.²⁰ In these highly doped solids of original concentration 1:500, dissociation could not be carried out to completion due to photomobility induced recombination of otherwise stably trapped Cl atoms (it is experimentally determined that at $P > 5 \text{ GPa}$ and $T = 300 \text{ K}$, Cl atoms remain stably trapped in Xe for at least 6 months). The photomobility in this case is induced through the charge-transfer excitation of the atomic centers and their subsequent radiative dissociation. The process is subject to an induction period ascribed to the creation of defects, however, once triggered a migration range of 30 Å is deduced.

In the case of two-photon-induced charge-transfer transitions, real intermediate states can play a significant role in determining resonances, most significantly due to the evolution of vertical electron affinities as a function of intermediate-state configurations.⁴⁰⁷ This consideration has been exploited in part in studies of ICl near the solid–liquid coexistence, where it has been shown that the branching of the harpoon reaction to form Xe₂⁺Cl[−] or Xe₂⁺I[−] is strongly controlled by the structural order of the solvent.⁴⁰⁶ Even in the absence of real intermediate resonances, the two-photon-induced contact charge-transfer transitions have large cross sections in the solid state. This has been most clearly demonstrated in the case of HCl/Xe, where the two-photon process can be carried out with 3.5 eV photons, i.e., 0.8 eV

below the dissociation limit of the molecule.²⁴⁸ The terminal ion-pair resonance which was postulated in this case was subsequently identified through the DIIS calculations¹⁰⁴ and through ab initio theory.³⁶⁶ Finally, we should note that these two-photon-induced charge-transfer transitions have giant cross sections, on the order of $10^{-42} \text{ cm}^4 \text{ s}$, and very broad resonances, which makes them difficult to avoid.

The halogens and hydrogen halides isolated in the heavier rare gases have allowed the dissection of the condensed-phase harpoon reactions with some clarity. The principles identified in these studies can be expected to be more broadly applicable. The observation of species such as HSXeH,³³⁷ HXeX, and HKrX ($X = \text{Cl}, \text{Br}, \text{I}$),^{105,115} the two-photon-induced dissociation of SH in Kr but not in Ar,³⁵ the exciton-mediated dissociation of N₂O, which is representative of all molecular impurities with dissociative negative ions,¹⁴ are examples where chemistry along ionic surfaces occurs. We may also recognize that in the lighter rare gases, where Rg⁺M[−] states are embedded in a high density of excited states of the guest, the ion-pair states can rapidly relax via nonadiabatic transitions, passing the control of subsequent dynamics to neutral states. A good example of the latter is provided by the studies of F₂ in Ne.^{321,413} Also, intramolecular charge-transfer states may compete with intermolecular charge transfer. This is illustrated in the case of iodine, where the molecular ion pair state, I⁺I[−](D'), is stable and relaxes radiatively in Ar and Kr²⁵³ while it undergoes either insertion or predissociation via the intermolecular charge-transfer configuration, Xe⁺I₂[−], in Xe.^{200,258}

In the solid state, charge delocalization effects cannot be ignored in describing intermolecular charge-transfer states. Since we focus on Rg⁺M[−]-type states, it is clear that in ordered lattices the vertically created state must initially involve a delocalized hole. This is best demonstrated in solid Xe doped with atomic halogens, where the guest–host intermolecular charge-transfer transitions are described as a progression of Rydberg holes orbiting the central negative ion.⁶⁶ With an extension of the DIIS model,¹⁰⁷ this picture of extensive delocalization is fully retrieved formally.⁷² A similar description is valid for H isolated in Xe, in which at least in the octahedral interstitial site the excited state is identified as Xe₆⁺H[−].^{372,414} The vertically excited states of halogens and hydrogen in solid Kr are also interpreted as a central negative ion with the hole delocalized over the entire cage.^{372,415} As the valence bandwidth of the host is reduced, the extent of delocalization will be reduced and a picture of resonant hole hops become more appropriate. Nevertheless, as long as the system has structural symmetry, the localized states cannot be stationary. Thus, even in Ne, we may expect hole mobility prior to trapping via hole–phonon coupling. A recent rigorous analysis of this process in small clusters of helium is quite informative;⁴¹⁶ earlier, a classical model was used to test the role of hole hopping in harpoon reactions.⁴¹⁷ In all cases, the delocalized hole states are unstable. They will localize and trap most generally as Rg⁺ through a process that involves positive feedback between

hole localization and bond compression. Since this is a rapid, kinetically driven process, after Rg^+X^- -type excitations, in addition to formation of $Rg_2^+X^-$, charge separation can occur, i.e., the hole may trap outside the first shell of atoms surrounding the X^- center. Experimentally, in the case of solid Xe doped with atomic halogens, it is found that the extent of charge separation is independent of the particular Rydberg state accessed.^{249,418} Quite clearly, charge separation will be enhanced by the presence of defects or nearby impurities with hole affinity, a mechanism that leads to the formation of H^+ centers upon UV irradiation of HX-doped solid Xe.¹⁰⁸ Delocalization of holes generated by excitation of charge-transfer transitions and their subsequent trapping at various impurity sites has led to a very stimulating field of studies on the structural and dynamical aspects of ionic centers in rare gas solids. Their consideration is also relevant since their photodynamics interferes with the photophysics of neutrals.

IR spectroscopic analysis of UV-irradiated matrixes containing hydrogen halides has led to the discovery of and identification of a large family of ionic species. At first ionic molecules of the form Rg_2H^+ with the hole trapped at the H atom were identified, including Ar_2H^+ , Kr_2H^+ , Xe_2H^+ , and their deuterated analogues.^{108,419} These species had previously been prepared by high-energy excitation in discharges and with X-rays,^{420,421} and now it has been shown that soft UV irradiation is sufficient to generate these ions. Further, the negative ionic centers X_2H^- with an electron trapped at the H atom were identified for $X = Cl, Br, I$ and their deuterated analogues.⁴¹⁹ This was followed by the identification of the HRgX trimers, which although overall neutral, derive their stability from the charge-transfer configuration (HRg^+X^-). These included HXeCl, HXeBr, HXeI, and HKrCl.¹⁰⁵ Following the same electronic principle, HXeH, HXeD, and DXeD were identified in Xe matrixes.¹¹⁵ All of these ionic and neutral trimers are linear, and all except HRgX are centrosymmetric. Evidently ionic contributions are essential in the binding energies of all these molecules.

The first step in the preparation of these compounds requires dissociation of the precursor: 248 nm is sufficient for HBr and HI while 193 nm is needed for HCl. Excitation of the charge-transfer states $X^-Rg_n^+$ is the second step, for which excitation by lamps in the 300–350 nm region or 248 nm can be used. The ionic species are formed without further treatment through hole trapping. The H atoms separate sufficiently from the halogen so that the vibrational fingerprints of the Rg_2H^+ molecules are not influenced by the halogen counterion. Generation of the neutral compounds requires significant annealing, and the two types of neutrals can be separated by selective bleaching of the HRgX molecules with 248 nm whereas 193 nm bleaches both types of neutrals. Besides this important access to new rare gas photochemistry, these “hidden processes” represent a severe obstacle for migration studies. The manifold of bleaching and charge-detrappling channels may mask the spectroscopic detection of the H and X content via the $Rg_2^+H^-$ and $Rg_2^+X^-$ emissions

in an uncontrolled way. In addition, H-migration processes are involved in the generation of the Rg_2H^+ centers. Finally, the Rg_2H^+ centers provide insight in local H-atom dynamics. These centers are unstable at 15 K and bleach on a time scale of 6000 (ArHAr)⁺ to 40000 s (XeHXe)⁺.⁴¹⁹ A bending motion of the H atom around one Rg atom leading to an unstable Rg–Rg–H geometry is the most likely decay channel according to the calculated potential energy surface.¹¹⁰ The barrier seems to be too high for a thermally activated crossing at 15 K and tunneling is more likely: a conclusion corroborated by the much higher stability of the deuterated analogues.

XII. Acknowledgments

We thank our co-workers who have been instrumental in creating the body of science reviewed here. Among our colleagues, Professors R. B. Gerber and H. Gabriel with their teams have inspired and led the theoretical maturation of the field since inception, Professor M. Chergui who has been a long-time partner in Berlin, and Professor C. C. Martens who has enthusiastically charged in ultrafast dynamics. We have been enriched through collaborations with T. F. George, A. V. Nemukhin, and K. R. Wilson. Yet, the true praise goes to our students and postdoctoral associates, many of whom have since become independent leaders in the field. From the first team members—M. E. Fajardo, L. Wiedeman, F. Okada, W. Lawrence, and H. Kunttu in Irvine; R. Alimi in Jerusalem; M. Chergui, R. Schriever, and H. Kunz in Berlin—to the most recent contributors—R. Zadayan, M. Ovchinnikov, A. Benderskii, and J. Almy in Irvine; C. Bressler and K. Gödderz in Berlin—there has been a long list of contributors whose work we recognize with this review. We thank S. Fiedler whose recalculations are shown in Figure 2 and B. Schmidt for providing Figure 3.

XIII. References

- (1) Kramers, H. *Physica* **1940**, *7*, 284.
- (2) Hägggi, P.; Talkner, P.; Borkovec, M. *Rev. Mod. Phys.* **1990**, *62*, 251.
- (3) Flynn, C. P. *Point Defects and Diffusion*; Clarendon: Oxford, 1972.
- (4) Borg, R. J.; Dienes, G. J. *An Introduction to Solid State Diffusion*; Academic Press: Boston, 1988.
- (5) Perutz, R. *Chem. Rev.* **1985**, *85*, 75.
- (6) Danilychev, A.; Apkarian, V. A. *J. Chem. Phys.* **1993**, *99*, 8617.
- (7) Benderskii, A. V.; Wight, C. A. *J. Chem. Phys.* **1996**, *104*, 85.
- (8) Krueger, H.; Weitz, E. *J. Chem. Phys.* **1992**, *96*, 2846.
- (9) Ryan, E. T.; Weitz, E. *J. Chem. Phys.* **1993**, *99*, 8628.
- (10) Ryan, E. T.; Weitz, E. *J. Chem. Phys.* **1993**, *99*, 1004.
- (11) Danilychev, A.; Apkarian, V. A. *J. Chem. Phys.* **1994**, *100*, 5556.
- (12) Ford, M. B.; Foxworthy, A. D.; Mains, G. J.; Raff, L. M. *J. Phys. Chem.* **1993**, *97*, 12134.
- (13) Lawrence, W. G.; Apkarian, V. A. *J. Chem. Phys.* **1992**, *97*, 2229.
- (14) Lawrence, W. G.; Apkarian, V. A. *J. Chem. Phys.* **1992**, *97*, 6199.
- (15) Ryan, E. T.; Weitz, E. *Chem. Phys.* **1994**, *189*, 293.
- (16) Ozin, G. A.; Huber, H. *Inorg. Chem.* **1978**, *17*, 155.
- (17) Kometer, R.; Schwentner, N. *J. Chem. Phys.* **1996**, *104*, 6967.
- (18) Ozin, G. A.; Mitchell, S. A.; Garcia-Pietro, J. *J. Phys. Chem.* **1982**, *86*, 473.
- (19) Feld, J.; Kunttu, H.; Apkarian, V. A. *J. Chem. Phys.* **1990**, *93*, 1009.
- (20) Katz, A. I.; Apkarian, V. A. *J. Phys. Chem.* **1990**, *94*, 6671.
- (21) Krylov, A. I.; Gerber, R. B. *Chem. Phys. Lett.* **1994**, *231*, 395.
- (22) Ebner, C.; Sung, C. C. *Phys. Rev. A* **1971**, *5*, 2625.
- (23) Zhou, M.; Ral, M.; Brison, J. P.; Sullivan, N. S. *Phys. Rev. B* **1990**, *42*, 1929.

- (24) Katunin, A. Y.; Lukashevich, I. I.; Orozmatov, S. T.; Skylarevski, V. V.; Suraev, V. V.; Filippov, V. V.; Filippov, N. I.; Shevtsov, V. A. *JETP Lett.* **1981**, *34*, 357.
- (25) Collins, G. W.; Souers, P. C.; Mainschein, J. L.; Mapoles, E. R.; Gaines, J. R. *Phys. Rev. B* **1992**, *45*, 549.
- (26) Kagan, Y.; Klingler, M. I. *J. Phys. C* **1974**, *7*, 2791.
- (27) Kagan, Y.; Maksimov, L. A. *Sov. Phys. JETP* **1984**, *38*, 307.
- (28) Takayanagi, T.; Masaki, N.; Nakamura, K.; Okamoto, M.; Sato, S.; Schatz, G. J. *Chem. Phys.* **1987**, *86*, 6133.
- (29) Miyazaki, T.; Morikita, H.; Fueki, K.; Hiraku, T. *Chem. Phys. Lett.* **1991**, *182*, 35.
- (30) Miyazaki, T.; Kumada, T.; Kitagawa, N.; Komaguchi, K.; Aratono, Y. *J. Low Temp. Phys.* **1998**, *111*, 453.
- (31) Fujitani, Y.; Miyazaki, T.; Masaki, N. M.; Aratono, Y.; Takikawa, E. *Chem. Phys. Lett.* **1993**, *214*, 301.
- (32) Komaguchi, K.; Kumada, T.; Aratono, Y.; Miyazaki, T. *Chem. Phys. Lett.* **1997**, *268*, 493.
- (33) Perry, M. D.; Mains, G. J.; Raff, L. M. *J. Phys. Chem.* **1994**, *98*, 13771.
- (34) Pan, R.; Raff, L. M. *J. Phys. Chem. A* **1997**, *101*, 235.
- (35) Zoval, J.; Apkarian, V. A. *J. Phys. Chem.* **1994**, *98*, 7945.
- (36) Verlet, L. *Phys. Rev.* **1967**, *159*, 98.
- (37) Bayliss, W. E. *J. Chem. Phys.* **1969**, *51*, 2665.
- (38) Bayliss, W. E. *J. Phys. B* **1977**, *10*, L477.
- (39) Pollock, E. L.; Alder, B. J. *Phys. Rev. Lett.* **1978**, *41*, 903.
- (40) Aziz, R. A. *Inert Gases*; Springer: New York, 1984.
- (41) Axilrod, B.; Teller, E. *J. Chem. Phys.* **1943**, *11*, 299.
- (42) Muto, Y. *Proc. Phys. Math. Soc. Jpn.* **1943**, *17*, 629.
- (43) Elrod, M. J.; Saykally, R. J. *Chem. Rev.* **1994**, *94*, 1975.
- (44) Barker, J. A.; Watts, R. O.; Lee, K.; Schaefer, T. P.; Lee, Y. T. *J. Chem. Phys.* **1974**, *61*, 3081.
- (45) Toennies, J. P.; Welz, W.; Wolf, G. *J. Chem. Phys.* **1979**, *71*, 614.
- (46) Hishinuma, N. *J. Chem. Phys.* **1981**, *75*, 4960.
- (47) Maitland, G. C.; Rigby, H.; Smith, E. B.; Wakeham, W. A. *Intermolecular Forces*; Clarendon Press: Oxford, 1981.
- (48) Tang, K. T.; Toennies, J. P. *Chem. Phys.* **1991**, *156*, 413.
- (49) Tang, K. T.; Toennies, J. P. *Z. Phys. D* **1986**, *1*, 91.
- (50) Mavroyannidis, C.; Stephen, M. J. *Mol. Phys.* **1962**, *5*, 629.
- (51) McLachlan, A. D. *Proc. R. Soc. London A* **1963**, *271*, 387.
- (52) Schriever, R.; Chergui, M.; Kunz, H.; Stepanenko, K. V.; Schwentner, N. *J. Chem. Phys.* **1989**, *91*, 4128.
- (53) Theodorakopoulos, G.; Farantos, S. C.; Buerker, R. J.; Peyerimhoff, S. D. *J. Phys. B: At. Mol. Phys.* **1984**, *17*, 1453.
- (54) Theodorakopoulos, G.; Petsalakis, I. D. *Chem. Phys. Lett.* **1988**, *149*, 196.
- (55) Schriever, R.; Chergui, M.; Schwentner, N. *J. Chem. Phys.* **1990**, *93*, 9206.
- (56) Aquilanti, V.; Grossi, G. *J. Chem. Phys.* **1980**, *73*, 1165.
- (57) Ellison, F. O. *J. Am. Chem. Soc.* **1963**, *85*, 3540.
- (58) Tully, J. C. *Semiempirical Methods of Electronic Structure Calculation*; Plenum: New York, 1977.
- (59) Kuntz, P. J. In *Atom-Molecule Collision Theory—A guide for the experimentalist*; Bernstein, R. B., Ed.; Plenum: New York, 1979.
- (60) Dawson, J. F.; Balling, L. C. *J. Chem. Phys.* **1979**, *71*, 836.
- (61) Balling, L. C.; Wright, J. J. *J. Chem. Phys.* **1983**, *79*, 2941.
- (62) Maillard, D.; Fournier, J.; Mohammed, H. H.; Girardet, C. *J. Chem. Phys.* **1983**, *78*, 5480.
- (63) Last, I.; George, T. F. *J. Chem. Phys.* **1987**, *87*, 1183.
- (64) Last, I.; George, T. F.; Fajardo, M. E.; Apkarian, V. A. *J. Chem. Phys.* **1987**, *87*, 5917.
- (65) Fajardo, M. E.; Apkarian, V. A. *J. Chem. Phys.* **1988**, *89*, 4102.
- (66) Schwentner, N.; Fajardo, M. E.; Apkarian, V. A. *Chem. Phys. Lett.* **1989**, *154*, 237.
- (67) Grigorenko, B. L.; Nemukhin, A. V.; Apkarian, V. A. *J. Chem. Phys.* **1996**, *104*, 5510.
- (68) Grigorenko, B. L.; Nemukhin, A. V.; Apkarian, V. A. *Chem. Phys.* **1997**, *219*, 161.
- (69) Grigorenko, B. L.; Nemukhin, A. V.; Apkarian, V. A. *J. Chem. Phys.* **1998**, *108*, 4413.
- (70) Grigorenko, B.; Nemukhin, A. V.; Ozhegova, N. V. *J. Chem. Phys.* **1998**, *296*, 84.
- (71) Von Grünberg, H. H.; Gersonde, I. H.; Gabriel, H. *Z. Phys. D: At. Mol. Clusters* **1993**, *28*, 145.
- (72) Von Grünberg, H. H.; Gabriel, H. *J. Chem. Phys.* **1996**, *105*, 4173.
- (73) Lawrence, W. G.; Apkarian, V. A. *J. Chem. Phys.* **1994**, *101*, 1820.
- (74) Fajardo, M. E. *J. Chem. Phys.* **1993**, *98*, 119.
- (75) Boatz, J. A.; Fajardo, M. E. *J. Chem. Phys.* **1994**, *101*, 3472.
- (76) Corbin, R. A.; Fajardo, M. E. *J. Chem. Phys.* **1994**, *101*, 2678.
- (77) Fajardo, M. E.; Boatz, J. A. *J. Comput. Chem.* **1997**, *18*, 381.
- (78) Fajardo, M. E.; Carrick, P. G.; Kenney, J. W. *J. Chem. Phys.* **1991**, *94*, 5812.
- (79) Fajardo, M. E. *J. Chem. Phys.* **1993**, *98*, 110.
- (80) Tam, S.; Fajardo, M. E. *J. Chem. Phys.* **1993**, *99*, 854.
- (81) Langhoff, P. W. *J. Phys. Chem.* **1996**, *100*, 2974.
- (82) Li, Z.; Apkarian, V. A.; Harding, L. B. *J. Chem. Phys.* **1997**, *106*, 942.
- (83) Danilychev, A. V.; Bondybey, V. E.; Apkarian, V. A.; Tanaka, S.; Kajihara, H.; Koda, S. *J. Chem. Phys.* **1995**, *103*, 4292.
- (84) Kuntz, P. *Chem. Phys.* **1999**, *240*, 19.
- (85) Krylov, A. I.; Gerber, R. B.; Apkarian, V. A. *Chem. Phys.* **1994**, *189*, 261.
- (86) Krylov, A. I.; Gerber, R. B.; Coalson, R. D. *J. Chem. Phys.* **1996**, *105*, 4626.
- (87) Kizer, K.; Apkarian, V. A. *J. Chem. Phys.* **1995**, *103*, 4945.
- (88) Crepin, C.; Tramer, A. *J. Chem. Phys.* **1992**, *97*, 4772.
- (89) Kerins, P. N.; McCafferey, J. G. *J. Chem. Phys.* **1998**, *109*, 3131.
- (90) Breckenridge, W. H.; Morse, M. D.; McCafferey, J. G. *J. Chem. Phys.* **1998**, *109*, 3137.
- (91) Alimi, R.; Gerber, R. B.; Apkarian, V. A. *J. Chem. Phys.* **1988**, *89*, 174.
- (92) Gersonde, I. H.; Gabriel, H. *J. Chem. Phys.* **1993**, *98*, 2094.
- (93) Gersonde, I. H.; Hennig, S.; Gabriel, H. *J. Chem. Phys.* **1994**, *101*, 9558.
- (94) Krylov, A. I.; Gerber, R. B. *J. Chem. Phys.* **1997**, *106*, 6574.
- (95) Batista, V. S.; Coker, D. F. *J. Chem. Phys.* **1997**, *106*, 6923.
- (96) Batista, V. S.; Coker, D. F. *J. Chem. Phys.* **1996**, *105*, 4033.
- (97) Buchachenko, A. A.; Stepanov, N. F. *J. Chem. Phys.* **1996**, *104*, 9913.
- (98) Buchachenko, A. A.; Stepanov, N. F. *J. Chem. Phys.* **1997**, *106*, 4358.
- (99) Zadoyan, R.; Sterling, M.; Apkarian, V. A. *J. Chem. Soc., Faraday Trans.* **1996**, *92*, 1821.
- (100) Zadoyan, R.; Sterling, M.; Ovchinnikov, M.; Apkarian, V. A. *J. Chem. Phys.* **1997**, *107*, 8446.
- (101) Alberti, S. F.; Halberstadt, N.; Beswick, J. A.; Echave, J. *J. Chem. Phys.* **1998**, *109*, 2844.
- (102) Tully, J. C. *J. Chem. Phys.* **1990**, *93*, 1061.
- (103) Hammes-Schiffer, S. T. *J. Chem. Phys.* **1994**, *101*, 4657.
- (104) Last, I.; George, T. *J. Chem. Phys.* **1988**, *89*, 3071.
- (105) Pettersson, M.; Lundell, J.; Rasanen, M. *J. Chem. Phys.* **1995**, *102*, 6423.
- (106) Pettersson, M.; Nieminen, J.; Khriachtchev, L.; Rasanen, M. *J. Chem. Phys.* **1997**, *107*, 8423.
- (107) Last, I.; George, T. F. *J. Chem. Phys.* **1990**, *93*, 8925.
- (108) Kunttu, H.; Seetula, J.; Rasanen, M.; Apkarian, V. A. *J. Chem. Phys.* **1992**, *96*, 5630.
- (109) Rasanen, M.; Seetula, J.; Kunttu, H. *J. Chem. Phys.* **1993**, *98*, 3914.
- (110) Lundell, J.; Kunttu, H. *J. Phys. Chem.* **1992**, *96*, 9774.
- (111) Lundell, J.; Nieminen, J.; Kunttu, H. *Chem. Phys. Lett.* **1993**, *208*, 247.
- (112) Lundell, J. *J. Mol. Struct.* **1995**, *355*, 291.
- (113) Lundell, J.; Rasanen, M.; Kunttu, H. *THEOCHEM* **1995**, *14*, 358.
- (114) Nieminen, J.; Kauppi, E.; Lundell, J.; Kunttu, H. *J. Chem. Phys.* **1993**, *98*, 8698.
- (115) Pettersson, M.; Lundell, J.; Rasanen, M. *J. Chem. Phys.* **1995**, *103*, 205.
- (116) Raff, L. M. *J. Chem. Phys.* **1990**, *93*, 3160.
- (117) Raff, L. M. *J. Chem. Phys.* **1991**, *95*, 8901.
- (118) Gross, M.; Spiegelmann, F. *J. Chem. Phys.* **1998**, *108*, 4149.
- (119) Tersoff, J. *Phys. Rev. B: Condens. Matter* **1989**, *39*, 5566.
- (120) Shugard, M.; Tully, J. C.; Nitzan, A. *J. Chem. Phys.* **1978**, *69*, 336.
- (121) Nitzan, A.; Shugard, M.; Tully, J. C. *J. Chem. Phys.* **1978**, *69*, 2525.
- (122) Alimi, R.; Garcavela, A.; Gerber, R. B. *J. Chem. Phys.* **1992**, *96*, 2034.
- (123) Zadoyan, R.; Li, Z.; Martens, C. C.; Apkarian, V. A. *J. Chem. Phys.* **1994**, *101*, 6648.
- (124) Sterling, M.; Li, Z.; Apkarian, V. A. *J. Chem. Phys.* **1995**, *103*, 5679.
- (125) Li, Z.; Apkarian, V. A. *J. Chem. Phys.* **1997**, *107*, 1544.
- (126) Cao, J.; Voth, G. A. *J. Chem. Phys.* **1994**, *101*, 6168.
- (127) Jang, S.; Voth, G. A. *J. Chem. Phys.* **1998**, *108*, 4098.
- (128) Lax, M. *J. Chem. Phys.* **1952**, *20*, 1752.
- (129) Kubo, R.; Toyozawa, Y. *Prog. Theor. Phys.* **1955**, *13*, 160.
- (130) Gordon, R. G. *J. Chem. Phys.* **1965**, *43*, 1307.
- (131) Gordon, R. G. *Adv. Magn. Reson.* **1968**, *3*, 1.
- (132) Heller, E. J. *Acc. Chem. Res.* **1981**, *14*, 368.
- (133) Cao, J.; Voth, G. A. *J. Chem. Phys.* **1993**, *99*, 10070.
- (134) Alimi, R.; Gerber, R. B. *Chem. Phys. Lett.* **1990**, *173*, 393.
- (135) Manz, J.; Saalfrank, P.; Schmidt, B. *J. Chem. Soc., Faraday Trans.* **1997**, *93*, 957.
- (136) Neugebauer, F.; May, V. *J. Lumin.* **1997**, *72*–*74*, 963.
- (137) Neugebauer, F.; May, V. *Chem. Phys. Lett.* **1998**, *289*, 67.
- (138) Gödderz, K. H.; Schwentner, N.; Chergui, M. *J. Chem. Phys.* **1996**, *109*, 91.
- (139) Jungwirth, P.; Fredj, E.; Gerber, R. B. *J. Chem. Phys.* **1997**, *107*, 8963.
- (140) Messina, M.; Coalson, R. D. *J. Chem. Phys.* **1989**, *90*, 4015.
- (141) Liu, L.; Guo, H. *Chem. Phys. Lett.* **1995**, *237*, 299.
- (142) Liu, L.; Guo, H. *J. Chem. Phys.* **1996**, *104*, 528.
- (143) Howard, W. F., Jr.; Andrews, L. *J. Raman Spectrosc.* **1975**, *2*, 447.
- (144) Grzybowski, J. M.; Andrews, L. *J. Raman Spectrosc.* **1975**, *4*, 99.
- (145) Kono, H.; Lin, S. H. *J. Chem. Phys.* **1986**, *84*, 1071.

- (146) Xu, J.; Schwentner, N.; Hennig, S.; Chergui, M. *J. Chim. Phys.* **1995**, *92*, 541.
- (147) Jungwirth, P.; Gerber, R. B. *J. Chem. Phys.* **1995**, *102*, 8855.
- (148) Jungwirth, P.; Fredj, E.; Gerber, R. B. *J. Chem. Phys.* **1996**, *104*, 9332.
- (149) Ovchinnikov, M.; Apkarian, V. A. *J. Chem. Phys.* **1996**, *105*, 10312.
- (150) Ovchinnikov, M.; Apkarian, V. A. *J. Chem. Phys.* **1997**, *106*, 5775.
- (151) Ovchinnikov, M.; Apkarian, V. A. *J. Chem. Phys.* **1998**, *108*, 2277.
- (152) Herman, M. F.; Kluk, E. *Chem. Phys.* **1984**, *91*, 27.
- (153) Herman, M. F. *J. Chem. Phys.* **1986**, *85*, 2069.
- (154) Heller, E. J. *J. Chem. Phys.* **1981**, *75*, 2993.
- (155) Mandelshtam, V. A.; Ovchinnikov, M. *J. Chem. Phys.* **1998**, *108*, 9206.
- (156) Spath, B. W.; Raff, L. M. *J. Phys. Chem.* **1992**, *96*, 2179.
- (157) Raff, L. M. *J. Chem. Phys.* **1992**, *97*, 7459.
- (158) Agrawal, P. M.; Thompson, D. L.; Raff, L. M. *J. Chem. Phys.* **1994**, *101*, 9937.
- (159) *Vibrational Spectroscopy of Trapped Species*; Hallam, E. H., Ed.; Wiley: London, 1973.
- (160) Moskovits, M.; Andrews, L. E. *Chemistry and Physics of Matrix-Isolated Species*; North-Holland Physics Publishing Amsterdam, 1988.
- (161) Ball, D. W.; Kafafi, Z. H.; Fredin, L.; Hauge, R. H.; Margrave, J. L. *A Bibliography of Matrix Isolation Spectroscopy 1954–1985*; Rice University Press: Houston, 1988.
- (162) Ochsner, D. W.; Ball, D. W.; Kafafi, Z. H. *A Bibliography of Matrix Isolation Spectroscopy 1985–1997*; NTIS: Washington, DC, 1998.
- (163) Bondybey, V. E.; Smith, A. M.; Agreiter, J. *Chem. Rev.* **1996**, *96*, 2113.
- (164) Perutz, R. *Chem. Rev.* **1985**, *85*, 97.
- (165) *Photophysics of Matrix-Isolated molecules*; Apkarian, V. A., Bondybey, V. E., Eds.; 1994; Vol. 189.
- (166) Schwentner, N. *J. Mol. Struct.* **1990**, *222*, 151.
- (167) Schwentner, N.; Chergui, M.; Kunz, H.; McCaffrey, J. G. In *In Reaction Dynamics in Clusters and Condensed Phases*; Jortner, J. L., Pullmann, B., Ed.; Kluwer Academic Publishers: Dordrecht, 1993.
- (168) Chergui, M.; Schwentner, N. *Trends Chem. Phys.* **1992**, *2*, 89.
- (169) Haas, Y.; Samuni, U. In *Research in chemical kinetics*; Hancock, C., Lampton, R., Eds.; Clackwell Science: 1998.
- (170) Schwentner, N.; Koch, E.-E.; Jortner, J. *Electronic excitations in Condensed rare gases*; Springer-Verlag: Berlin, 1985.
- (171) Klein, M. L.; Venables, J. A. *Rare gas solids*; Academic Press: New York, 1976.
- (172) Klein, M. L.; Venables, J. A. *Rare gas solids*; Academic Press: New York, 1977.
- (173) *Inert Gases: Potentials, Dynamics, and Energy Transfer in Doped Crystals*; Klein, M. L., Ed.; Springer-Verlag: Berlin, 1984; Vol. 34.
- (174) Benderskii, V. A.; Makarov, D. E.; Wight, C. A. *Chemical Dynamics at Low Temperatures*; John Wiley & Sons Inc.: New York, 1994.
- (175) Klein, M. L.; Lewis, L. *J. Chem. Rev.* **1990**, *90*, 459.
- (176) Dubost, H. In *Inert Gases*; Klein, M. L., Ed.; Springer-Verlag: Berlin, 1984; Vol. 34.
- (177) Whitnell, R. M.; Wilson, K. R. In *Reviews of Computational Chemistry*; Lipkowitz, K. B., Boyd, D. B., Eds.; VCH: New York, 1994; Vol. IV.
- (178) Gerber, R. B.; McCoy, A. B.; Garcia-Vela, A. *Annu. Rev. Phys. Chem.* **1994**, *45*, 273.
- (179) Legay, F. In *Chemical and biochemical applications of lasers*; Moore, C. B., Ed.; Academic Press: New York, 1977; Vol. 2.
- (180) Bondybey, V. E.; Brus, L. E. In *Radiationless Transitions*; Lin, S. H., Ed.; Academic Press: New York, 1980.
- (181) Salloum, A.; Dubost, H. *Chem. Phys.* **1994**, *189*, 179.
- (182) Egorov, S. A.; Skinner, J. L. *J. Chem. Phys.* **1995**, *103*, 1533.
- (183) Egorov, S. A.; Skinner, J. L. *J. Chem. Phys.* **1996**, *105*, 10153.
- (184) Egorov, S. A.; Berne, B. J. *J. Chem. Phys.* **1997**, *107*, 6050.
- (185) Egorov, S. A.; Skinner, J. L. *J. Chem. Phys.* **1997**, *106*, 1034.
- (186) Bachir, I. H.; Charneau, R.; Dubost, H. *Chem. Phys.* **1992**, *164*, 451.
- (187) Bachir, I. H.; Charneau, R.; Dubost, H. *Chem. Phys.* **1993**, *177*, 675.
- (188) Apkarian, V. A. *Chem. Phys. Lett.* **1984**, *110*, 168.
- (189) Jasmin, D.; Brosset, P.; Dahoo, R.; Gautier-Roy, B.; Abouaf-Marguin. *J. Chem. Phys.* **1998**, *108*, 2302.
- (190) Dubost, H.; Charneau, R.; Chergui, M.; Schwentner, N. *J. Lumin.* **1991**, *48*–*49*, 853.
- (191) Kühle, H.; Fröhling, R.; Bahrdt, J.; Schwentner, N. *J. Chem. Phys.* **1986**, *84*, 666.
- (192) Kusznier, D.; Schwentner, N. *J. Lumin.* **1991**, *48/49*, 273.
- (193) Bahrdt, J.; Schwentner, N. *J. Chem. Phys.* **1988**, *88*, 2869.
- (194) Chergui, M.; Schriever, R.; Schwentner, N. *J. Chem. Phys.* **1988**, *89*, 7083.
- (195) Chergui, M.; Schwentner, N. *J. Chem. Phys.* **1989**, *91*, 5993.
- (196) Vigliotti, F.; Chergui, M.; Dickgiesser, M.; Schwentner, N. *Faraday Discuss.* **1997**, *108*, 139.
- (197) Hoffman, G. J.; Imre, D. G.; Zadayan, R.; Schwentner, N.; Apkarian, V. A. *J. Chem. Phys.* **1993**, *98*, 9233.
- (198) Zadayan, R.; Li, Z.; Martens, C. C.; Ashjian, P.; Apkarian, V. A. *Chem. Phys. Lett.* **1994**, *218*, 504.
- (199) Li, Z.; Zadayan, R.; Apkarian, V. A.; Martens, C. C. *J. Phys. Chem.* **1995**, *99*, 7453.
- (200) Zadayan, R.; Almy, J.; Apkarian, V. A. *J. Chem. Soc., Faraday Discuss.* **1997**, *108*, 255.
- (201) Bader, J. S.; Berne, B. J.; Pollak, E.; Hanggi, P. *J. Chem. Phys.* **1996**, *104*, 1111.
- (202) Bardeen, C. J.; Che, J.; Wilson, K. R.; Yakovlev, V. V.; Apkarian, V. A.; Martens, C. C.; Zadayan, R.; Kohler, B.; Messina, M. *J. Chem. Phys.* **1997**, *106*, 8486.
- (203) Zadayan, R.; Schwentner, N.; Apkarian, V. A. *Chem. Phys.* **1998**, *233*, 353–363.
- (204) Broquier, M.; Dubost, H.; Kolos, R.; Lefevre, J.; Tramer, A.; Berset, J. M.; Ortega, J. M.; Peremans, A. *Opt. Commun.* **1995**, *118*, 255.
- (205) Roubin, P.; Berset, J. M.; Cardonatto, S.; Dubost, H.; Lefevre, J.; Ortega, J. M. *J. Phys. IV* **1994**, *4*, 385.
- (206) Roubin, P.; Berset, J. M.; Cardonatto, S.; Dubost, H.; Lefevre, J.; Ortega, J. M. *J. Chem. Phys.* **1994**, *101*, 3403.
- (207) Winn, J. S. *J. Chem. Phys.* **1991**, *94*, 5275.
- (208) Anderson, D. T.; Winn, J. S. *Chem. Phys.* **1994**, *189*, 171.
- (209) Lang, V. I.; Winn, J. S. *J. Chem. Phys.* **1991**, *94*, 5270.
- (210) Wurfel, B. E.; Schallmoser, G.; Lask, G. M.; Agreiter, J.; Thoma, A.; Schlachta, R.; Bondybey, V. E. *Chem. Phys.* **1993**, *174*, 255.
- (211) Schallmoser, G.; Thoma, A.; Wurfel, B. E.; Bondybey, V. E. *Chem. Phys. Lett.* **1994**, *219*, 101.
- (212) Thoma, A.; Schallmoser, G.; Smith, A. M.; Wurfel, B. E.; Bondybey, V. E. *J. Chem. Phys.* **1994**, *100*, 5387.
- (213) Blindauer, C.; Van Riesenbeck, N.; Seranski, K.; Winter, M.; Becker, A. C.; Schurath, U. *Chem. Phys.* **1991**, *150*, 93.
- (214) Blindauer, C.; Peric, M.; Schurath, U. *J. Mol. Spectrosc.* **1993**, *158*, 177.
- (215) Hennig, S.; Cenian, A.; Gabriel, H. *Chem. Phys. Lett.* **1993**, *205*, 354.
- (216) Perutz, R. N.; Turner, J. J. *J. Chem. Soc., Faraday Trans. 1* **1973**, *69*, 452.
- (217) Schulze, W.; Kolb, D. M. *J. Chem. Soc., Far. Trans. 1* **1974**, *70*, 1098.
- (218) Schulze, W.; Becker, H. U.; Abe, H. *Phys. Chem.* **1978**, *82*, 138.
- (219) Schilling, G.; Ernst, W. E.; Schwentner, N. *IEEE J. Quantum Electron.* **1993**, *29*, 2702.
- (220) Schilling, G.; Ernst, W. E.; Schwentner, N. *Appl. Phys. B: Lasers Opt.* **1994**, *58*, 267.
- (221) Silverman, D. C.; Fajardo, M. E. *J. Chem. Phys.* **1997**, *106*, 8964.
- (222) Macler, M.; Fajardo, M. E. *Appl. Phys. Lett.* **1994**, *65*, 2275.
- (223) Thoma, A.; Wurfel, B. E.; Schlachta, R.; Lask, G. M.; Bondybey, V. E. *J. Phys. Chem.* **1992**, *96*, 7231.
- (224) Varding, D.; Reimand, I.; Zimmerer, G. *Phys. Status Solidi b* **1994**, *185*, 301.
- (225) Bressler, C.; Dickgiesser, M.; Schwentner, N. *J. Chem. Phys.* **1997**, *107*, 10268.
- (226) Schuberth, E. M.; Creuzburg, E. M. *Phys. Status Solidi B* **1975**, *71*, 797.
- (227) Rudnick, W.; Haensel, R.; Nahme, H.; Schwentner, N. *Phys. Status Solidi a* **1985**, *87*, 319.
- (228) Schwentner, N.; Apkarian, V. A. *Chem. Phys. Lett.* **1989**, *154*, 413.
- (229) Hoffman, G. J.; Apkarian, V. A. *J. Phys. Chem.* **1991**, *95*, 5372.
- (230) Lawrence, W. G.; Apkarian, V. A. *J. Chem. Phys.* **1992**, *97*, 2224.
- (231) Koga, K.; Takami, A.; Koda, S. *Chem. Phys. Lett.* **1998**, *293*, 180–184.
- (232) Kajihara, H.; Okamura, T.; Koda, S. *J. Mol. Spectrosc.* **1997**, *183*, 72.
- (233) Kizer, K. S. UC, Irvine, 1998.
- (234) Misochko, E. Y.; Akimov, A. V.; Wight, C. A. *Chem. Phys. Lett.* **1998**, *293*, 547.
- (235) Fraenkel, R.; Haas, Y. *Chem. Phys. Lett.* **1994**, *220*, 77.
- (236) Fraenkel, R.; Haas, Y. *Chem. Phys.* **1994**, *186*, 185.
- (237) Fraenkel, R.; Haas, Y. *J. Chem. Phys.* **1994**, *100*, 4324.
- (238) Becker, A. C.; Lodemann, K. P.; Schurath, U. *J. Chem. Phys.* **1987**, *87*, 6266.
- (239) Seranski, K.; Winter, M.; Schurath, U. *Chem. Phys.* **1992**, *159*, 247.
- (240) Fajardo, M. E.; Tam, S.; Thompson, T. L.; Cordonnier, M. E. *Chem. Phys.* **1994**, *189*, 351.
- (241) Fajardo, M. E.; Tam, S. *J. Chem. Phys.* **1998**, *108*, 4237–4241.
- (242) Momose, T.; Shida, T. *Bull. Chem. Soc. Jpn.* **1998**, *71*, 1–15.
- (243) Momose, T. *J. Low Temp. Phys.* **1998**, *111*, 469–474.
- (244) Fujisaki, A.; Sano, K.; Kinoshita, T.; Takahashi, Y.; Yabuzaki, T. *Phys. Rev. Lett.* **1993**, *71*, 1039.
- (245) Hui, Q.; Persson, J. L.; Beijersbergen, J. H. M.; Takami, M. Z. *Phys. B* **1995**, *98*, 353.
- (246) Toennies, J. P.; Vilesov, A. F. *Annu. Rev. Phys. Chem.* **1998**, *49*, 1.

- (247) Hill, M. W.; Zadayan, R.; Apkarian, V. A. *Chem. Phys. Lett.* **1992**, *200*, 251.
- (248) Fajardo, M. E.; Apkarian, V. A. *J. Chem. Phys.* **1986**, *85*, 5660.
- (249) Fajardo, M. E.; Apkarian, V. A. *J. Chem. Phys.* **1988**, *89*, 4124.
- (250) Gudipati, M. S. *J. Phys. Chem.* **1997**, *101*, 2003–2009.
- (251) Schwentner, N.; Bressler, C.; Lawrence, W.; Xu, J.; Chergui, M. *Chem. Phys.* **1994**, *189*, 205.
- (252) Macler, M.; Nicolai, J. P.; Heaven, M. *J. Chem. Phys.* **1989**, *91*, 674.
- (253) Macler, M.; Heaven, M. *Chem. Phys.* **1991**, *151*, 219.
- (254) Borrmann, A.; Martens, C. C. *J. Chem. Phys.* **1995**, *102*, 1905.
- (255) Cenian, A.; Hennig, S.; Gabriel, H. *J. Chem. Phys.* **1995**, *102*, 9276.
- (256) Rose, D. A.; Martens, C. C. *J. Phys. Chem. A* **1997**, *101*, 4613.
- (257) Brus, L. E.; Bondybey, V. E. *J. Chem. Phys.* **1976**, *65*, 71.
- (258) Benderskii, A. V.; Zadayan, R.; Apkarian, V. A. *J. Chem. Phys.* **1997**, *107*, 8437.
- (259) Becker, A. C.; Schurath, U.; Dubost, H.; Galaup, J. P. *J. Chem. Phys.* **1988**, *125*, 321.
- (260) Bondybey, V. E.; Brus, L. E. *J. Chem. Phys.* **1976**, *64*, 3724.
- (261) Bondybey, V. E.; Brus, L. E. *J. Chem. Phys.* **1975**, *65*, 620.
- (262) Bondybey, V. E.; Fletcher, C. *J. Chem. Phys.* **1976**, *64*, 3615.
- (263) Bondybey, V. E.; Bearder, S. S.; Fletcher, C. *J. Chem. Phys.* **1976**, *64*, 5243.
- (264) Beeken, P.; Mandich, M.; Flynn, G. *J. Chem. Phys.* **1982**, *76*, 5995.
- (265) Mandich, M.; Beeken, P.; Flynn, G. *J. Chem. Phys.* **1982**, *77*, 702.
- (266) Beeken, P.; Hanson, E. A.; Flynn, G. *J. Chem. Phys.* **1983**, *78*, 5892.
- (267) Fajardo, M. E.; Withnall, R.; Feld, J.; Okada, F.; Lawrence, W.; Wiedeman, L.; Apkarian, V. A. *Laser Chem.* **1988**, *9*, 1.
- (268) Lai, L.-H.; Liu, C.-P.; Lee, Y.-P. *J. Chem. Phys.* **1998**, *109*, 988.
- (269) Liu, C.-P.; Lai, L.-H.; Lee, Y.-Y.; Hung, S.-C.; Lee, Y.-P. *J. Chem. Phys.* **1998**, *109*, 978.
- (270) Kölml, J.; Schrems, O.; Beichert, P. *J. Phys. Chem. A* **1998**, *102*, 1083.
- (271) Johnsson, K.; Engdahl, A.; Ouis, P.; Nelander, B. *J. Phys. Chem.* **1992**, *96*, 5778.
- (272) Johnsson, K.; Engdahl, A.; Ouis, P.; Nelander, B. *J. Mol. Struct.* **1993**, *293*, 137.
- (273) Muller, H. S. P.; Willner, H. *J. Phys. Chem.* **1993**, *97*, 10589.
- (274) Gole, J. L. *J. Phys. Chem.* **1980**, *84*, 1333.
- (275) Arkell, A.; Schwager, I. *J. Am. Chem. Soc.* **1967**, *89*, 5999.
- (276) Rochkind, M. M.; Pimentel, G. C. *J. Chem. Phys.* **1967**, *46*, 4481.
- (277) Alcock, W. G.; Pimentel, G. C. *J. Chem. Phys.* **1968**, *48*, 2373.
- (278) Peterson, K. A.; Werner, H. J. *J. Chem. Phys.* **1992**, *96*, 8948.
- (279) Peterson, K. A.; Werner, H. J. *J. Chem. Phys.* **1996**, *105*, 9823.
- (280) Esposito, A. P.; Foster, C. E.; Beckman, R. A.; Reid, P. J. *J. Phys. Chem. A* **1997**, *101*, 5309.
- (281) Qian, J. W.; Tannor, D. J.; Amatatsu, Y.; Morokuma, K. *J. Chem. Phys.* **1994**, *101*, 9597.
- (282) Yabushita, S.; Morokuma, K. *Chem. Phys. Lett.* **1990**, *175*, 518.
- (283) Amatatsu, Y.; Yabushita, S.; Morokuma, K. *J. Chem. Phys.* **1994**, *100*, 4894.
- (284) Amatatsu, Y.; Morokuma, K. *Chem. Phys. Lett.* **1995**, *245*, 469.
- (285) Krylov, A. I.; Gerber, R. B. *J. Chem. Phys.* **1994**, *100*, 4242.
- (286) Benjamin, I.; Wilson, K. R. *J. Chem. Phys.* **1989**, *90*, 4176.
- (287) Benjamin, I. *J. Chem. Phys.* **1995**, *103*, 2459.
- (288) Fraenkel, R.; Haas, Y. *Chem. Phys. Lett.* **1993**, *214*, 234.
- (289) Fraenkel, R.; Haas, Y. *Chem. Phys. Lett.* **1994**, *226*, 610.
- (290) Samuni, U.; Kahana, S.; Fraenkel, R.; Haas, Y.; Danovich, D.; Shaik, S. *Chem. Phys. Lett.* **1994**, *225*, 391.
- (291) Samuni, U.; Kahana, S.; Fraenkel, R.; Haas, Y.; Danovich, D.; Shaik, S. *Chem. Phys. Lett.* **1994**, *231*, 124.
- (292) Easley, W. C.; Weltner, W. J. *J. Chem. Phys.* **1970**, *52*, 197.
- (293) Wan, C.; Gupta, M.; Zewail, A. H. *Chem. Phys. Lett.* **1996**, *256*, 279.
- (294) Mulliken, R. S. *J. Chem. Phys.* **1971**, *55*, 288.
- (295) Steinfeld, J. I. *Acc. Chem. Res.* **1970**, *3*, 313.
- (296) Schroeder, J.; Troe, J. *Annu. Rev. Phys. Chem.* **1987**, *38*, 163.
- (297) Smalley, R. E.; Wharton, L.; Levy, D. H. *J. Chem. Phys.* **1978**, *68*, 671.
- (298) Chuang, T. J.; Hoffman, G. W.; Eisenthal, K. B. *Chem. Phys. Lett.* **1974**, *25*, 201.
- (299) Chuang, T. J.; Hoffman, G. W.; Eisenthal, K. B. *Acc. Chem. Res.* **1975**, *8*, 118.
- (300) Harris, A. L.; Brown, J. K.; Harris, C. B. *Annu. Rev. Phys. Chem.* **1988**, *39*, 341.
- (301) Potter, E. D.; Liu, Q.; Zewail, A. H. *Chem. Phys. Lett.* **1992**, *200*, 605.
- (302) Liu, Q. L.; Wang, J. K.; Zewail, A. H. *J. Phys. Chem.* **1995**, *99*, 11321.
- (303) Liu, Q.; Wan, C.; Zewail, A. H. *J. Chem. Phys.* **1996**, *105*, 5294.
- (304) Scherer, N. F.; Jonas, D. M.; Fleming, G. R. *J. Chem. Phys.* **1993**, *99*, 153.
- (305) Xu, J.; Schwentner, N.; Chergui, M. *J. Chem. Phys.* **1994**, *101*, 7381.
- (306) Xu, J.; Schwentner, N.; Hennig, S.; Chergui, M. *J. Raman Spectrosc.* **1997**, *28*, 433.
- (307) Ben-Nun, M.; Levine, R. D.; Jonas, M.; Flemming, G. R. *Chem. Phys. Lett.* **1995**, *245*, 629.
- (308) Ben-Nun, M.; Levine, R. D.; Flemming, G. R. *J. Chem. Phys.* **1996**, *105*, 3035.
- (309) Tellinghuisen, J. *J. Chem. Phys.* **1985**, *82*, 4012.
- (310) Chergui, M.; Schwentner, N. *J. Chem. Phys.* **1992**, *97*, 2881.
- (311) Chergui, M.; Schwentner, N. *Chem. Phys. Lett.* **1994**, *219*, 237.
- (312) May, V.; Suisky, D.; Chergui, M.; Schwentner, N. *Chem. Phys. Lett.* **1992**, *200*, 325.
- (313) Zerza, G.; Vigliotti, F.; Sassara, A.; Chergui, M.; Stepanenko, V. *Chem. Phys. Lett.* **1996**, *256*, 63.
- (314) Portella-Oberli, M. T.; Jeannin, C.; Chergui, M. *Chem. Phys. Lett.* **1996**, *259*, 475.
- (315) Jeannin, C.; Portella-Oberli, M. T.; Vigliotti, F.; Chergui, M. *Chem. Phys. Lett.* **1997**, *279*, 65.
- (316) Jimenez, S.; Pasquarello, A.; Car, R.; Chergui, M. *Chem. Phys.* **1998**, *233*, 343.
- (317) Eloranta, J. V. K.; Hakkanen, H.; Kiljunen, T.; Kunttu, H. *J. Chem. Phys.* **1998**, *109*, 7784.
- (318) Kraas, M.; Görtler, P. *Chem. Phys. Lett.* **1991**, *183*, 264.
- (319) Kraas, M.; Görtler, P. *Chem. Phys. Lett.* **1991**, *187*, 527.
- (320) Zerza, G.; Sliwinski, G.; Hoffman, J.; Imre, D. G.; Apkarian, V. A. *J. Chem. Phys.* **1993**, *99*, 10178.
- (321) Bressler, C.; Lawrence, W.; Schwentner, N. *J. Chem. Phys.* **1996**, *105*, 1318.
- (322) Wörmer, J.; Möller, T.; Stapelfeldt, J.; Zimmerer, G.; Haaks, D.; Kampf, S.; Le Calvé, I.; Castex, M. *C. Z. Phys. D* **1988**, *7*, 383.
- (323) Görtler, P.; Kunz, H.; Le Calvé, J. *J. Chem. Phys.* **1989**, *91*, 6020.
- (324) McCaffrey, J. G.; Kunz, H.; Schwentner, N. *J. Chem. Phys.* **1992**, *96*, 155.
- (325) McCaffrey, J. G.; Kunz, H.; Schwentner, N. *J. Chem. Phys.* **1992**, *96*, 2825.
- (326) Gödderz, K. H.; Schwentner, N.; Chergui, M. *J. Chem. Phys.* **1996**, *105*, 451.
- (327) Chergui, M.; Schwentner, N.; Stepanenko, V. *Chem. Phys.* **1994**, *187*, 153.
- (328) Zoval, J.; Imre, D.; Apkarian, V. A. *J. Chem. Phys.* **1993**, *98*, 1.
- (329) Tiee, J. J.; Ferris, M. J.; Loge, G. W.; Wampler, F. B. *Chem. Phys. Lett.* **1983**, *96*, 422.
- (330) Hirst, D. M.; Guest, M. F. *Mol. Phys.* **1982**, *46*, 427.
- (331) Wheeler, M. D.; Orr-Ewing, A. J.; Ashfold, M. N. R. *J. Chem. Phys.* **1997**, *107*, 7591.
- (332) Kunz, H.; McCaffrey, J. G.; Chergui, M.; Schriever, R.; Ünal, Ö.; Schwentner, N. *J. Lumin.* **1991**, *48/49*, 621.
- (333) Yang, M.-C.; Salzberg, A. P.; Chang, B.-C.; Carter, C. C.; Miller, T. A. *J. Chem. Phys.* **1993**, *98*, 4301.
- (334) Yang, M. C.; Carter, C. C.; Miller, T. A. *J. Chem. Phys.* **1997**, *107*, 3437.
- (335) Applegate, B. E.; Yang, M. C.; Miller, T. A. *J. Chem. Phys.* **1998**, *109*, 162–169.
- (336) Korambath, P. P.; Wu, X. T.; Hayes, E. F.; Carter, C. C.; Miller, T. A. *J. Chem. Phys.* **1997**, *107*, 3460.
- (337) Khriachtchev, L.; Pettersson, M.; Isoniemi, E.; Rasanen, M. *J. Chem. Phys.* **1998**, *108*, 5747.
- (338) Dunning, T. H.; Hay, P. J. *J. Chem. Phys.* **1977**, *66*, 3767.
- (339) Dunning, T. H.; Hay, P. J. *J. Chem. Phys.* **1981**, *74*, 3718.
- (340) Becker, C. H.; Casavecchia, P.; Lee, Y. T. *J. Chem. Phys.* **1979**, *70*, 2986.
- (341) Aquilanti, V.; Luzzati, E.; Pirani, E.; Volpi, G. G. *J. Chem. Phys.* **1988**, *89*, 6165.
- (342) Lo, G.; Setsler, D. W. *J. Chem. Phys.* **1994**, *100*, 5432.
- (343) Nemukhin, A. V.; Grigorenko, B. L.; Granovsky, A. A. **1998**, Submitted for publication.
- (344) Goodman, J.; Tully, J. C.; Bondybey, V. E.; Brus, L. *J. Chem. Phys.* **1977**, *66*, 4802.
- (345) Goodman, J.; Brus, L. E. *J. Chem. Phys.* **1976**, *65*, 3808.
- (346) Schröder, D.; Harvey, J. N.; Aschi, M.; Schwarz, H. *J. Chem. Phys.* **1998**, *108*, 8446.
- (347) Hoffman, G. J.; Swafford, L. A.; Cave, R. J. *J. Chem. Phys.* **1998**, *109*, 10701.
- (348) Kunttu, H.; Apkarian, V. A. *Chem. Phys. Lett.* **1990**, *171*, 423.
- (349) Alimi, R.; Gerber, R. B.; Apkarian, V. A. *J. Chem. Phys.* **1990**, *92*, 3551.
- (350) Alimi, R.; Gerber, R. B.; Apkarian, V. A. *Phys. Rev. Lett.* **1991**, *66*, 1295.
- (351) Benderskii, A. V.; Wight, C. A. *J. Chem. Phys.* **1994**, *101*, 292.
- (352) Brosset, P.; Dahoo, R.; Gauthier-Roy, B.; Abouaf-Marguin, L.; Lakhli, A. *Chem. Phys.* **1993**, *172*, 315.
- (353) Lakhli, A.; Girardet, C.; Dahoo, R.; Brosset, P.; Gauthier-Roy, B.; Abouaf-Marguin, L. *Chem. Phys.* **1993**, *177*, 31.
- (354) Dahoo, P. R.; Berrodier, I.; Raducu, V.; Teffo, J. L.; Chabi, H.; Lakhli, A.; Abouaf-Marguin, L. *Eur. Phys. J.* **1999**, *D 5*, 71.
- (355) Schriver-Mazzuoli, L.; de Saxe, A.; Lugez, C.; Camy-Peyret, C.; Schriver, A. *J. Chem. Phys.* **1995**, *102*, 690.
- (356) Bahou, M.; Schriver-Mazzuoli, L.; Camy-Peyret, C.; Schriver, A. *Chem. Phys. Lett.* **1997**, *273*, 31.

- (357) Dyer, M. J.; Bressler, C. G.; Copeland, R. A. *Chem. Phys. Lett.* **1997**, *266*, 548.
- (358) Benderskii, A. V.; Wight, C. A. *Chem. Phys.* **1994**, *189*, 307.
- (359) Bahou, M.; Schriver-Mazzuoli, L.; Camy-Peyret, C.; Schriver, A. *J. Chem. Phys.* **1998**, *108*, 6884.
- (360) Tanaka, S.; Kajihara, H.; Koda, S.; Apkarian, V. A. *Chem. Phys. Lett.* **1995**, *233*, 555.
- (361) Gerber, R. B.; Alimi, R. *Chem. Phys. Lett.* **1990**, *93*, 393.
- (362) Lawrence, W.; Okada, F.; Apkarian, V. A. *Chem. Phys. Lett.* **1988**, *150*, 339.
- (363) Schriever, R.; Chergui, M.; Ünal, Ö.; Schwentner, N.; Stepanenko, V. *J. Chem. Phys.* **1990**, *93*, 3245.
- (364) Schriever, R.; Chergui, M.; Schwentner, N. *J. Phys. Chem.* **1991**, *95*, 6124.
- (365) Cheng, B. M.; Lo, W. J.; Lai, L. H.; Hung, W. C.; Lee, Y. P. *J. Chem. Phys.* **1995**, *103*, 6303.
- (366) Adams, G. F.; Chabalowski, C. F. *J. Phys. Chem.* **1994**, *98*, 5878.
- (367) Gersonde, I. H. Freie Universität Berlin, 1992.
- (368) Tarasova, E. I.; Ratner, A. M.; Stepanenko, V. M.; Fugol, I. Y.; Chergui, M.; Schriever, R.; Schwentner, N. *J. Chem. Phys.* **1993**, *98*, 7786.
- (369) Alimi, R.; Brokman, A.; Gerber, R. B. *J. Chem. Phys.* **1989**, *91*, 1611.
- (370) Alimi, R.; Apkarian, V. A.; Gerber, R. B. *J. Chem. Phys.* **1993**, *98*, 331.
- (371) Alimi, R.; Gerber, R. B.; McCaffrey, J. G.; Kunz, H.; Schwentner, N. *Phys. Rev. Lett.* **1992**, *69*, 856.
- (372) Kunz, H.; McCaffrey, J. G.; Chergui, M.; Schriever, R.; Ünal, Ö.; Stepanenko, V.; Schwentner, N. *J. Chem. Phys.* **1991**, *95*, 1466.
- (373) Kunz, H.; McCaffrey, J. G.; Schriever, R.; Schwentner, N. *J. Chem. Phys.* **1991**, *94*, 1039.
- (374) Katz, A. I.; Feld, J.; Apkarian, V. A. *Opt. Lett.* **1989**, *14*, 441.
- (375) Kunttu, H.; Lawrence, W. G.; Apkarian, V. A. *J. Chem. Phys.* **1991**, *94*, 1692.
- (376) Zerza, G.; Knopp, F.; Kometer, R.; Sliwinski, G.; Schwentner, N. *SPIE* **1991**, *1410*, 202.
- (377) Zerza, G.; Sliwinski, G.; Schwentner, N. *Appl. Phys. B* **1992**, *55*, 331.
- (378) Sliwinski, G.; Schwentner, N. *SPIE* **1996**, 23.
- (379) Kunttu, H.; Feld, J.; Alimi, R.; Becker, A.; Apkarian, V. A. *J. Chem. Phys.* **1990**, *92*, 4856.
- (380) Kunttu, H.; Sekreta, E.; Apkarian, V. A. *J. Chem. Phys.* **1991**, *94*, 7819.
- (381) Misochko, E. Y.; Benderskii, A. V.; Wight, C. A. *J. Phys. Chem.* **1996**, *100*, 4496.
- (382) Misochko, E. Y.; Benderskii, V. A.; Goldschleger, A. U.; Akimov, A. V.; Benderskii, A. V.; Wight, C. A. *J. Chem. Phys.* **1997**, *106*, 3135.
- (383) Goldschleger, A. U.; Misochko, E. Y.; Akimov, A. V.; Goldschleger, I. U.; Benderskii, V. A. *Chem. Phys. Lett.* **1997**, *267*, 288.
- (384) Becker, C. H.; Casavecchia, P.; Lee, Y. T. *J. Chem. Phys.* **1979**, *70*, 2986.
- (385) Muto, H.; Nunome, K.; Iwasaki, M. *J. Phys. Chem.* **1980**, *84*, 3402.
- (386) Toriyama, K.; Nunome, K.; Iwasaki, M. *J. Phys. Chem.* **1980**, *84*, 2374.
- (387) Wittl, F.; Eberlein, J.; Epple, T.; Dechant, M.; Creuzburg, M. *J. Chem. Phys.* **1993**, *98*, 9554.
- (388) Eberlein, J.; Creuzburg, M. *J. Chem. Phys.* **1997**, *106*, 2188.
- (389) LaBrake, D.; Weitz, E. *Chem. Phys. Lett.* **1993**, *211*, 430.
- (390) Vaskonen, K. E. J.; Kiljunen, T.; Kunttu, H. *J. Chem. Phys.* **1999**, *110*, 2122.
- (391) LaBrake, D.; Ryan, E. T.; Weitz, E. *J. Chem. Phys.* **1995**, *102*, 4112.
- (392) Fairbrother, D. H.; LaBrake, D.; Weitz, E. *J. Phys. Chem.* **1996**, *100*, 18848.
- (393) Eloranta, J.; Vaskonen, K.; Kunttu, H. *J. Chem. Phys.* **1999**, in press.
- (394) Von Grünberg, H. H.; Gabriel, H. *Chem. Phys. Lett.* **1992**, *192*, 503.
- (395) Schuberth, E. M.; Creuzburg, E. M.; Müller-Liesheim, W. *Phys. Status Solidi B* **1976**, *76*, 301.
- (396) Kometer, R.; Legay, F.; Legay-Sommaire, N.; Schwentner, N. *J. Chem. Phys.* **1994**, *100*, 8737.
- (397) Dubov, V. S.; Gudzenko, L. I.; Gurvich, L. V.; Iakovlenko, S. I. *Chem. Phys. Lett.* **1977**, *45*, 330.
- (398) Tamagake, K.; Kolts, J. H.; Setser, D. W. *J. Chem. Phys.* **1979**, *71*, 1264.
- (399) Nelson, T. O.; Setser, D. W.; Qin, J. *J. Phys. Chem.* **1993**, *97*, 2585.
- (400) Boivineau, M.; Le Calve, J.; Castex, M.-C.; Jouvet, C. *J. Chem. Phys.* **1986**, *84*, 4712.
- (401) Boivineau, M.; Le Calve, J.; Castex, M. C.; Jouvet, C. *Chem. Phys. Lett.* **1986**, *128*, 528.
- (402) Boivineau, M.; le Calve, J.; Castex, M. C.; Jouvet, C. *Chem. Phys. Lett.* **1986**, *130*, 208.
- (403) Dedonder-Lardeux, C.; Berdah, M.; Jouvet, C.; Martrenchard-Barra, S.; Mestdagh, J. M.; Solgadi, D.; Visticot, J. P. *J. Chem. Phys.* **1996**, *104*, 2740.
- (404) Mestdagh, J. M.; Berdah, M.; Auby, N.; Dedonder-Lardeux, C.; Jouvet, C.; Martrenchard-Barra, S.; Solgadi, D.; Visticot, J. P. *J. Chem. Phys.* **1998**, *4*, 291.
- (405) Okada, F.; Apkarian, V. A. *J. Chem. Phys.* **1991**, *94*, 133.
- (406) Okada, F.; Wiedeman, L.; Apkarian, V. A. *J. Phys. Chem.* **1989**, *93*, 1267.
- (407) Lawrence, W. G.; Apkarian, V. A. *Isr. J. Chem.* **1990**, *30*, 135.
- (408) Zadoyan, R.; Apkarian, V. A. *Chem. Phys. Lett.* **1993**, *206*, 475.
- (409) Hill, M. W.; Apkarian, V. A. *J. Chem. Phys.* **1996**, *105*, 4023.
- (410) Hoffman, G. J.; Sekreta, E.; Apkarian, V. A. *Chem. Phys. Lett.* **1992**, *191*, 401.
- (411) Dubov, V. S. *Chem. Phys.* **1992**, *97*, 7342.
- (412) Last, I.; George, T. F. *Chem. Phys. Lett.* **1991**, *177*, 315.
- (413) Bressler, C.; Lawrence, W.; Chergui, M.; Schwentner, N. *J. Lumin.* **1994**, *60/61*, 570.
- (414) Creuzburg, M.; Wittl, F. *J. Mol. Struct.* **1990**, *222*, 127.
- (415) Creuzburg, M.; Eberlein, J. *Chem. Phys. Lett.* **1998**, *285*, 379.
- (416) Ovchinnikov, M.; Grigorenko, B. L.; Janda, K. C.; Apkarian, V. A. *J. Chem. Phys.* **1998**, *108*, 9351.
- (417) Gerber, R. B.; Alimi, R.; Apkarian, V. A. *Chem. Phys. Lett.* **1989**, *158*, 257.
- (418) Fajardo, M. E.; Apkarian, V. A.; Moustakas, A.; Krueger, H.; Weitz, E. *J. Phys. Chem.* **1988**, *92*, 357.
- (419) Kunttu, K. M.; Seetula, A. *Chem. Phys.* **1994**, *189*, 273.
- (420) Bondybey, V. E.; Pimentel, G. C. *J. Chem. Phys.* **1972**, *56*, 3832.
- (421) Milligan, P. E.; Jacox, M. E. *J. Mol. Spectrosc.* **1973**, *46*, 460.

CR9404609